UNIVERSITY OF TROMSØ UIT

# Mineralogy, Geochemistry and Ore Potential of an ultramafic rock from the Kvaløya Island, North Norway

**Anna Pryadunenko**

GEO-3900 Master's Thesis in Geology

December 2013

**Acknowledgements**

This study was made possible by financial support from Norwegian Centre for International Cooperation in Education (SIU). The University of Tromsø and the Department of Geology in particular is thanked for great opportunities and facilities they provide students.

I would like to thank my supervisor, Kåre Kullerud for the topic he suggested for my master thesis, that turned out to be very interesting to work on. I am very grateful to Kåre K. for the time he spend with me during field work, analytical work and his great support in the interpretation of data. Also, Kåre K. is warmly thanked for his unlimited patience in correcting my English. Thank you, Kåre for everything!

I would like to express my sincere gratitude towards A. Bekker for great discussions and advises that influenced my work and my attitude a lot. Steffen G. Bergh is warmly acknowledged for valuable advises on making this work more pervasive. Muriel Erambert is thanked for great assistance during the microprobe work.

Furthermore, I would like to thank Tatyana Pryadunenko, for her useful advises on improving the structure of this thesis.

I would like to express huge thanks to Nadezda Priyatkina in particular, for the scientific inspiration and positive energy she was providing me during all the time.

All my international friends: Yulia, Alexey, Pierrick, JB, Valeria, Lidia, Thomas, Regina, Marketa, Karina, Patrick, Kristoffer, Alexander and many others, thank you all for great time we spent together in Tromsø. Thank you, Alvaro. Your presence has been of great support for me.

**Anna P. 29.12.2013**

## Abstract

A low-grade metamorphic ultramafic rock at the Kvaløya Island, North Norway, shows Ni content up to 2 500 ppm. Olivine is absent from the rock, and Ni is principally bonded in pentlandite, violarite and millerite. Among other sulphide minerals found in the rock are pyrite, pyrrhotite, chalcopyrite, sphalerite, galena and heazlewoodite (?). Two generations of pyrite are observed in the rock. Second generation is Ni-rich. The rock represents a zone of supergene alteration. The rock was most likely formed in the intracontinental environment.

The serpentinized ultramafic rock from the Kvaløya Island can be an example of low-grade Ni-ore if integrated approach is used for waste minerals. One possible use of many of the traditional waste materials from mining is for $CO_2$ sequestration, i.e. by reacting the waste minerals with $CO_2$ in order to permanently store $CO_2$ in carbonates.

In this work we present an overview of sulphide mineral content, data on conditions of sulphides formation along with geochemical investigations and some constraints on tectonic settings of the rock.

**Keywords**: ultramafic rock, low-grade metamorphism, Ni sulfides, serpentine, $CO_2$ sequestration

Abbreviations of the mineral names are given after Whitney & Bernard (2010), except for:

Amf – Amphibol (GROUP)
Vl – violarite

Term **“ore”** is used in the work referred to the studied ultramafic rock. However, the author does not mean under this term that it is economically profitable for mining.

**Content**

## Introduction.

*A posse ad esse non valet cosequentia…*

The Fennoscandian Shield is a wide territory of exposed Precambrian rocks in northern Europe, that is in many aspects similar to other Precambrian shields in different parts of the world. Precambrian shields are of great interest because of their huge potential for mineral resources. From this prospective the Fennoscandian Shield is a major metal supplier not only for Scandinavia, but also for the whole Europe. Numerous of economic deposits are revealed within the shield in Finland and Sweden, such as the giant nickel-cobalt-copper-zinc deposit in Talvivaara, the copper-zinc deposit in Outokumpu, the chromium deposit in Kemi and the PGE deposit in Suhanko in Finland, and the iron ore deposit in Kiruna and the VMS and gold deposits in the Skellefte district in Sweden. Some small occurrences are also known in Norway. Anyway the number of economic deposits of mineral resources within the Fennoscandian Shield is far from those for other Precambrian shields all over the world (e.g. Russia, Canada, Australia, Zimbabwe). One reason for this relatively un-mineralized character of the Fennoscandian Shield could be that some deposits are simply not discovered yet. This is why it is important to concentrate research on the areas that are potentially ore bearing. The West Troms Basement Complex (WTBC) is a broad area of Precambrian rocks that is considered to be a continuation of the Fennoscandian Shield exposed in a window within the Norwegian Caledonides.

Another factor that should be taken into consideration is a constant increase of metal prices on global market that allows mineral occurrences and previously economically uninteresting deposits to acquire industrial significance. Moreover, the complex approach to mining of new objects could help with minimization of expenses and with solving the problems with waste rock storage.

The ultramafic rock described in this work is probably not the best example of a low-grade ore even with today's prices on Ni. However, the purpose of this study is to

give a comprehensive overview of the mineralogical composition and ore mineral content, as well as to show possibilities of multipurpose usage of the same mineral resource. Furthermore, it will be focused on the ore mineral chemistry and the temperature conditions during formation of the ore minerals, which will shed light on nature of ore-forming processes. In addition, the author makes an attempt to place the ultramafic rock into the tectono-magmatic framework of the region and define its tectonic settings.

## Chapter 1. Regional geology

The area of research is located in the northeastern part of the Kvaløya Island, a component of the West Troms Basement Complex (WTBC), which is considered to be the northwestern fringe of the Fennoscandian Shield.

### 1.1. Geology of the Fennoscandian Shield

From geographical point of view, the Fennoscandian Shield includes territories of Sweden, Finland, the northwestern part of Russia, and parts of Norway (Fig. 1.1.1).

The oldest rocks of the shield are Archean in age, formed between 3.5 and 2.5 Ga, and they are mainly represented by TTG- and other types of gneisses and greenstone belts. These rocks are found in the northeastern part of the shield (Kola Peninsula, Karelia and northeastern Finland). From 2.5 Ga to 1.95 Ga the Archean crust was exposed to an extensional regime. Stratified mafic intrusions as well as abundant mafic dyke swarms were formed during this period. NW-SE trending rift zones formed and the Kola Ocean opened. This was followed by ocean closure and the Karelian Orogeny.

The next prominent event in the crust formation within the Fennoscandian Shield is the Svecofennian orogeny, which was responsible for the formation of the Svecofennian province of the Fennoscandian Shield. This province makes up northern and central Sweden and southwestern Finland. This tectonic event took place during the period 1.96 – 1.76 Ga. The province includes island arcs, microcontinents and different terrains that initially were positioned west of the continent, which afterwards were juxtaposed due to the collision. The province is composed of both metasedimentary and metavolcanic rocks (Ojala and Iljina 2008).

The phase of crustal accretion was followed by the emplacement of large volumes of plutonic rocks, intruded into the western part of Svecofennian Province. The so-called Trans-Scandinanavian Igneous Belt (TIB) stretches from Småland in southern Sweden through Värmland and western Dalarna and then continues below much of the

Caledonian mountain chain up to northern Norway (the Lofoten-Vestrålen district). The TIB comprises of mostly undeformed granitoids, characteristic rapakivi granits and anorthosites.

Southwest of the TIB, the Sveconorwegian Province (also known as the Southwestern Gneiss Province) occurs, which had a complex evolution ranging from c. 1700 to 900 Ma ago. Most of the rocks originally formed during the Gothian Orogeny 1700-1500 Ma ago and the following Sveconorwegian Orogeny c. 1130-900 Ma ago. The province is dominated by supracrustal and igneous rocks.

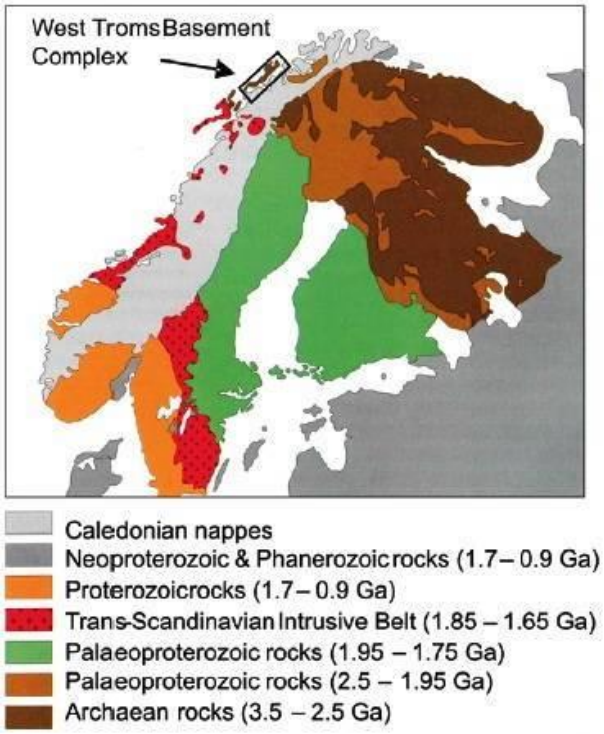


***Figure 1.1.1.*** *Simplified geological map of the Fennoscandian Shield with major tectonic domains. Ages are given in the legend. Area of study indicated with black rectangle. After Bergh et al. (2010).*

The Scandinavian Caledonides, which stretch through most of Norway and include adjacent parts of Sweden, are made up of Neoproterozoic to Silurian metasedimentary and metavolcanic rocks, deposited in the Iapetus Ocean 700 to 400 Ma ago. Together with slices of older basement, these rocks were thrust several 100 km eastwards over the edge of the Fennoscandian Shield in several large thrust sheets

known as nappes, when Laurentia collided with Baltica during the Caledonian orogeny c. 400 Ma ago (Andersson 2009).

## 1.2. Mafic-ultramafic associations within the Basement Windows in Northern Norway

Mafic-ultramafic rock associations occur within several basement provinces in Northern Norway (Fig. 1.2.1). The majority of these rocks are interpreted to have similar origin and age as the WTBC.

For the present study, the composition of the Kvaløya ultramafic rock has been compared with the compositions of mafic-ultramafic rocks from these other basement provinces in Northern Norway (see chapter 8). An overview on the geology of these provinces is given here.

South of the study area two provinces are exposed. These are the Rombak Tectonic Window exposed within Norwegian Caledonides and the Lofoten-Vesterålen area west of the Caledonian Nappes.

The Altenes, Reppafjord and Alta-Kvænangen tectonic windows are located in the western part of Finnmark, the northernmost county of Norway. These tectonic windows are juxtaposed closely to each other. The Alta-Kvænangen window is separated from the Altenes window by the Alta Fjord. The boundary between the Altenes and Reppafjord windows is marked by a 6 km wide zone of Caledonian rocks. The metamorphic grade of the rocks in these basement provinces increases northwards from greenschist to amphibolite facies conditions. In all three windows, the rocks display a weak metamorphic Caledonian overprint. The Proterozoic rocks exposed in Western Finnmark were unified in the Raipas Supergroup by Pharaoh (1983).

### *Rombak Tectonic Window*

The Rombak Tectonic Window is defined as an area of 1900 $km^2$ occurring on both sides of the border between Norway and Sweden (Fig. 1.2.1). The window is situated on the boundary between the Archean and Paleoproterozoic domains of the Fennoscandian Shield. A big variety of sedimentary rocks, mafic to felsic volcanic rocks and mafic to felsic plutonic rock are exposed in the area. The rocks occurring in the window underwent metamorphism at amphibolite facies conditions, but evidence for a later greenschist facies retrogressive metamorphism have developed to a varying degree in different parts of the window. According to the description of the geology from the area (Korneliussen et al., 1989), the abundances of rock types such as sedimentary rocks and mafic to felsic volcanics vary significantly from one supracrustal unit to another within the basement window. The age relationships between different supracrustal units are unclear. The Ruvssot-Sjangeli area, where mafic volcanics were dated to 2.3 Ga (after Romer 1989), represents the oldest rock in the eastern part of the Rombak window. It is separated from other supracrustal belts of the window by the N-S trending Muohtaguobla Tectonic Zone. The oldest rocks in the southern part of the window, which not have been dated, are the Gautelis Tonalites. The supracrustal sequences of the Rombak window are spatially associated with mafic to felsic plutonic rocks intruded 1.8 – 1.7 Ga ago (Korneliussen et.al., 1989).

In the present thesis, whole rock chemical analyses (XRF) of mafic to intermediate volcanic rocks from the Ruvssot-Sjangeli area are used. The analyses are from Korneliussen and Sawyer (1989). Korneliussen and Sawyer (1989) suggested that the rocks of the window formed in a mature magmatic arc environment that existed about 1.9 – 1.7 Ga ago.

### *Lofoten-Vesterålen Basement Province*

The Lofoten-Vesterålen area of the North Norway (Fig. 1.2.1) Neoarchaean and Palaeoproterozoic continental crust (2.9 - 1.67 Ga) occur as a basement horst. To the east it borders with the Scandinavian Caledonides and to the west with offshore Mesozoic basins (Bergh et. al., 2012). The entire Lofoten–Vesterålen region is considered to be a part of the Svecofennian Orogen. The territory of the Lofoten – Vesterålen region as well as the territory of the above-described Rombak Basement Window roughly coincide with the southern boundary of the Archean domain of the Fennoscandian Shield. The western parts of Lofoten and Vesterålen Basement Province are represented by granulite facies rocks, while the eastern part of the region is dominated by various amphibolite facies gneisses, migmatites, greenstone belts and granitic plutons (Corfu 2007). Formation of the oldest crust of the Lofoten – Vesterålen area took place during the major crustal accretion event in Meso- Neoarchean at 2.85-2.7 Ga, as evidenced from U-Pb zircon data (Corfu 2007). The region underwent a major orogenic event at about 2.64 Ga involving high-grade metamorphism including migmatization (Corfu 2007). The most significant event during the Proterozoic crustal evolution of the Lofoten – Vesterålen area is marked by the intrusion of an anorthosite-mangerite-charnockite-granite (AMCG) suite, which took place during two distinct events; the first one at 1.87 – 1.86 Ga and second and major event at 1.8 – 1.79 Ga (Corfu 2004). The latest and most prominent event was characterized by the emplacement of pegmatitic melt. This plutonic rock suite is considered to be the northwestern most tip of the Transscandinavian Igneous Belt. The rocks of the area also show some indications of a cryptic tectono-thermal event at about 1100 Ma and very weak metamorphic overprint as a result of the Caledonian Orogeny. Early Proterozoic supracrustal rocks present in the Lofoten – Vesterålen area mainly consist of fine-grained quartz, two-feldspar gneisses. However, large areas on Austvågøy consist of quartz-rich plagioclase gneisses, while other areas (Hinnøy) include considerable amounts of more basic rocks. Rocks of obvious sedimentary origin, including marble,

graphite schist and iron formations, occur throughout the region as lenses within the feldspatic gneisses (Griffin et al., 1978). The analyses of the Early Proterozoic supracrustal rocks used in this thesis, which generally are intermediate in composition, are taken from the work of Griffin et al. (1978). It has been interpreted that the rocks have an arc-related origin, similar to the rocks of the Rombak tectonic window (Jensen 1996) and rocks occurring in the Kiruna and Skellefte districts of northern Sweden (Griffin et al., 1978; Korneliussen & Sawyer 1989).

### *Altenes Tectonic Window*

An at least 10 km wide zone of Paleoproterozoic supracrustal rocks is exposed in the Altenes window (Fig. 1.2.1). The Paleoproterozoic rocks are uncomformably overlain by the Neoproterozoic Rafsbotn group. The Paleoproterozoic rocks of the window are divided into two groups, the Brattholmen group with 8 formations and the Sagelv group with two formations. These two groups are separated by an angular unconformity. The igneous rocks of the Brattholmen group are represented by calc-alkaline metavolcanics with varying in composition from basalts via andesites to rhyolites, while the igneous rocks of the younger Turelv formation of the Sagelv group have tholeiitic affinity (Jensen 1996). A suite of Paleoproterozoic mafic dykes crosscuts these two regionally developed metavolcanic sequences. The dykes have a predominant SW-NE trend. The dykes were geochemically investigated and compared with two metavolcanic successions from the Altenes window by Jensen (1996), where it was shown that the dykes display characteristics that strongly support their formation in an arc-related tectono-magmatic regime. Furthermore, the calc-alkaline metavolcanic rocks of the Brattholmen group were interpreted as representatives for subduction-related magmatic activity. The younger meta-tholeiites of the Turelv formation of the Sagelv group were suggested to be formed in a back-arc spreading basin. Dating of rocks from Altenes tectonic window has not been performed, but the metamorphic peak of the correlative Holmvann Group exposed in Reppafjord window was obtained as 1.84 Ga

(Pharoah et. al., 1982). In this thesis, analyses of the mafic dykes from Altenes window are used for comparison. Analyses are taken from the work of Jensen (1996).

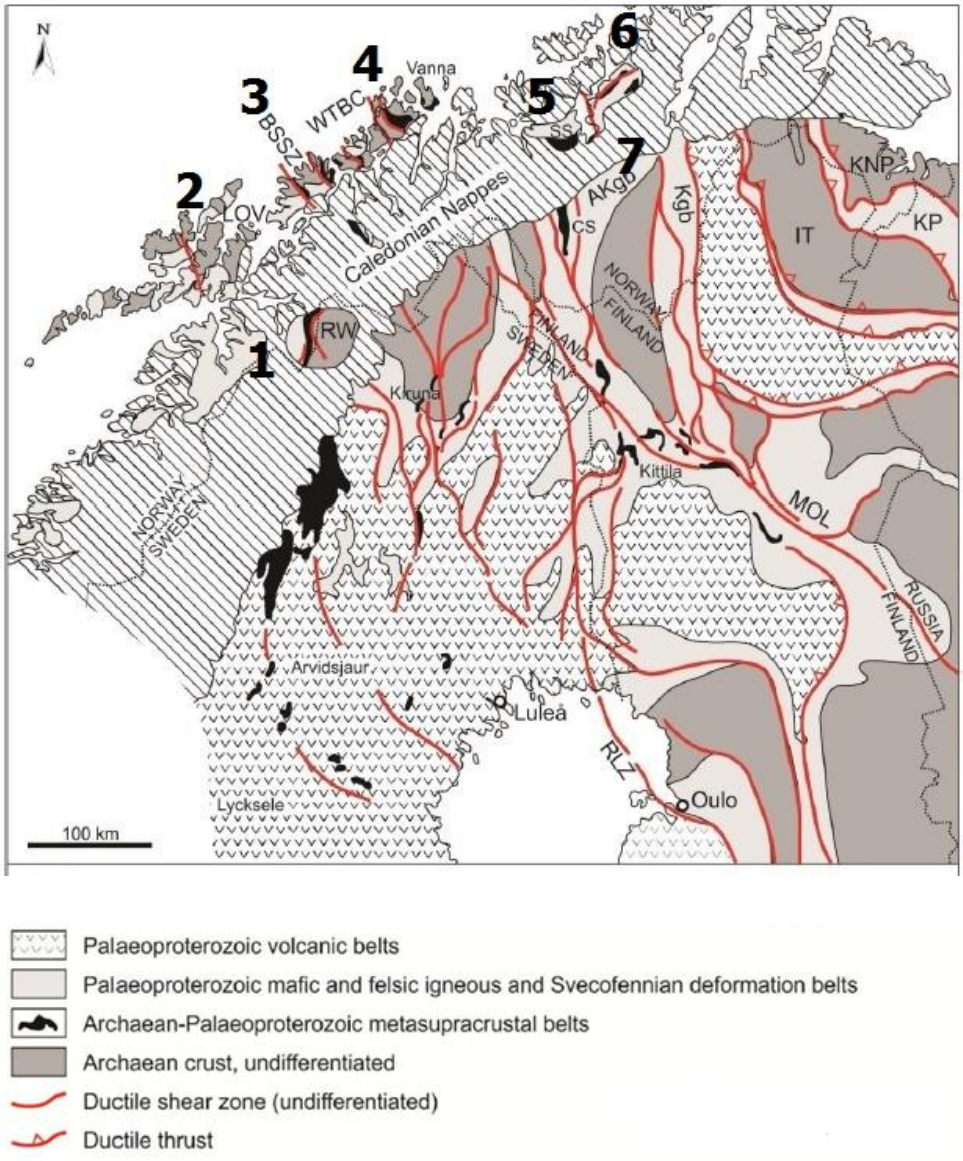


***Figure 1.2.1****. Schematic tectonic map of the Fennoscandian Shield after Bergh et al. (2013). Ultramafic and mafic rocks (overviewed in this chapter) occur within Rombak Tectonic Window (1), Lofoten and Vesterålen islands (2), Senja Shear Belt (3), Ringvassøya Island (4), Alta-Kvænangen Tectonic Window (5), Reppafjord Tectonic Window (6) Altenes Tectonic Window (7).*

### *Repparfjord Tectonic Window*

The Porsa Group is the oldest group in the Reppafjord window (Fig. 1.2.1). It is composed of metasedimentary rocks (dolomites, schists, metasandstones). The Nussir Group is represented by metabasalts and can be correlated to the Turelv formation of the Sagelv group of the Altenes window. The next group is the Saltvann Group composed of metasandstones. These three groups are concordant and represent together a continuous volcano-sedimentary succession with calc-alkaline magmatism as dominant (Jensen 1996). The youngest rocks of the Reppafjord window belong to the Holmvann group, represented by nine formations of metavolcanics and metasediments. This group is correlative with the Brattholmen group of the Altenes window. In the present thesis, whole rock chemical analyses of the Aisaroaivi formation of the Holmvann group from Jensen (1996) were chosen for comparison. The reasons for this is that the Aisaroaivi formation, which contains ultramafic, boninite-like metavolcanics (Jensen 1996) is correlated to the Brattholmen group of the Altenes window. Comprehensive geochemical studies, reinforced by detailed studies of the supracrustal units allowed Jensen (1996) to conclude that the metavolcanic rocks from the Reppafjord window formed in continental arc tectonic settings.

### *Alta-Kvænangen Tectonic Window*

In the Alta-Kvænangen tectonic window (Fig. 1.2.1), the Kvenvik Greenstone Formation (KGF) appears to be the lowermost part of the Proterozoic Raipas Supergroup. The unit is correlated with the Nussir Group in the Repparfjord Window and the Turelv formation of the Sagelv Group of the Altenes Window (Jensen 1996). Primary volcano-sedimentary structures are well preserved in the rocks of KGF, since the rocks only have been subjected to low grade metamorphic conditions. Significant studies of the rocks of KGB have been done by Zwaan and Gautier (1980), Bergh (1986), Bergh and Torske (1986). Whole rock chemical analyses of the least altered

volcanic rocks given in Bergh (1986) have been used in the present thesis. Based on geochemical data (mostly incompatible elements and REE), the mafic metavolcanics from the Kvenvik greenstone formation were identified by Bergh (1986) as tholeiitic basalts formed in transitional settings, such as continental rifts or back-arc basins. Furthermore, REE patterns support their affiliation to N-MORB. The presence of thick siliciclastic units indicates deposition in shallow water to terrestrial subsiding rift basin. All in all, plate margin tectonic settings with magmatism transitional between within plate basalts and plate margin basalts with a signature of MORB tholeiites was established for KGF (Bergh 1986).

## 1.3 Geology of the West Troms Basement Complex. Senja, Kvaløya, Ringvassøya and Vanna Islands.

North of the Lofoten and Vesterålen Basement Province, the West Troms Basement Complex is exposed along the coast on a chain of islands stretching from Senja in south to Vanna in north (Fig. 1.3.1).

### *The Senja Island*

The Island of Senja is located on the suspected continuation of the boundary between the Achaean and Svecofennian domains of the Fennoscandian Shield. In the southwestern part of the island of Senja, intrusive rocks of 1.8-1.77 Ga in age are widespread. These rocks are confined to the Transscandinavian Igneous Belt. In the northeastern part of the island the major unit is the 30 km wide Senja Shear Belt that comprises Achaean basement gneisses with age 2.8 - 2.75 Ga (Kullerud et al., 2006a) and lens-shaped embedments of folded Paleoproterozoic metasupracrustals (Astridal, Torsnes and Svanfjellet belts). The supracrustal belts are represented by mafic volcanics and mainly terrigenous sedimentary successions. Myhre et al. (2011) provide results on U-Pb zircon dating from a gabbroic rock in the Mjelde-Skorelvatn belt and of detrital

zircon dating from a metapsammite in the Torsnes. The gabbro yielded an age of 1992±2 Ma of an intrusive event, while 1970±14 Ma is interpreted as the maximum deposition age of the metapsammites. The same age is proposed for the Astridal belt by Bergh et al. (2010). Analyses used in this work were performed on rock samples from a mafic-ultramafic association from NW Senja. The rocks of the association occur both within the Archean gneisses and within the Astridal Supracrustal Belt (Priyatkina, 2013). Samples analyzed were mostly collected along the southwestern shore of Baltsfjord within the supracrustal zone. The rocks underwent metamorphism under greenschist to amphibolite facies conditions. With reference to structural features and isotope data from the Astridal belt, the metamorphism and deformation of the belt is inferred to be a result of the Svecofennian Orogeny, with only a weak Caledonian overprint (Bergh et al., 2010). This situation is similar for the whole WTBC.

The layered mafic-ultramafic association comprises ultramafic olivine-pyroxene-amphibole rocks, mafic amphibolite and hornblendite. The deformation is intense and the contacts with the Archean gneisses are tectonically modified. Sharp contacts within the mafic-ultramafic bodies are more abundant than gradational contacts. The transition from olivine-rich to pure hornblendite layers occurs through a gradual increase of the amphibole content relative to that of olivine (Priyatkina, 2013).

The rocks are interpreted to be igneous olivine-amphibole cumulates; the hornblendite and metagabbroic rocks initially formed through various degree of fractionation and were later modified during high-grade metamorphism. In terms of tectonic settings, Priyatkina (2013) suggested that the ultramafic-mafic layered association might represent ophiolite cumulates crystallized within the oceanic crust in a MORB-like tectonic setting, with similarities to the Eocene Skaergaard intrusion in Greenland. Priyatkina (2013) concluded that even though the Archean continental crust is present towards SW of the study area within the Lofoten and Vesterålen Islands, it cannot be excluded that the suture of the Svecofennian Ocean may be found within the Senja Shear Belt.

### *The Ringvassøya Island*

The Island of Ringvassøya is located north of Kvaløya. The Ringvassøya Grenstone Belt (RGB) is a suprucrustal unit containing mafic to felsic volcanic rock. The belt which is 10 to 15 km wide, is enclosed between segments of the tonalitic Dåfjord gneisses. The mafic volcanic unit (MVU) of our interest is outcropping in the central part of the Ringvassøya Greenstone Belt and comprises mainly amphibolite of different types (Motuza 2000). Based on geochemical data, the amphibolites of the mafic volcanic unit were interpreted by Motuza (2000) as primary basalts of the tholeitic series. Within the amphibolites, a few meters thick layers of felsic material with biotite and hornblende are common. They belong to the same unit (MVU) and were interpreted as primary volcanites of andesitic to rhyolitic composition, mainly pyroclastic (Motuza 2000). The oldest ages obtained from the Ringvassøya greenstone belt are c. 2.85-2.83 Ga (Motuza et al., 2001; Kullerud et al., 2006a). Whole rock chemical analyses were taken from Motuza (2000). Analyses of intrusive mafic rocks and felsic volcanics were also included for comparison in the present thesis, since it is inferred that the igneous rocks of the Ringvassøya Greenstone Belt (including dykes), form continues series from picrobasalts, basalts and basaltic andesites via andesites and dacites to rhyolites (Motuza 2010). Geochemical investigations allowed dividing all igneous rocks of the central part of RGB into two distinct groups:

1. Tholeiitic, with all amphibolites and some samples of andesitic lapilli tuff belonging to this group.
2. Calc-Alkaline, with all dacitic and rhyolitic rocks and partly andesitic metavolcanic rocks included.

The tectonic setting of the rocks from RGB was interpreted as volcanic island arc environment adjacent to an active continental margin. The presence of both tholeiitic and calc-alkaline rock series indicate the existence of different volcanic centers at the same time (Motuza 2010).

### *The Kvaløya Island*

The main geological units of the Kvaløya Island are gneisses of different composition, predominantly tonalitic, plutonic suites, mafic dyke swarms and metasupracrustal belts. Most of the rocks of the island are Neorcheaen in age They were intruded by plutonic rocks of mafic, intermediate and granitic compositions, such as the Ersfjord Granite, during Svecofennian time

The gneisses occur as megablocks that are separated by metasupracrustal belts. The northeastern block is represented by intermediate-mafic banded gneisses. The Gråtind Migmatite occurs in the southeastern part of the island and comprises highly deformed tonalitic to dioritic gneisses. Further west, the Bakkejord Diorite occurs, which is composed of gabbro, diorite and tonalite. The southwestern part of the island is made up of the Kattfjord Complex, which is represented by biotite gneiss of tonalitic composition (Corfu et al. 2003)

Metasupracrustal belts occur on the Kvaløya Island as narrow stripes accompanied by steep ductile-shear zones. They are composed of sedimentary and metavolcanic rocks, with the latter occurring as amphibolitic units. The most prominent supracrustal belt is Mjelde-Skorelvvatn Zone, which is striking in a NNW-SSE direction. The rocks of the supracrustal belts have undergone metamorphism under greenschist- to amphibolite-facies conditions.

Undeformed mafic dyke swarms are abundant in the massive Bakkejord Diorite, while they are scarce further to the east in the Gråtind Migmatite. East of the Mjelde-Skorelvvatn they are exposed as highly deformed amfibolitic lenses. The age obtained from the dykes in this part of the island is 2670 Ma (Kullerud et al., 2006a). A later generation of mafic dykes intruded tonalitic gneisses at the Ringvassøya Island 2403±3 Ma ago. Trace element geochemistry suggests that this generation of dykes can be classified as continental basalts (Kullerud et al., 2006b).

The latest prominent intrusive event for the whole WTBC is represented by the Ersfjord Granite, which is exposed in the central and northwestern parts of the Kvaløya

Island. This unit has given a U-Pb zircon crystallization age of 1792 ± 5 Ma (Corfu et al. 2003). The complex shows only gentle metamorphic overprint as a result of the Caledonian Orogeny.

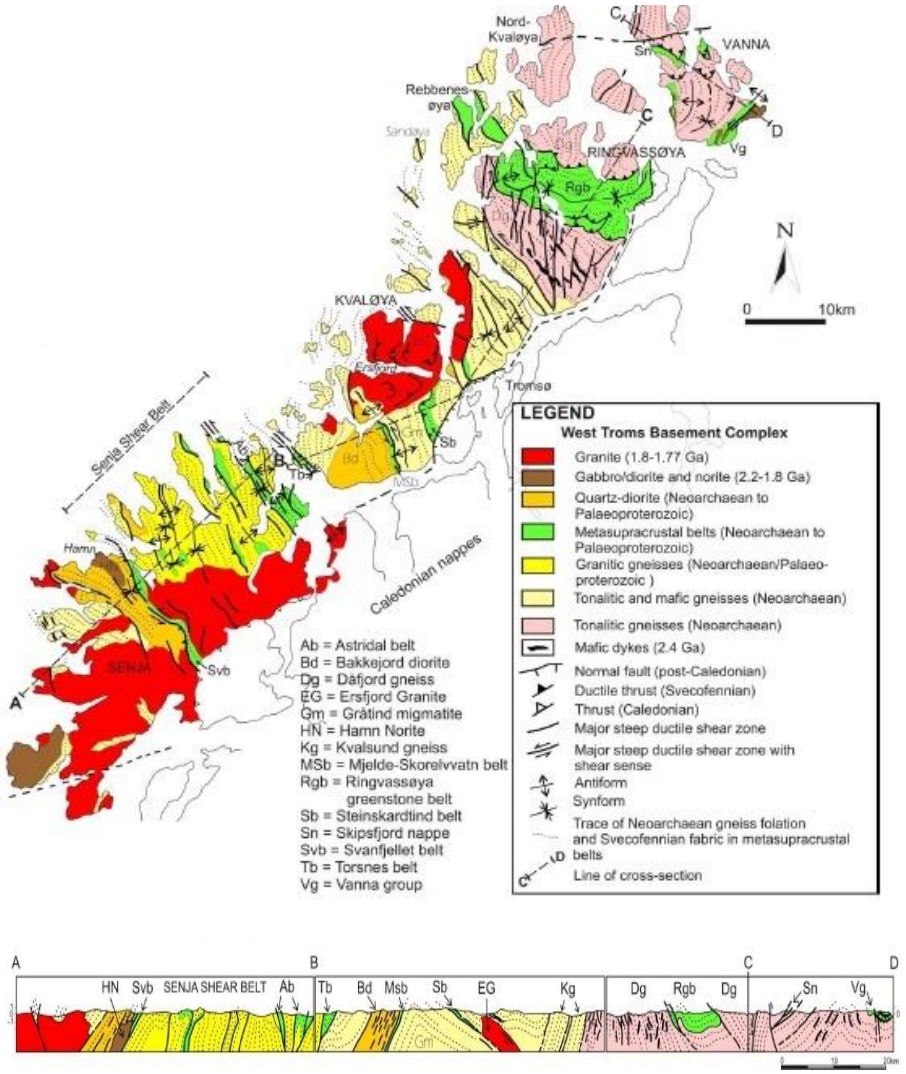


***Figure 1.3.1.*** *Regional geologic-tectonic map and cross-section of the West Troms Basement Complex (from Bergh et al., 2010)*

The studied ultramafic rock occurs as elongated bodies with length up to 300 meters, hosted by Archean gneisses. The maximum width of the lenses is up to 30 meters. Lenses are abundant in the northeastern part of the island (Fig. 1.3.2.)

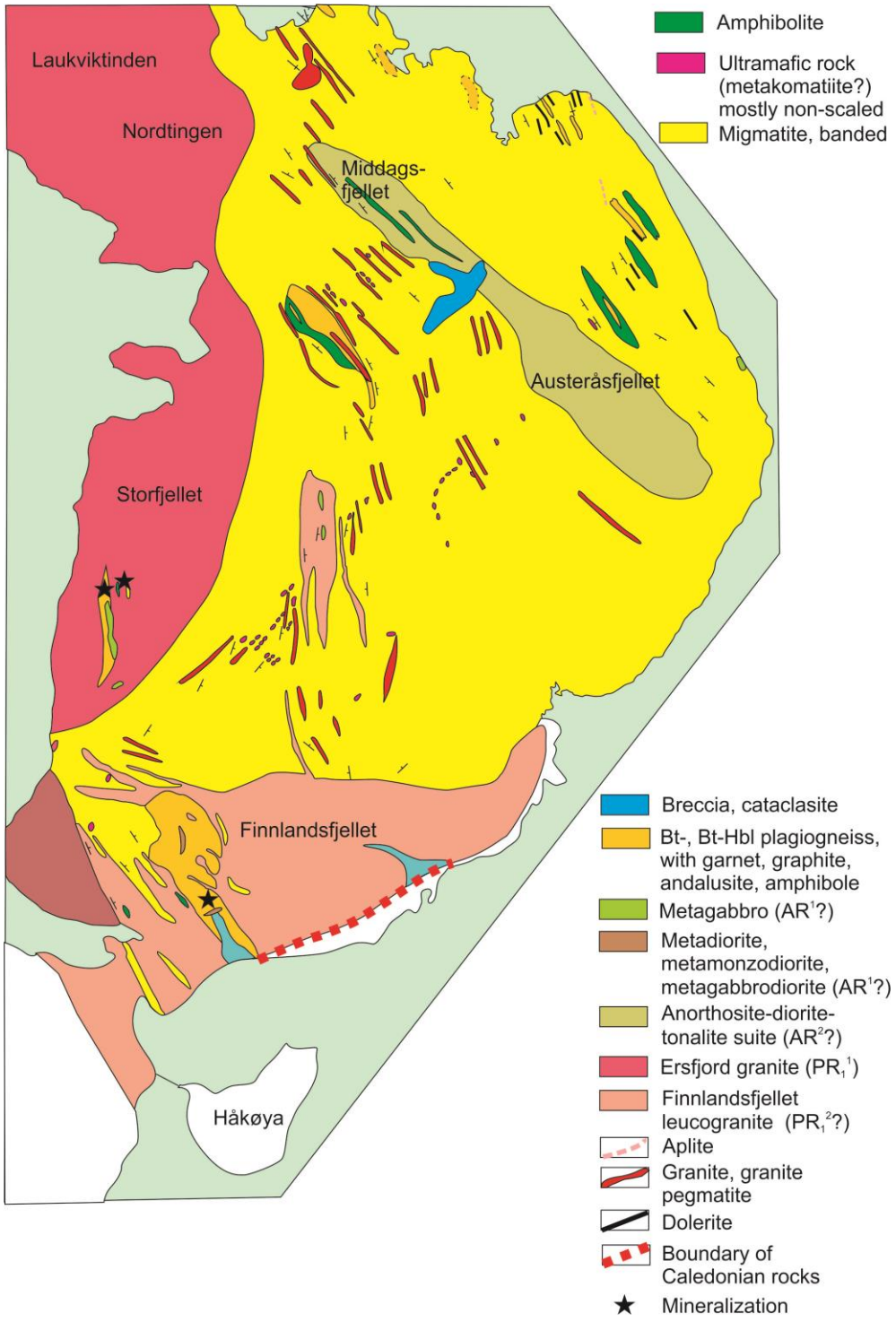


***Figure 1.3.2.*** *Schematic geological map of the Kvaløya Island (after Gedeminas Motuza, personal communication to Kåre Kullerud, 2011)*

## Chapter 2. Field occurrence of the ultramafic rock.

The studied ultramafic rock is hosted by Archean gneisses. The composition of the gneisses in the northeastern part of Kvaløya Island is quite homogeneous. The mineral assemblage of the gneiss includes plagioclase as a dominant mineral phase, and quartz, biotite and amphibole. The gneisses are medium- to coarse-grained with foliation striking N-S to NNW-SSE and dipping with angles 60-80° variably to the WSW and ENE (Fig. 2.1).


***Figure 2.1.*** *Foliation in the gneiss.*

The ultramafic rock occurs within the Archean gneisses as lens-shaped bodies with rusty brownish weathering surface, with length varying from 10 to 100 meters (the longest observed is at least 300 meters) and width up to 30 meters (Fig. 2.2).

The contacts between the ultramafic lenses and the host rock are tectonically reworked, making it impossible to argue about the primary relationships between the different rocks (Fig. 2.3)


***Figure 2.2.*** *Field occurrence of the ultramafic rock. (a) Rusty, brownish colored rock, bounded by red lines is a lens of ultramafic rock, surrounded by gneisses. (b) Small lens with rusty color on weathered surface. Strike is sub-parallel to the foliation in the gneiss.*

***Figure 2.3.*** *Tectonically modified contact between the ultramafic rock (right) and an amfibolite dyke (left). The contact is poorly exposed, however it is notable that it was sheared (b).*

Crosscutting relationships has been observed between gneisses and amphibolite dykes (Fig. 2.4). Such dykes are abundant in the area. The thickness of the amphibolite dykes varies between 1 and 2 m. They strike towards N-NW, which is similar to the ultramafic lenses. However, no direct relationship between amphibolite dykes and the ultramafic rock has been observed (except for sheared contacts).


***Figure 2.4.*** *Field relationships between amphibolite dyke (dark colored rock) and gneiss (light-colored rock). The dyke is crosscutting the foliation of the gneiss.*

The ultramafic rock is characterized by a massive texture, rusty color on weathered surface and dark-grey color on fresh surface. Some lenses show spotty texture with circles 0.5-0.7 cm in diameter (samples AP-47, AP-50, AP-53). The origin of this texture is likely due to alteration.

Some lenses are enriched in opaque minerals (sulfides), while in others mineralization is not visible with a naked eye. No special pattern in the distribution of sulfide mineralization was observed in the field. Sulfides are normally equally distributed within the lenses, without being confined to veins or fractures.

## Chapter 3. Petrology

The rock-forming mineral assemblage has been studied during thin-section microscopy in transmitted light. The dominating silicate phases are serpentine, amphibole and talc. Some textural variations as well as differences in the abundances of the rock-forming minerals were observed.

Textures preserved in the rock could be separated into two main types. The first type is represented by samples showing relatively homogenous texture characterized by random distribution of rock-forming minerals and opaque minerals. The second type comprises samples that have a "spotty" texture characterized by clusters of opaque minerals that occur spatially close to each other resulting in dark spots, while domains free of opaque minerals result in light spots. Another characteristic of the spotty textures in some thin-sections is the presence of domains dominated by serpentine or amphibole (Fig. 3.1 c).

The modal abundances of the rock-forming minerals show variations within samples with different texture. In most of the studied thin-sections serpentine represent the most abundant mineral phase. Serpentine forms tiny crystals that normally are less than 0.05 mm in size. Sometimes serpentine occurs as aggregates of randomly oriented crystals that are of the same in size (Fig. 3.1 a, b).

Amphibole is the second-most abundant mineral. It form crystals up to 0.7 mm, but also occurs insignificantly altered in very fine-grained aggregates. The fine-grained aggregates of amphibole show interference colors that are one order higher than that for the larger crystals (Fig. 3.1 d).

Chlorite form tabular grains up to 0.5 mm in size, with grayish to greenish interference colors (Fig. 3.1 e). However, very often chlorite flakes with interference colors of high order are observed. Interference colors change from dark brown to reddish and even violet, suggesting strong Mg-enrichment of these grains.

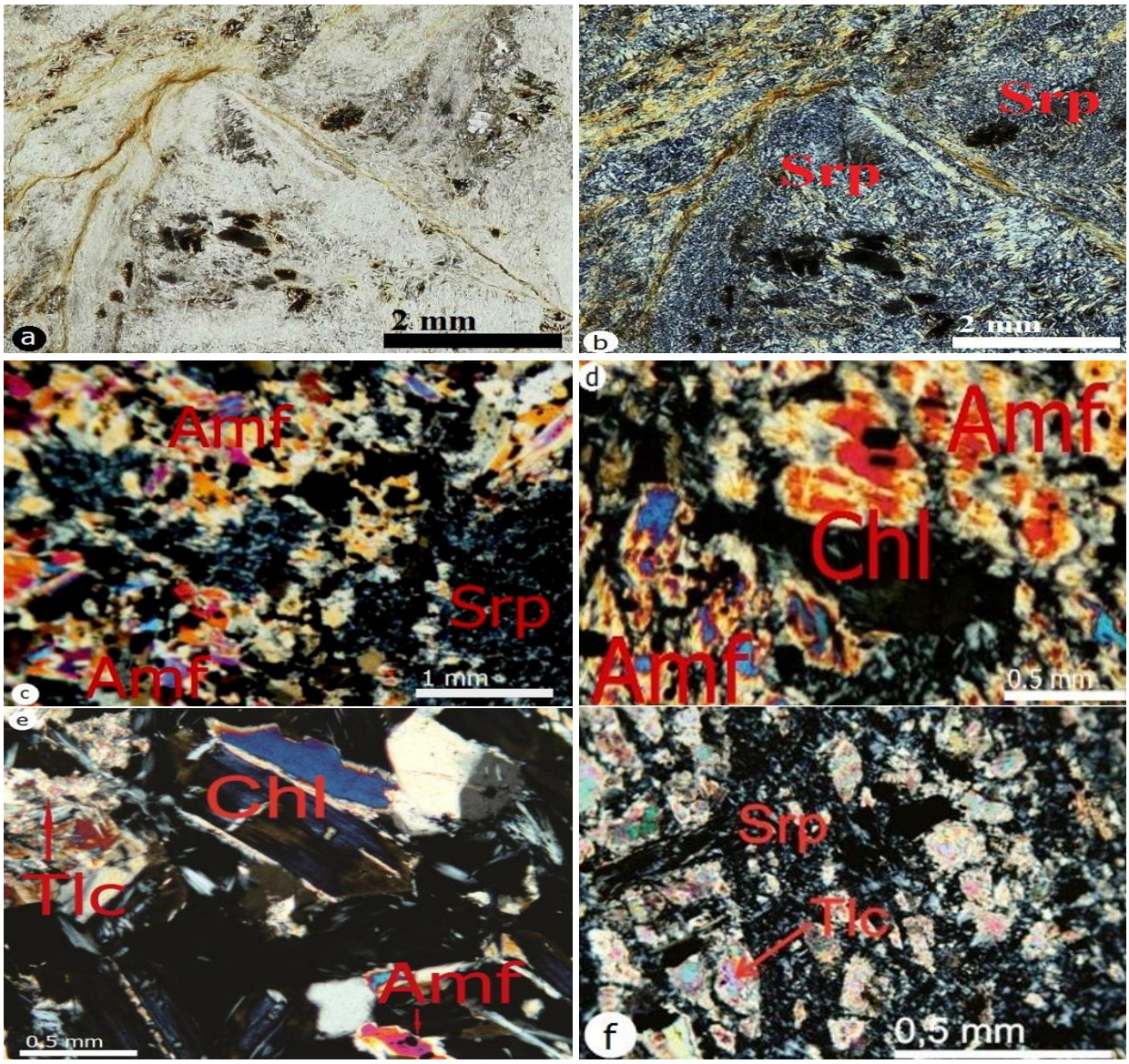


***Figure 3.1.*** *(a) Aggregates of small randomly oriented crystals of serpentine. Plain polarized light. (b) Same as in (a), crossed nicols. (c) Microphotograph of the representative sample with "spotty" texture. Some areas in the thin-section are highly dominated by serpentine, some by amphibole. (d) Two representative amphibole grains. One, in the upper part of the image shows red-brownish colors, while fine-grained aggregate in the lower part of the image has more intense violet colors. (e) Tabular flake of chlorite. (f) Sample dominated by talk.*

Talk is less abundant in the studied rock. It always form aggregates that are very fine-grained and does not exceed 0.3 mm in size. However, a few samples are dominated by talc (> 50 volume %) (Fig. 3.1 f). In these samples amphibole forms relatively big crystals (up to 1.5 mm in size). This amphibole is unaltered, except from along grain boundaries of a few grains, where it has been replaced by talk.

For samples that show the spotty texture, the modal abundances of serpentine and amphibole are approximately the same. In these samples, serpentine forms elongated crystals with size up to 0.5 mm. Amphibole, in its turn, show crystals up to 1.5 mm in size. Amphibole grains are slightly altered. Chlorite is Mg-rich.

The minerals observed from the studied ultramafic rock are clearly not in chemical equilibrium, which can be concluded from the talc alteration of amphibole grains. Based on the optical properties of amphibole, it is concluded that it most likely is represented by tremolite. Chlorite shows two different varieties. Anyhow, additional microprobe analyses are required for making conclusions about the chemical compositions of the silicate minerals of the rock.

## Chapter 4. Ore mineralogy

Thirty-six polished thin-sections were studied. Ore minerals observed from the Kvaløya ultramafic rock are given in Table 4.1.

The most abundant opaque minerals observed in thin sections are magnetite and ilmenite, with the first one as the most abundant. The sulfide content is dominated by pyrrhotite and pentlandite, which show approximately equal modal abundances. Pyrite and chalcopyrite are also common minerals, but they are less abundant than pyrrhotite and pentlandite. Galena and sphalerite were occasionally observed. Sphalerite sometimes occurs as individual grains, separated from other sulfides, while galena only has been observed in aggregates together with other sulfides or as inclusions in pyrite. Millerite was observed in 3 thin sections as coarse individual crystals (up to 0.3mm) or together with pentlandite and occasionally with violarite. Some grains from samples KV-660 and AP-54 show optical properties in reflected light characterizing heazelwoodite, although the presence of this mineral has not been confirmed by electron microprobe analysis.

### *Magnetite*

Magnetite is the most widespread ore mineral in all samples. The grain size varies from < 0.01 mm up to several mm. The mineral shows grey color in reflected light, usually with weak brownish tint. Magnetite grains demonstrate high relief. The mineral is isotropic with no birefringence as a result. Magnetite shows allotriomorphic grain shapes, but subidiomorphic grains are sometimes observed. Cleavage is lacking in all grains of magnetite. All grains of magnetite, especially the largest ones, show traces of internal fracturing. Twinning is not common for magnetite from the studied samples, although it has been observed in some thin-sections. Magnetite is often intergrown with other ore minerals; commonly with ilmenite (Fig. 4.1). Furthermore, it is observed intergrown with pyrrhotite and pentlandite. Small (< 0.01 mm) grains of magnetite are

enclosed in grains of other minerals, such as pyrite and pentlandite, indicating its earlier crystallization and afterwards being trapped by later formed minerals. Solid solution decay structures, that are very common for magnetite (Ramdor 1962) have not been noticed in any sample, all grains seem to be chemically homogeneous. The modal abundance of magnetite in all the samples is very high (up to 30 %). Commonly magnetite makes up to 50 % of all opaque minerals, sometimes up to 70%.

***Table 4.1. Opaque mineral content of the ultramafic rock from the Kvaløya Island.***

| **List of minerals, determined from the ultramafic rock at Kvaløya** | |
|---|---|
| Oxides | Magnetite $Fe_3O_4$ |
| | Ilmenite $FeTiO_3$ |
| Sulfides | Pyrrhotite $Fe_{1-x}S$ |
| | Pentlandite $(Fe, Ni)_9S_8$ |
| | Violarite $Fe^{2+}Ni_2^{3+}S_4$ |
| | Pyrite $FeS_2$ |
| | Chalcopyrite $CuFeS_2$ |
| | Sphalerite ZnS |
| | Galena PbS |
| | Millerite NiS |
| | Heazelwoodite $Ni_3S_2$ (?) |

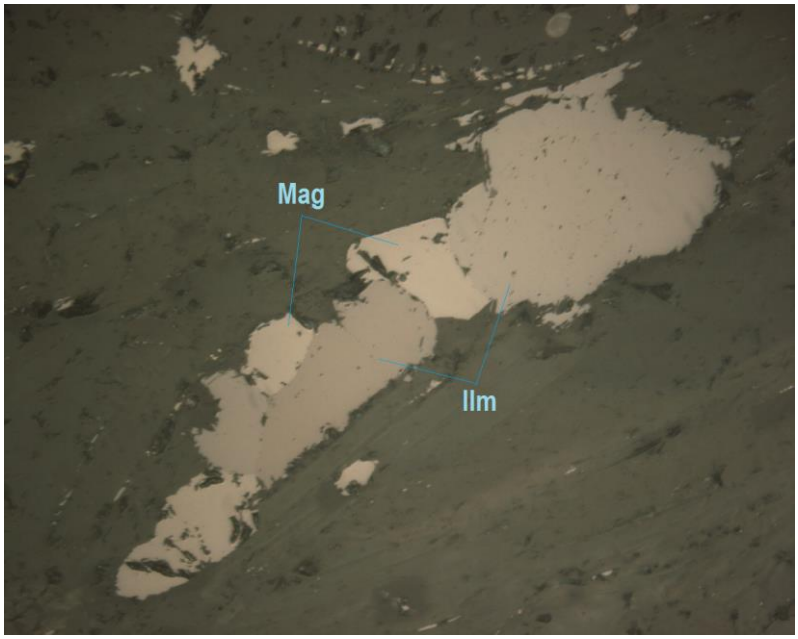


***Figure 4.1.*** *Intergrowth of magnetite with ilmenite.*

***Ilmenite***

Ilmenite is a common mineral for all the studied samples. The grain size of ilmenite varies from < 0.1 mm to 1 mm. Ilmenite is white-grayish in plain polarized reflected light, sometimes with brownish tint and is quite similar to magnetite. However, ilmenite is clearly anisotropic in cross-polarized light, distinguishing it from magnetite. The mineral shows high surface relief, more distinct than that for magnetite, which is isotropic. Ilmenite show strong birefringence. Grains of ilmenite show no cleavage, but are mostly deformed and show internal fracturing. Tabular crystals are common. Ilmenite often occurs in individual grains, but it is also often observed in association with pyrite, pyrrhotite, pentlandite and other ore minerals. According to Pichler et al. (1997) ilmenite associated magnetite in basic rocks typically shows laminar intergrowths. However, this kind of relationship between the two minerals has not been observed from the rock studied here. The reason for this could be the fresh surfaces of both ilmenite and magnetite grains of the studied thin-sections, which makes it difficult to see such kind of intergrowths. On oxidized surface or after structural etching,

however, these features can become visible. Ilmenite is slightly less abundant than magnetite.

### *Pyrrhotite*

Pyrrhotite has been determined in all of the studied samples. The size of pyrrhotite grains and pyrrhotite - pentlandite aggregates varies from < 0.01 mm up to about 1 mm. In plane polarized reflected light, pyrrhotite has light yellow color with brownish-pink hue. Compared to pyrite, the color of pyrrhotite is more washy. Pyrrhotite grains show low birefringence, often observed only along grain edges. The mineral is strongly anisotropic. All pyrrhotite grains in the studied thin-sections show moderately high surface relief. No twinnings were observed in pyrrhotite grains. Separate crystals of pyrrhotite were rarely observed, more often pyrrhotite is observed intergrown with pentlandite (Fig. 4.2 a, b). Most pyrrhotite grains are anhedral and they are split by multidirectional cracks, due to this fragmentation it is hard to say anything about the initial grain shape, although some grains are clearly idiomorphic. Pyrrhotite occurs together with pentlandite, chalcopyrite, sphalerite, and occasionally galena and pyrite. Pyrrhotite also commonly occurs together with magnetite and ilmenite. The modal abundance of pyrrhotite is approximately half of that for magnetite.

Pyrrhotite grains commonly contain inclusions of other sulfides, such as chalcopyrite and pentlandite. According to Ramdor (1962), pyrrhotite may contain some dissolved $CuFeS_2$ at high temperatures, which will segregate as chalcopyrite or cubanite during solid solution decay. In this case, the structure does not look like a result of decay, but more like mechanical inclusions of chalcopyrite in the pyrrhotite grain. They are confined to the edges of the grains and to cracks and fractures in pyrrhotite crystals.

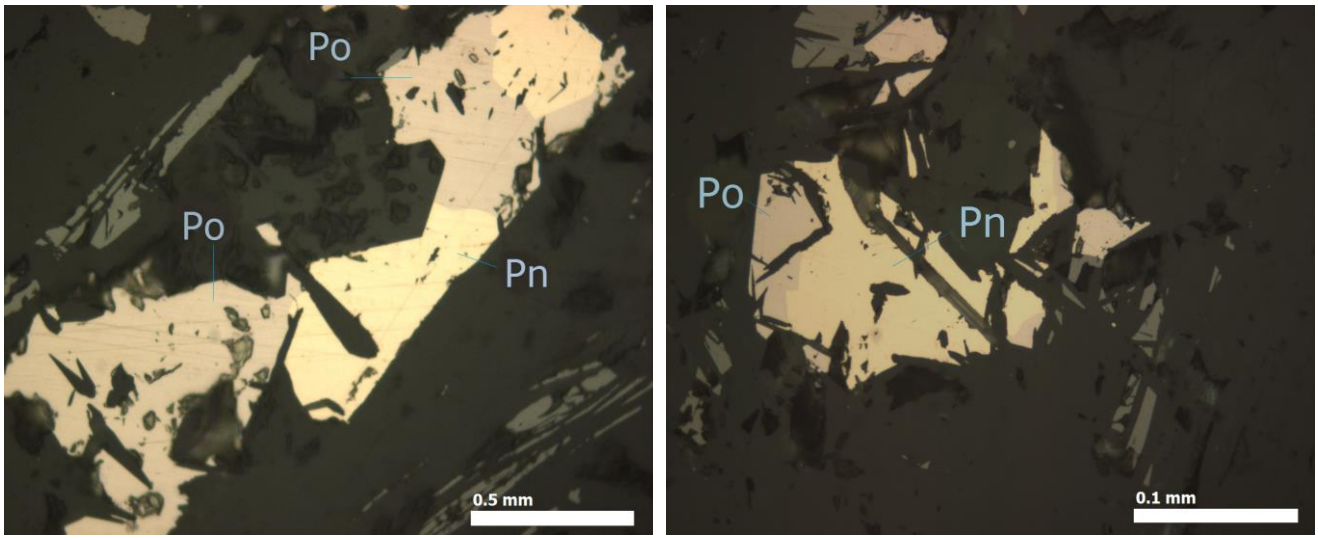


***(a)*** ***(b)***

***Figure 4.2.*** *(a), (b) Intergrowths of pyrrhotite and pentlandite.*

***Pentlandite***

As well as pyrrhotite, pentlandite was found in all of the studied the thin-sections. It forms grains ranging in size from < 0.01 mm up to several mm, in general exceeding the size of pyrrhotite grains. Pentlandite shows a light creamy-brown color in reflected light. Pentlandite is isotropic and has moderate relief. The mineral forms its own separate crystals as well as intergrowths with pyrrhotite, ilmenite and magnetite. Grains of pentlandite do not contain any products of solid solution decay or inclusions of other minerals. It frequently can be observed in mineral assemblages with chalcopyrite, pyrrhotite sometimes also with sphalerite and galena (Fig 4.3). As pentlandite usually forms later than pyrrhotite (Ramdor 1962; Kullerud 1963) it occurs as segregations, which are internally deformed. Subidiomorphic grains are observed very seldom.

***Violarite***

Violarite has been observed in close association with pentlandite and pyrrhotite, being a product of supergene alteration of these two minerals. In reflected light it is obviously different from pentlandite. Violarite has more intense color, while pentlandite

color is brighter. Violarite is isotropic. In the studied samples, the mineral has been observed in the association with pentlandite, pyrrhotite, chalcopyrite and magnetite (Fig 4.4). Furthermore, violatite can also be observed in association with millerite.

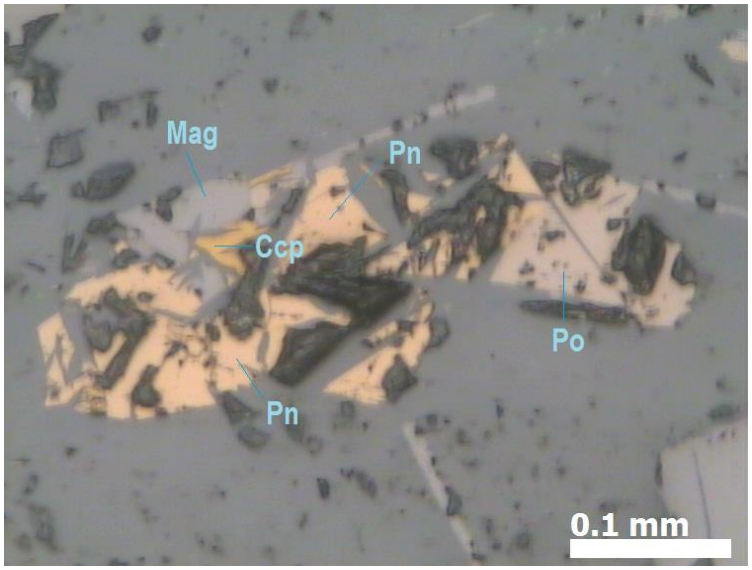


***Figure 4.3.*** *Typical mineral assemblage observed in thin-sections: pentlandite-pyrrhotite-chalcopyrite-magnetite.*

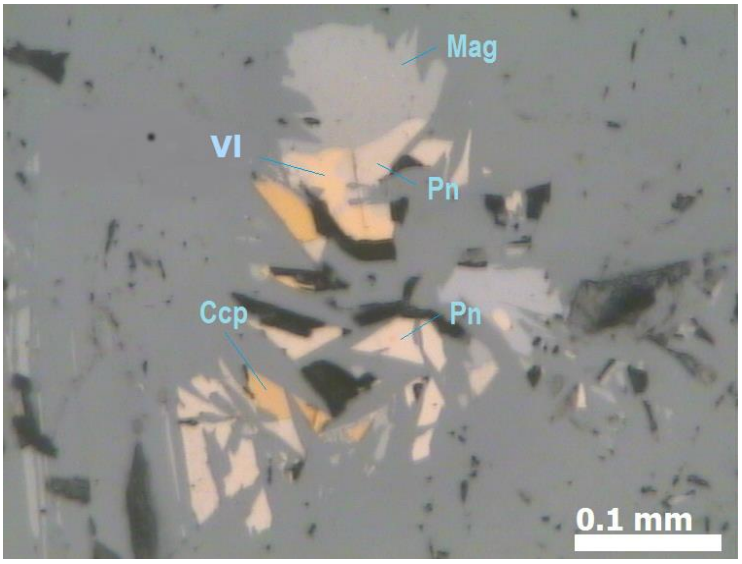


***Figure 4.4.*** *Mineral assemblage pentlandite – violarite – chalcopyrite-magnetite.*

***Millerite***

Millerite has been observed in three samples. It occurs in granular aggregates, up to 0.4-0.5 mm in diameter, as 0.01-0.02 mm long acicular crystals, and also as elongated crystals that commonly are highly deformed. In reflected light, millerite has bright, light yellow color and is quite similar to chalcopyrite. The mineral has very low birefringenceand moderate relief, and it is strongly anisotropic. Millerite grains do not show twinning or optical zoning. Millerite occurs together with pentlandite, most likely being a product of its decomposition (Fig. 4.5). Violarite has been observed together with millerite (Fig. 4.6), suggesting that these two minerals reflect a late low-temperature stage of ore mineral formation for the studied rock.

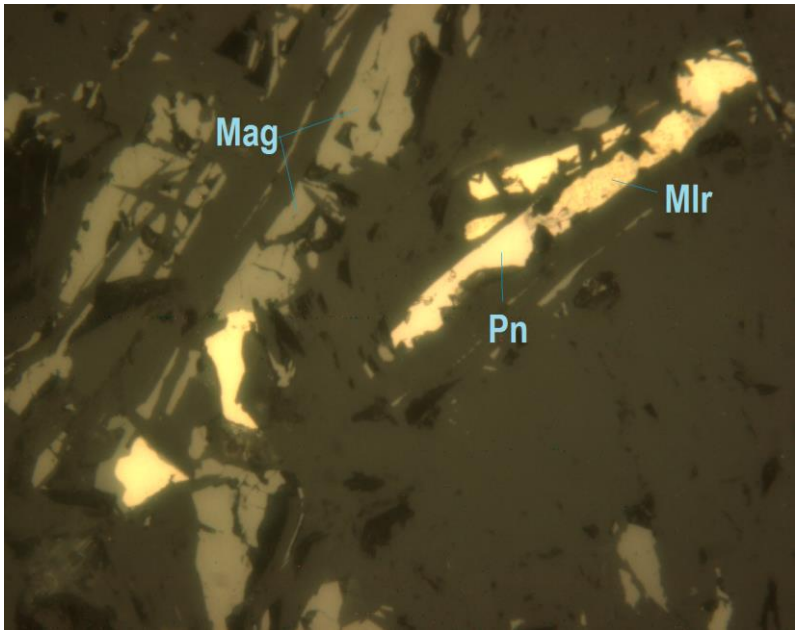


***Figure 4.5.*** *Elongated grain of pentlandite partly replaced by millerite.*

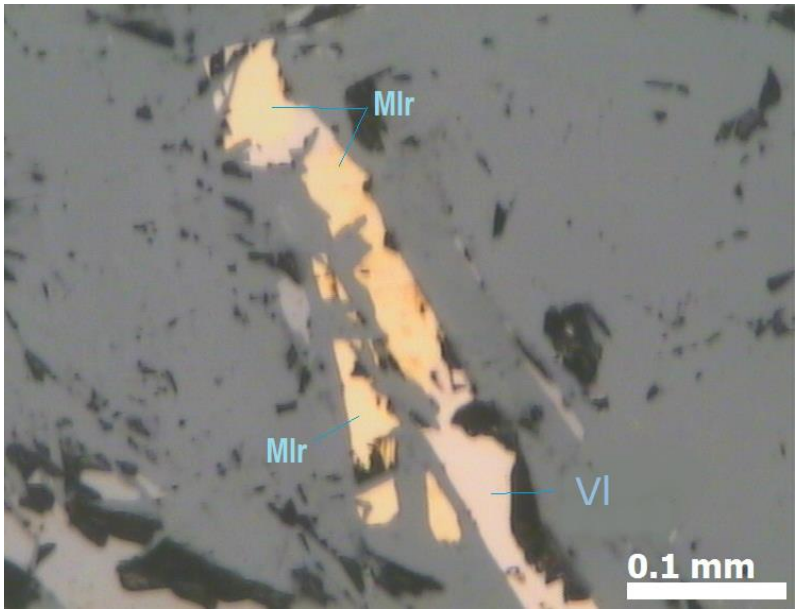


***Figure 4.6.*** *Millerite with violarite. The minerals most likely represent pseudomorph after pentlandite.*

***Chalcopyrite***

Chalcopyrite grains were observed almost in all thin-sections. In the studied samples,the size of the chalcopyrite grains does not exceed 0.3 mm. The color of the mineral in reflected light is bright, intensive yellow. The mineral shows no or very low birefringence. All grains of chalcopyrite are very weakly anisotropic. Anisotropy is more significantly manifested in those grains whose birefringence is notable. Grains of chalcopyrite very often show twinning. In reflected light, the mineral occurs as separate individual grains or aggregates of grains, as well as in intergrowths with pyrrhotite and as inclusions in pentlandite (Fig. 4.7). The shape of isolated grains is irregular, with jagged edges. Isometric crystals are rarely observed.

***Sphalerite***

Sphalerite was observed in less than half of the studied thin-sections. The grain size of sphalerite is commonly about 0.01 mm. In reflected light, the color of sphalerite

is dark-grey, sometimes with a bluish tint. It is isotropic with moderate relief. Some sphalerite grains show internal reflections from intensive red color to brown or very dark brown. Twinning is very common.The mineral appears as fine-grained aggregates or in association with pentlandite, pyrrhotite, pyrite, chalcopyrite and sometimes with magnetite (Fig. 4.8). Furthermore, it occurs as inclusions, sometimes together with galena, in pyrite grains. The grain shape is usually isometric. Very small (< 0.001) stilliform chalcopyrite grains can be observed in sphalerite ("Chalcopyrite disease" Ramdor, 1962).

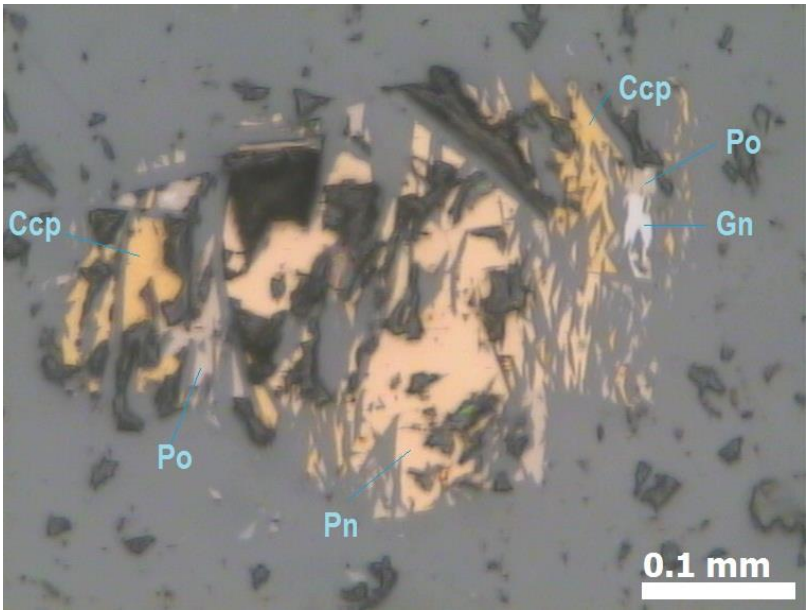


***Figure 4.7.*** *Intergrowths of pentlandite with pyrrhotite and chalcopyrite. Galena is present as a small euhedral grain, whose relation with pyrrhotite is not very clear.*

***Galena***

Only a few grains of galena have been observed. The grain size is less than 0.003 mm. In reflected, light galena is white and very bright. Scratches and other irregularities are common on crystal surfaces due to the low hardness of the mineral. Low relief, especially notable in the studied samples, where galena is observed in mineral assemblages together with minerals with high relief (e.g. magnetite). Most often galena

is present as small inclusions in pyrite, together with inclusions of sphalerite. In one single case, galena was observed as a part of the matrix mineral assemblage (Fig. 4.8). Relationships between galena and other sulfides are not very clear because of the very small grain sizes.

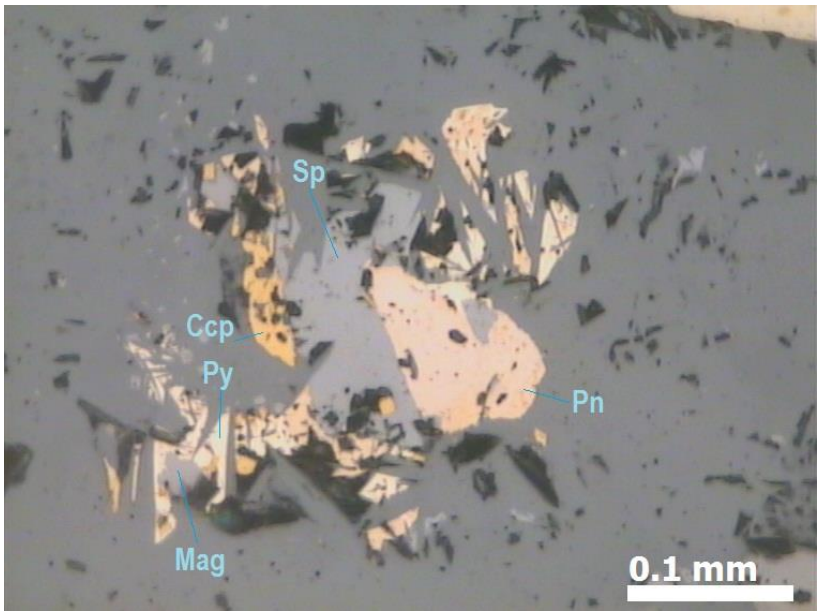


***Figure 4.8.*** *Multiple mineral assemblage chalcopyrite – pyrite – pentlandite – magnetite – sphalerite.*

***Pyrite***

Pyrite was observed in almost all of the studied thin-sections. The modal content of pyrite is approximately half of that of pyrrhotite. Sometimes it forms rather big grains up to 2-3 mm, but grain sizes of < 0.5 mm is more common. The mineral shows a pale yellow color in reflected light; compared to chalcopyrite it is less bright and less intensive. All pyrite grains in the studied thin-sections are isotropic. The relief is hard to describe, since most part of the grain show different relief in different directions during rotation of the stage of the microscope. These grains often show inhomogeneous internal structures, characterized by the presence of a large number of pores and cavities, and inclusions of other minerals such as sphalerite and galena. The grain shape is often

idiomorphic, but the crystals are mostly fractured. Some fractured grains are partly replaced by iron hydroxides along cracks. Anyhow, replacement of pyrite by Fe-hydroxides is rarely observed. It seems, that two generations of pyrite are present in studied samples. The earliest generation shows fractured crystals, partially replaced by Fe-hydroxides along cracks (Fig. 4.9). The grain size of this generation does not exceed 1 mm. Crystals of the later generation is larger, their size sometimes come up to 3 mm. They do not show any evidence of deformation, but they have a lot of early minerals as inclusions, entrapped during the growth (Fig. 4.10).

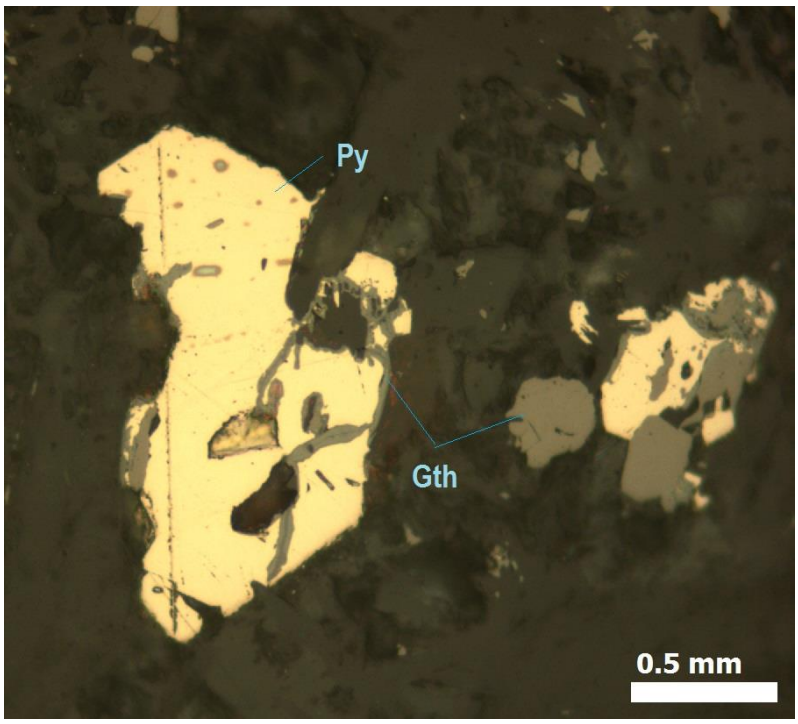


***Figure 4.9.*** *Pyrite grains of the early generation with Fe-hydroxides formed along cracks. Gth – goethite.*

Figure 4.11 shows relationships between different mineral phases from the ultramafic rock from the Kvaløya Island.

The high modal content of pentlandite compared to pyrrhotite and pyrite (Pn/Po ≈ 1.4) propose sulfur undersaturation during sulfide formation.

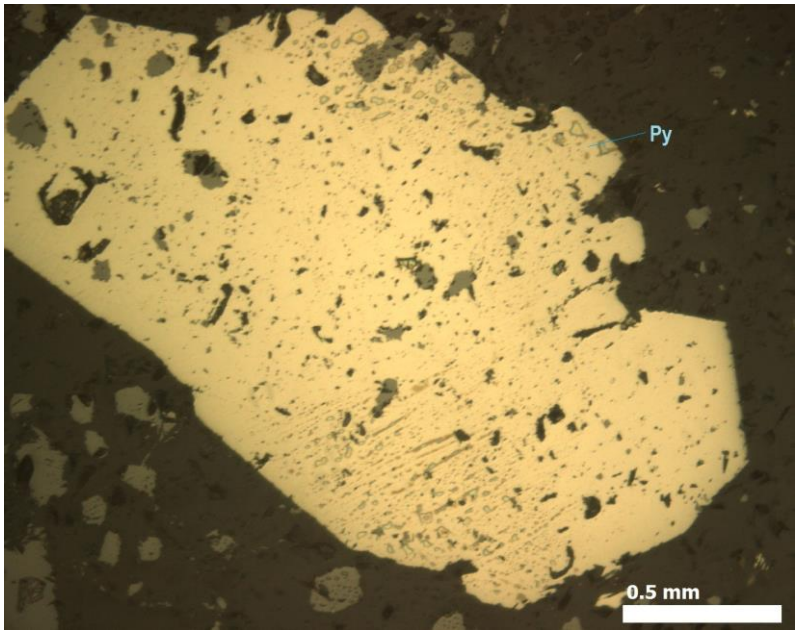


***Figure 4.10.*** *Grain of pyrite of the second generation with numerous inclusions of early sphalerite and with abundance of pores.*

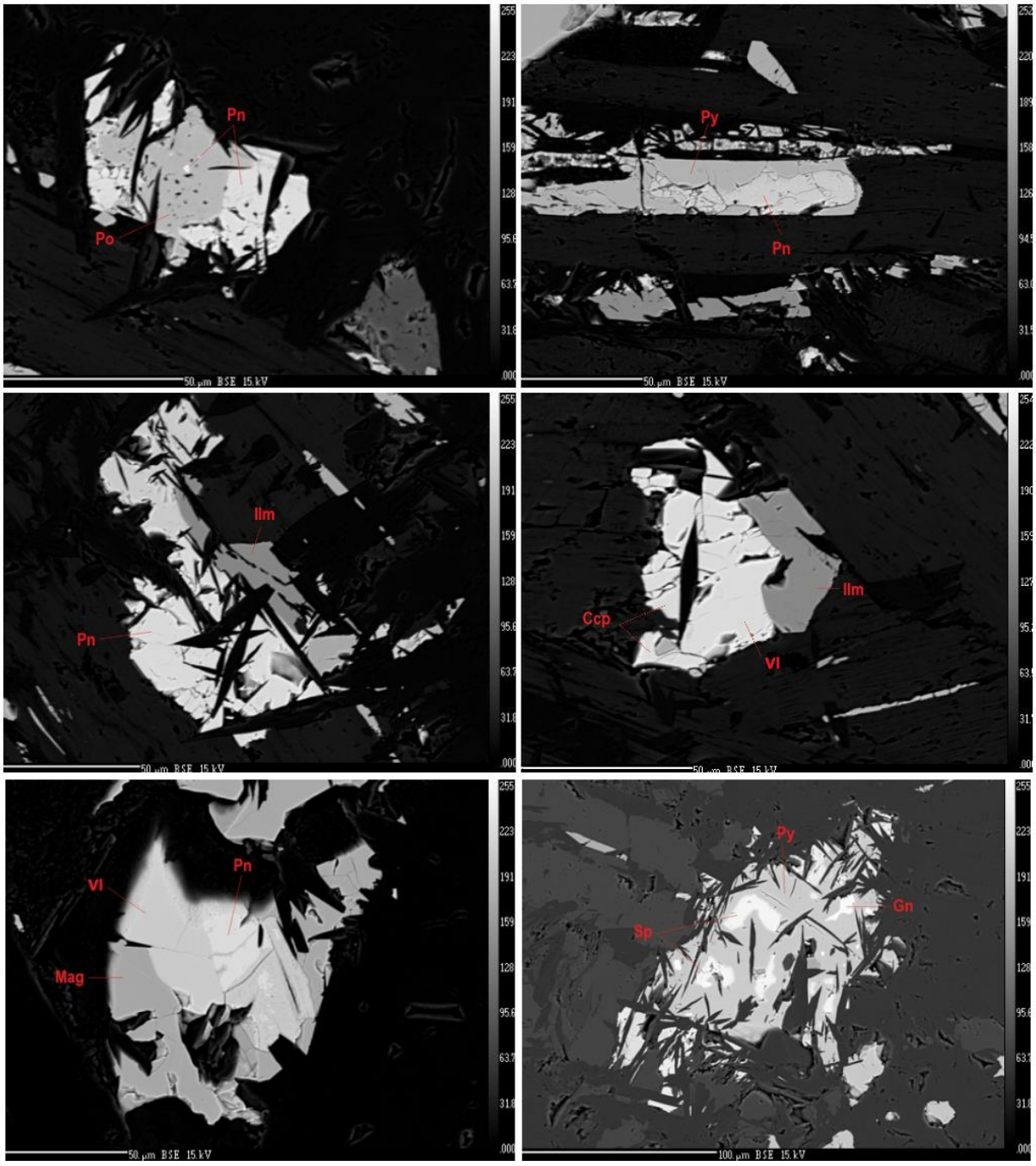


***Figure 4.11.*** *Back-scattered electron microprobe images of minerals and their relationships observed in the studied ultramafic rock. (a) Inclusion of pentlandite in pyrrhotite grain intergrown with pentlandite. (b) Pyrite overgrowing pentlandite grain. (c) Intergrowth of ilmenite with pentlandite. (d) The mineral assemblage ilmenite – chalcopyrite – violarite (e) Substitution of pentlandite by violarite. Relicts of pentlandite and substitution texture can be clearly observed from back scattered image. (f) Pyrite replacing sphalerite.*

## Chapter 5. Geochemistry

*Analytical procedure.*

Whole rock major oxides and trace element analyses for 40 samples were carried out by the author using fused and pressed pellets on a Bruker S8 TIGER XRF at the Department of Geology, University of Tromsø. For analysis of major elements, the powder was mixed together with Li-tetraborate ($Li_2B_4O_7$) in the ratio of 1:7 (0.6 g of rock powder and 4.2 g of Li-tetraborate). Then, the mixture was melted during approximately 6 minutes in a platinum pot at temperatures around 1200 $^0$C. Finally, the hot melt was cooled down in platinum molds. For trace element analysis the first stage of the analytical procedure was weighing up 9.0 g of rock powder and mixing it with 9 wax pills (POLYSIUS PORLAB® Mahlhilfe) in a mortar. After mixing, the final step was to place the sample material in a cylinder shaped container where it was pressed with a piston to a pill.

For other samples (Appendix I), analyses were performed at Activation Laboratories LTD, Ontario, Canada after Code 4LITHO (11+) Major Elements Fusion ICP (WRA) /Trace Elements Fusion ICP/MS (WRA4B2). Lithium metaborate/tetraborate fusion ICP Whole Rock Package and a trace element ICP/MS package were combined for the scope of the elements of our interest with appropriate detection limits. The fused samples are diluted and analyzed on a Perkin Elmer Sciex ELAN 6000, 6100 or 9000 ICP/MS. Three blanks and five controls (three before sample group and two after) are analyzed per group of samples. Duplicates are fused and analyzed for every 15 samples. The instrument is recalibrated for every 40 samples.

Six samples were analyzed at the Activation Laboratories LTD. Ontario, Canada after the method REE and Au 1C - Exp 2 - Fire Assay -Au, Pd, Pt- ICP/MS. Sample size of 30 grams was used. Samples are mixed with fire assay fluxes (borax, soda ash, silica, litharge) and with Ag added as a collector. The mixture is placed in a fire clay crucible, the mixture is preheated at 850°C, intermediate 950°C and finish 1060° C, the entire

fusion process last 60 minutes. After cooling, the lead button is separated from the slag and cupelled at 950°C to recover the Ag (doré bead) + Au, Pt, Pd.

The Ag doré bead is digested in hot (95° C) $HNO_3$+ HCl. After cooling for 2 hours the sample solution is analyzed for Au, Pt and Pd on a Perkin Elmer Sciex ELAN 6000, 6100 or 9000 ICP/MS. A blank and a digested standard are run every 15 samples. The instrument is recalibrated for every 45 samples. Duplicates are run when sample duplicates are received by the ICP/MS department.

*Results.*

The major oxide contents (see Appendix I) show that the studied rock belongs to the high magnesium (20-33 wt % of MgO) ultrabasic and basic (38-48 wt % $SiO_2$) rock classes. The $Al_2O_3$ and CaO contents of the rock vary significantly from 1.72 wt % to 5.68 wt % and from 0.2 wt % to 9.98 wt % respectively.

The content of $Fe_2O_3^{total}$ is relatively constant for the studied samples showing variations from 11 wt % to 15 wt %. The content of alkalis ($Na_2O$ and $K_2O$) in the rock is usually negligible, with $K_2O$ often below the detection limit, which is 0.01 wt %. The $P_2O_5$ and MnO contents of the rock are always less than 1 wt %.

The $TiO_2$ content is relatively constant at 0.5 wt %, sometimes exceeding 1 wt %. This increase does not seem to have any obvious correlation with the contents of other oxides, but it normally occurs for samples with $SiO_2$ content higher than 40 wt %.

Figure 5.1 shows that the compositional data from all samples form continuous trends on Harkers binary diagrams allowing to conclude that all lenses belong to the same suite, most likely reflecting different fractionation degrees. All major oxides, except $Fe_2O_3^{total}$ show negative correlation with the MgO content of the rock. In case of $Fe_2O_3$ it is difficult to see any correlation, because the data are scattered in the plot $Fe_2O_3$ versus MgO (Fig. 5.1).

The $CaO/Al_2O_3$ ratio of the rock varies significantly from 0.11 to 2.06. $Na_2O+K_2O$ is always < 1. The rock shows exceptionally high $Al_2O_3/TiO_2$ ratios ranging from 4.5 to 19.0.

For some bivariate Harker diagrams for REE and HFSE (Fig. 5.2), the compositional data for all elements form continuous trends, similar to those for major oxides. All elements shown in Fig. 5.2 are negatively correlated with MgO.

The compositional data for elements like Cu, Cr, Co and U are scattered and do not show any correlation to MgO (Fig. 5.3). Ni and Zn show positive correlations with MgO (Fig. 5.3). V and Th show negative correlations with MgO, although for Th the correlation is weakly manifested. The Th and U content of the rock is usually below 1 ppm, sometimes the content of U exceed this value. The Cu and Co contents of the rock vary from below detection limit to 180 ppm for Cu, and from 70 ppm to 135 ppm for Co. The Zn content is similar to that of Co. The V content of the rock varies between 55 ppm and 178 ppm. Elements like Ni and Cr have highest concentrations in the rock relative to other trace elements with Ni varying between 700 ppm to almost 2500 ppm and Cr content from 1000 ppm to more than 4000 ppm.

For five chosen samples PGE were analyzed (Appendix xx). Samples for PGE analyses were chosen based on the contents of elements like Ni, Co, and Cu. The maximum concentration of Au for the analyzed samples is 5 ppb; the lowest is below detection limit, which is 1 ppb. For Pt and Pd, the highest contents were recorded as 11 ppb and 11.3 ppb, respectively (sample AP – 038). The lowest content for Pt is 1 ppb and for Pd is 0.7 ppb. However, according to unpublished data of Gedeminas Motuza (personal communication to Kåre Kullerud, 2011), an average content of 122 ppb Pd was recorded for 15 samples of the same rock with up to 308 ppb in some samples.

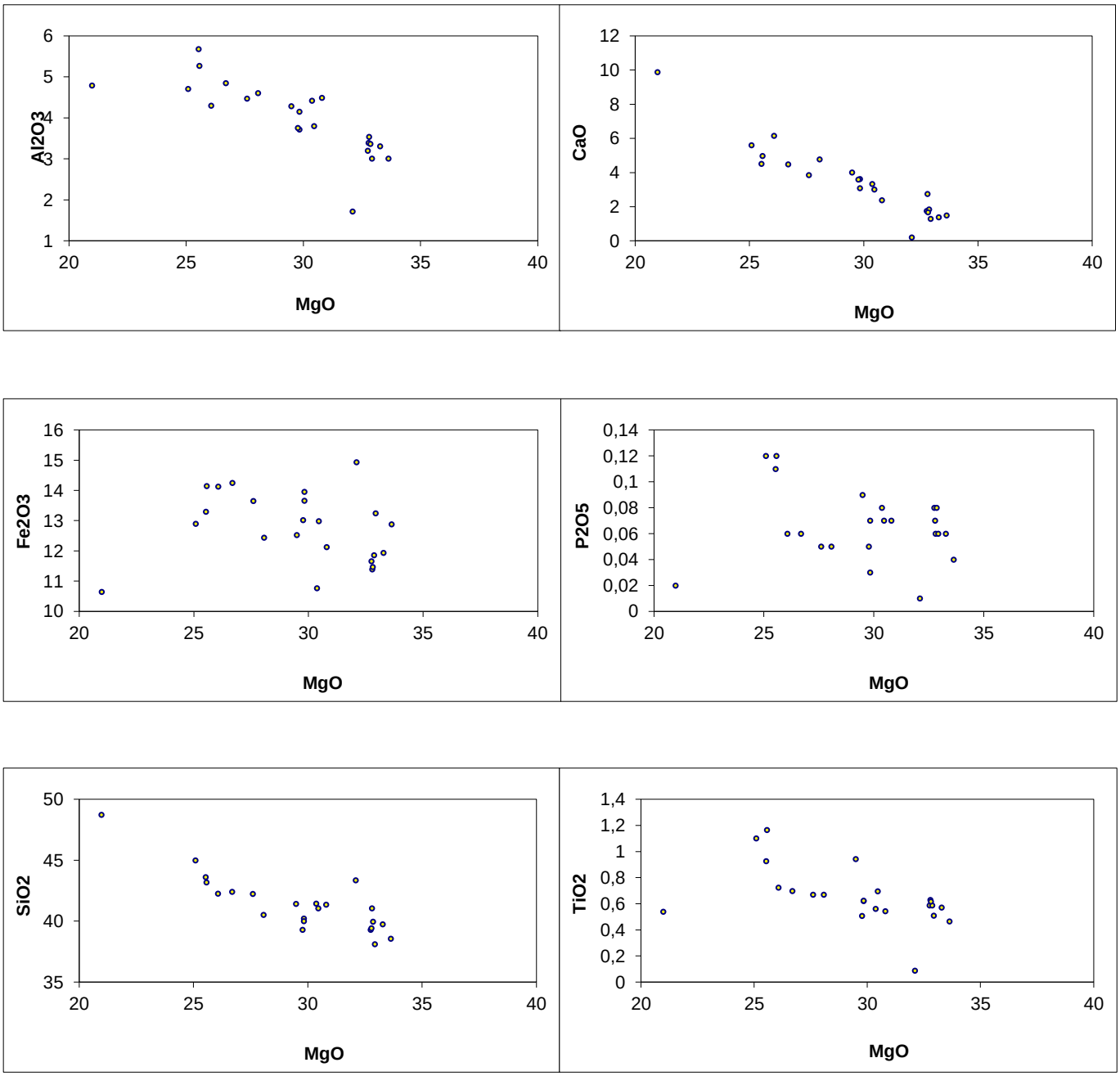


***Figure 5.1.*** *Bivariate plots showing major oxides vs. MgO for the ultramafic rock from the Kvaløya Island. The major oxide contents are presented in wt.%.*

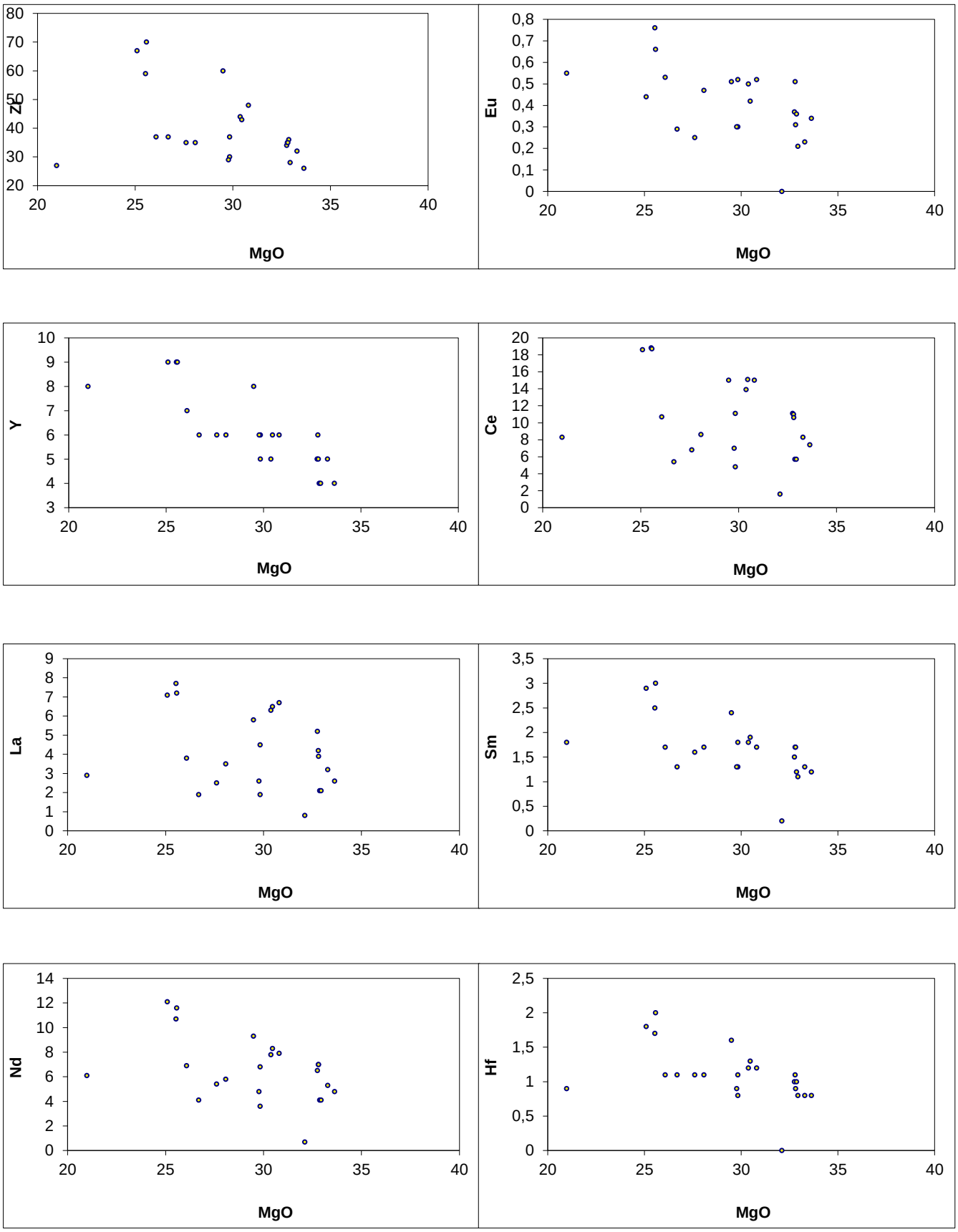


***Figure 5.2.*** *Bivariate plots showing REE and HFSE vs. MgO for the ultramafic rock from the Kvaløya Island. The concentrations of all elements are given in ppm.*

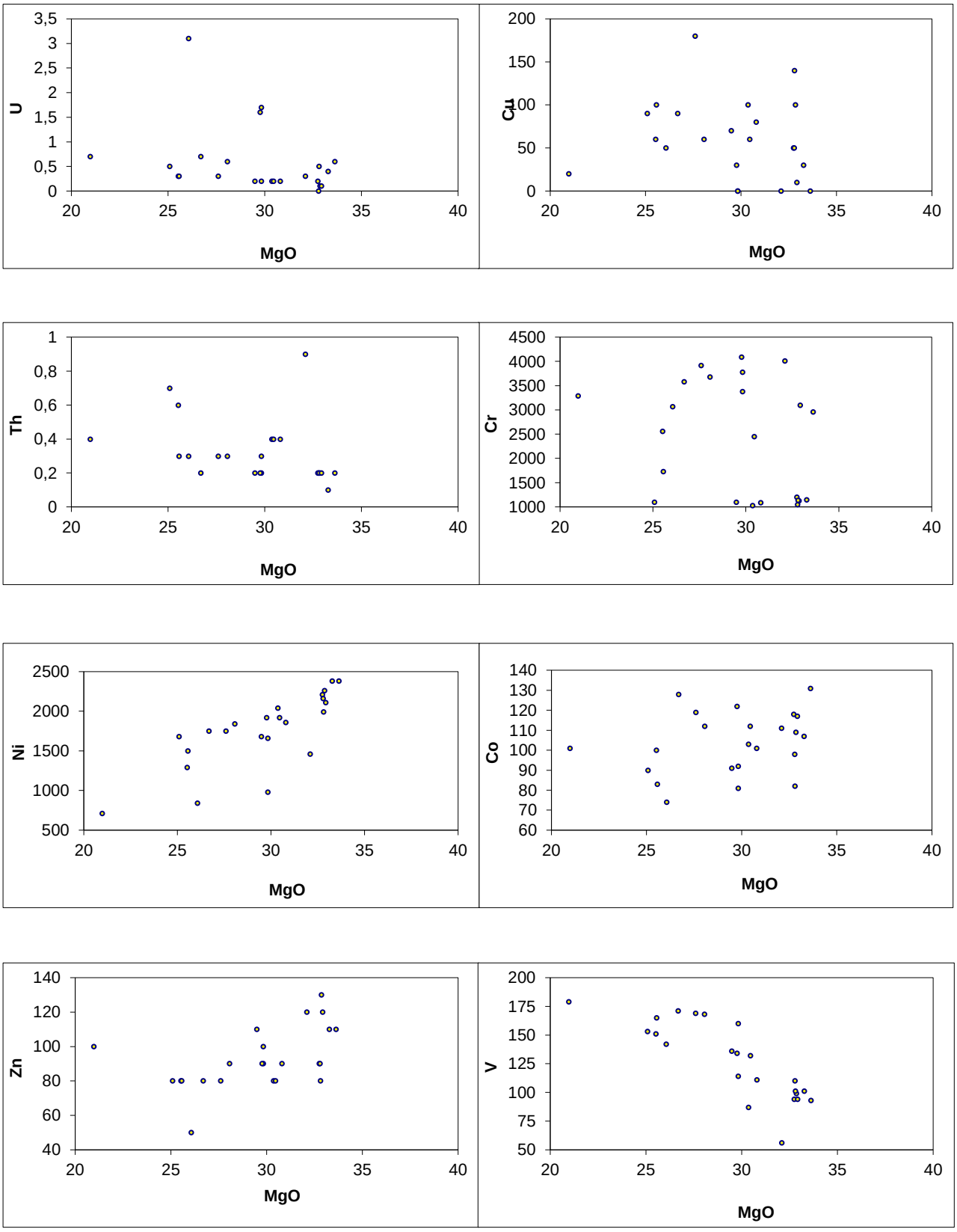


***Figure 5.3.*** *Bivariate plots showing trace elements vs. MgO for the ultramafic rock from the Kvaløya Island. The concentrations of all elements are given in ppm.*

REE patterns (chondrite normalized) show that the rock is depleted in HREE relative to LREE and extremely depleted in Y (Fig. 5.4). Except from for Eu, the REE patterns are similar for all samples. The REE patterns were divided in two groups based on the significance of Eu-anomalies in order to simplify the interpretation of the data (Fig. 5.4).

The REE patterns of the studied rock are similar to patterns of ultramafics (Aitken & Echeverria, 1984; Nesbitt, et al., 1979; Xie et al., 1995). The REE patterns are distinguished from the patterns from komatiites by a significantly stronger depletion in HREE, however, the Barberton komatiites show less significant depletion in HREE (Nesbitt, et. al., 1979). Komatiites from Gorgona are depleted in LREE (Aitken & Echeverria, 1984).

The Y and La content vary from 4 ppm to 9 ppm and from 1 ppm to 8 ppm respectively. The Nd content varies between 0.3 ppm to 12 ppm. The content of Hf is relatively constant varying from 0.8 ppm to 2 ppm. The concentration of Sm in the rock varies from 0.2 ppm to 3 ppm. Ce shows significant variations from 0.2 ppm to 20 ppm. The content of Eu is always below 1 ppm. Zr varies from 25 ppm to 70 ppm.

The rock shows Zr/Sm ratios in the range 20.5-30, and Hf/Sm ratios in the range 0.5-0.84, which is similar to the primitive mantle ratios of Zr/Sm = 25 and Hf/Sm = 0.69. (Xie et al., 1995). The Ce/Yb ratios vary from 9 to 27.8.

Total REE content of the samples varies significantly from 4.1 ppm to 60 ppm.

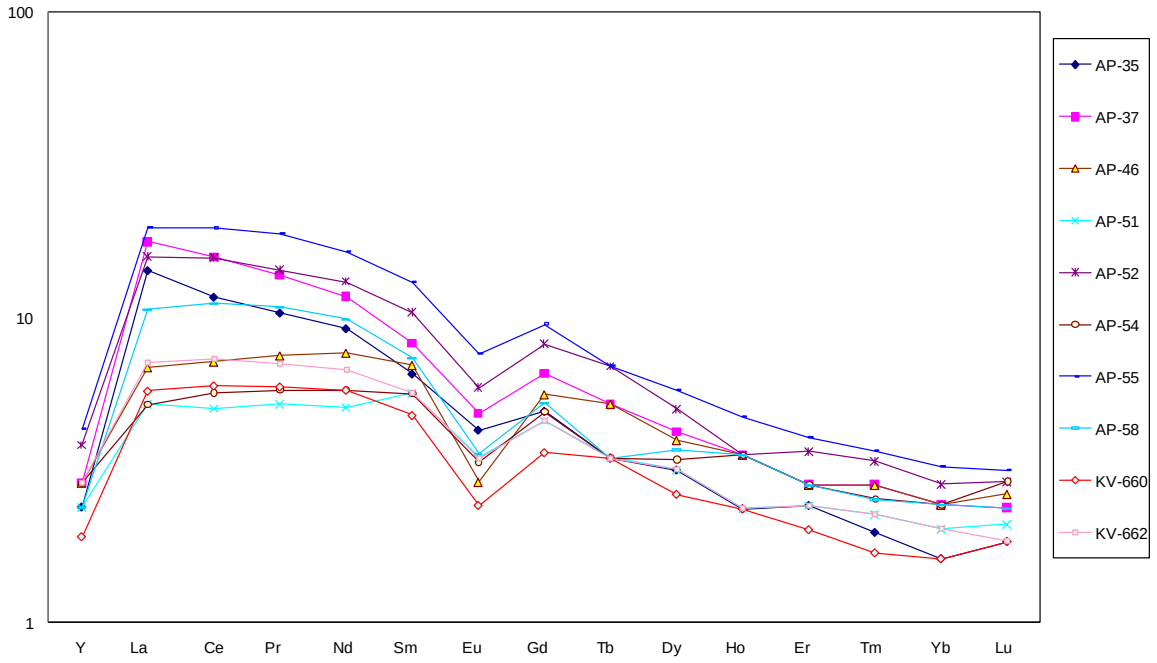


(a)

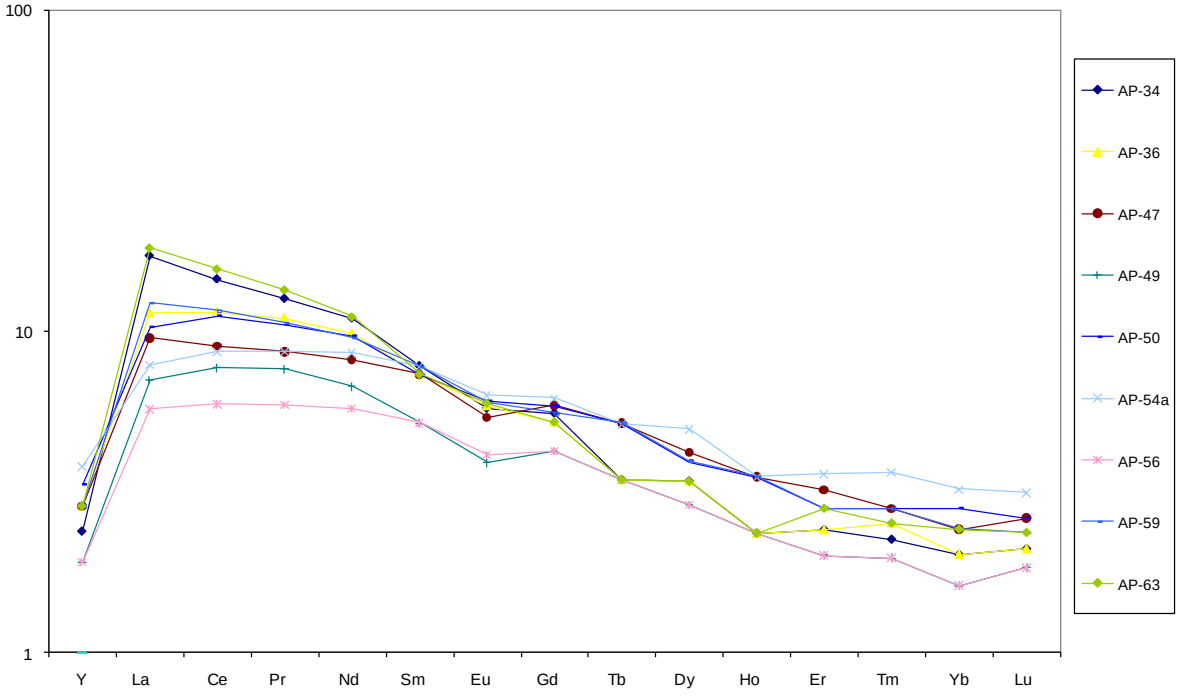


(b)

***Figure 5.4.*** *REE patterns for the ultramafic rock from Kvaløya Island normalized to chondrite after Boynton (1984). (a) for samples with relatively significantly manifested Eu-anomaly; (b) for samples with negligible Eu-anomaly.*

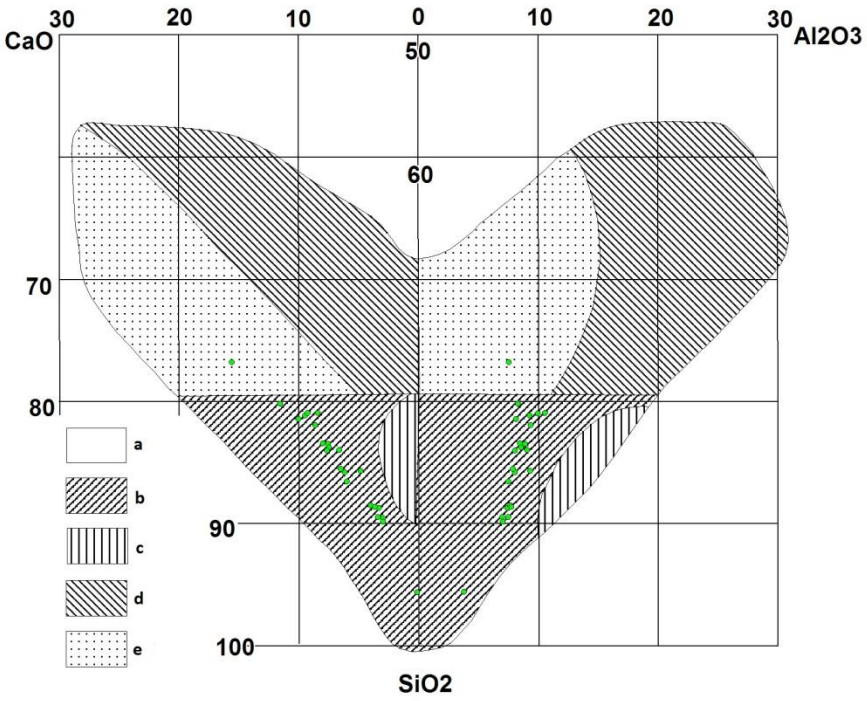


***Figure 5.5.*** *Diagram $CaO$-$Al_2O_3$-$SiO_2$ for ascertainment of the primary origin of metamorphic rocks. a – sedimentary rocks field, b – e – magmatic rocks fields; b – ultramafic rocks field, c – felsic rocks field, d – field of mafic, intermediate and alkaline rocks, e – field of uncertainty. After Domoracky (1964).*

As it was mentioned in chapter 2, the high-Mg rock from Kvaløya Island does not show any primary textures. In order to ascertain the primary origin of the rock, the compositional data of the analysed samples were plotted in the $CaO$-$Al_2O_3$-$SiO_2$ diagram (Fig.5.5) after Domoracky (1964). It is assumed that $SiO_2$, $Al_2O_3$ and $CaO$ were immobile during metamorphism. Although the stability of $CaO$ during metamorphism is controversial, the fields on the diagram were designed based on a large amount of analyses of metamorphic rocks, which origin was certainly known. For plotting in the diagram, the sum $CaO$-$Al_2O_3$-$SiO_2$ is normalized to 100%. The diagram shows that all data from studied samples plot within the fields of ultramafic rocks.

In order to discriminate between ultramafic rock types, a diagram for high-Mg rocks was used (Fig. 5.6). From the diagram we can see that the compositional data of samples of the rock from Kvaløya plot in the field of meimechites and komatiites. Taking into account the low $TiO_2$ content of the rock (usually less than 1 wt %), the studied rock is most similar to komatiites.

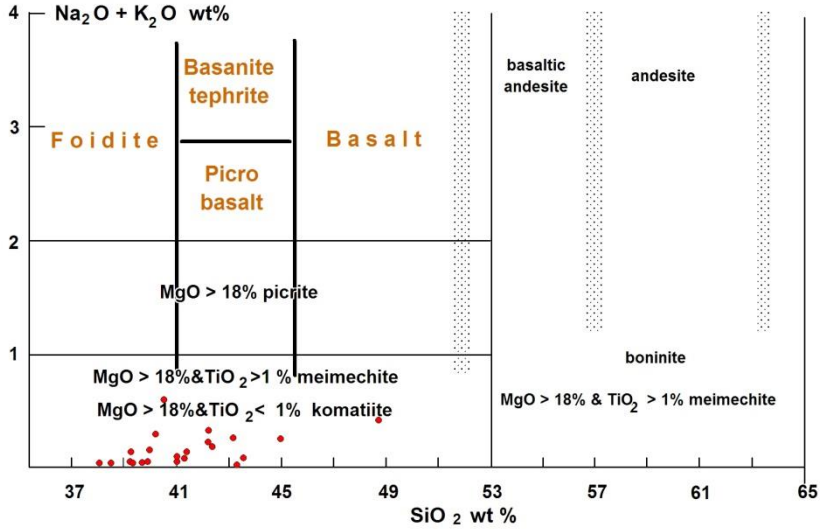


***Figure 5.6.*** *Discrimination diagram $SiO_2$ vs $Na_2O+K_2O$ for high-Mg ultramafic, mafic and intermediate rock classes. After Le Bas and Streckeisen (1991).*

In figure 5.7 $Fe_2O_3$+$TiO_2$-$Al_2O_3$-MgO discrimination diagram for mafic-ultramafic volcanic rocks was used. The compositional data of the ultramafic rock from Kvaløya cluster along the boundary between the fields representing komatiites and komatiitic basalts in the ternary diagram in Fig. 5.7, with the majority of samples within the komatiite field. The samples that plot in the komatiitic basalt field are those with elevated concentrations of $TiO_2$ relative to other samples (> 0.8 wt %).

The studied rock has further been compared with other komatiites and komatiitic rocks of different age that are well studied from other parts of the world, e.g. the Barberton komatiites, the Munro komatiites and the Gorgona komatiites (Fig. 5.8). In the $TiO_2$ vs. MgO diagram (Fig. 5.8) the compositional data of the samples from the Kvaløya ultramafic rock form a trend similar to those of the other komatiites, but the

slope of the trend is more steep, showing a clear negative correlation between the $TiO_2$ and MgO content. In the $Al_2O_3$ vs. MgO diagram, the Kvaløya ultramafic rock shows compositional variations very close to the Barberton komatiites.

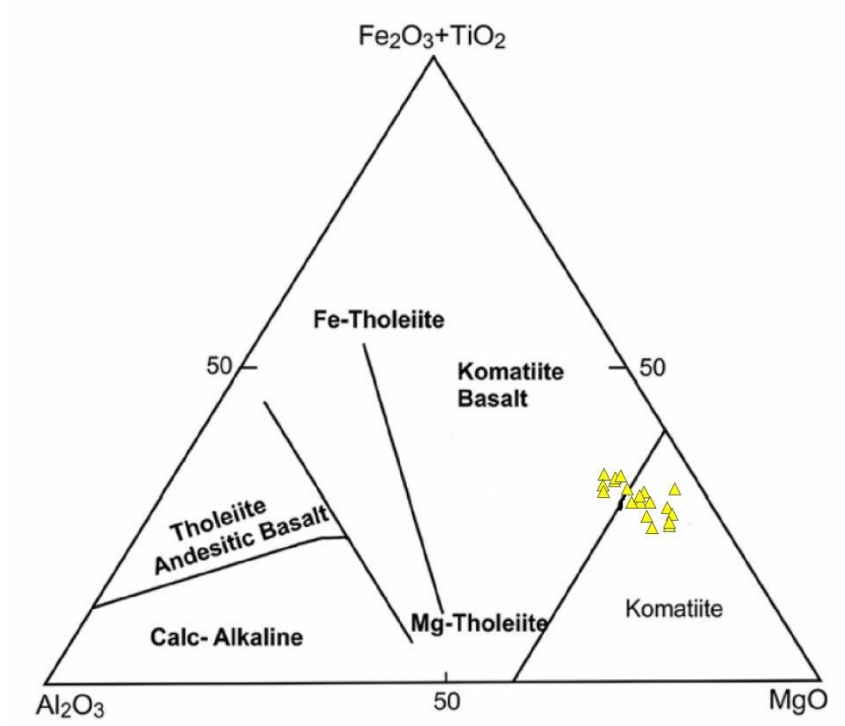


***Figure 5.7.*** *$Fe_2O_3$+$TiO_2$-$Al_2O_3$-MgO discrimination diagram for the studied ultramafic rock. Modified from Jensen (1976)*

Arndt and Lesher (2004) conclude that a MgO content of about 30 wt % is probably the maximum content for komatiites. Rocks with MgO content more than 30%, i.e. approximately half of studied samples, most likely represent olivine cumulates.

Figure 5.9 illustrates different types of komatiites based on $Al_2O_3/TiO_2$ and Gd/Yb ratios. The REE concentrations are chondrite normalized. Here we can see that the studied rock is slightly more depleted in $Al_2O_3$ than the Barberton type called Al-depleted and Ti-enriched. However, the REE ratios of the studied rock are significantly higher than that for the other types of komatiites. Gd/Yb is measure of relative HREE depletition. High Gd/Yb ratios as a function of garnet preserved in the residue melt indicate extreme depth of rock formation (Arndt and Lesher 2004).

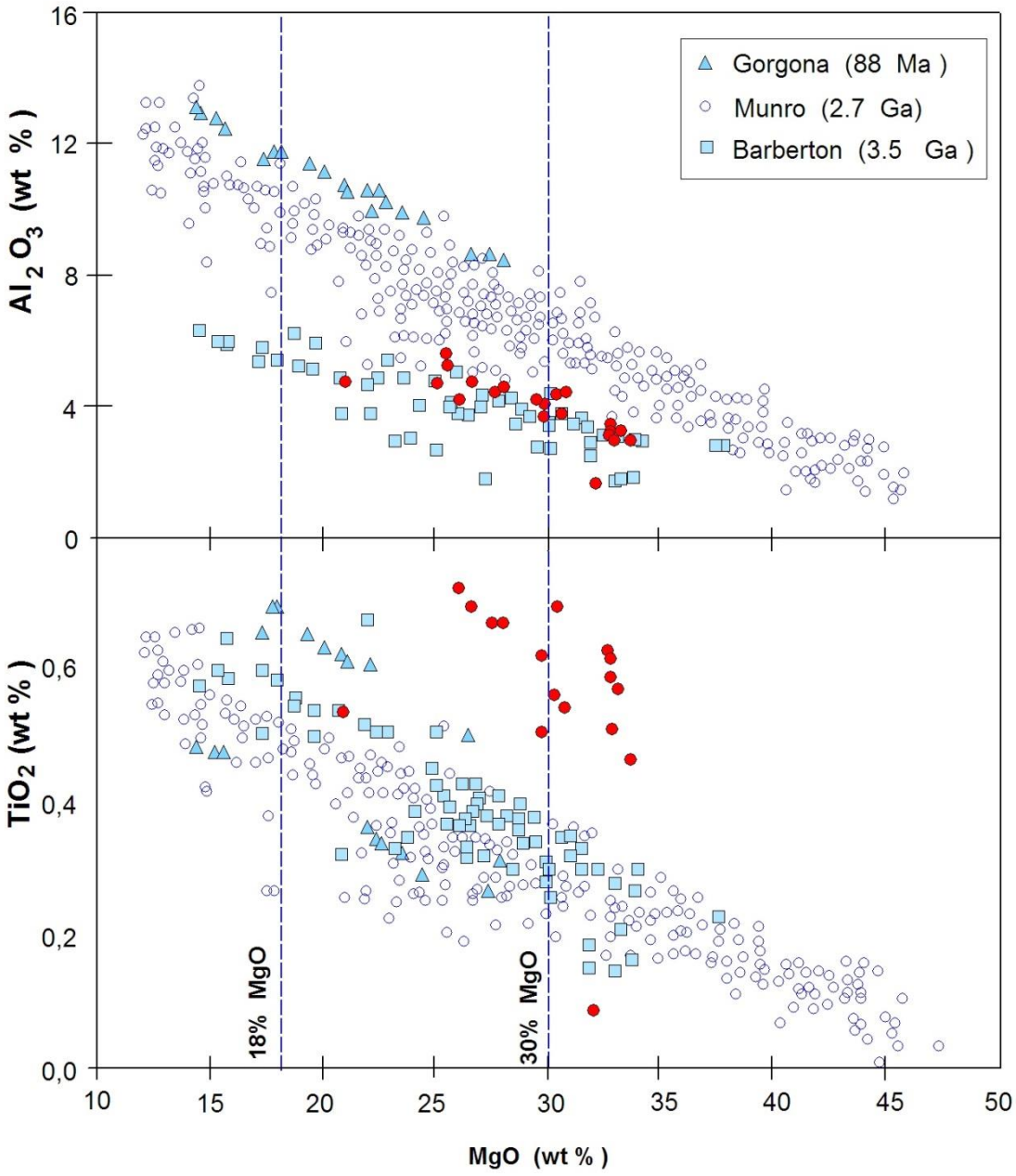


***Figure. 5.8.*** *Variation diagrams illustrating the range of compositions of the main types of komatiite. The limit at 18% MgO separates komatitic basalts from komatiites; the limit at 30% MgO indicates the probable maximum MgO content of komatiitic liquids. Compositions of the studied rock are indicated with red circles, other symbols are indicated in the diagram. After Arndt and Lesher (2004).*

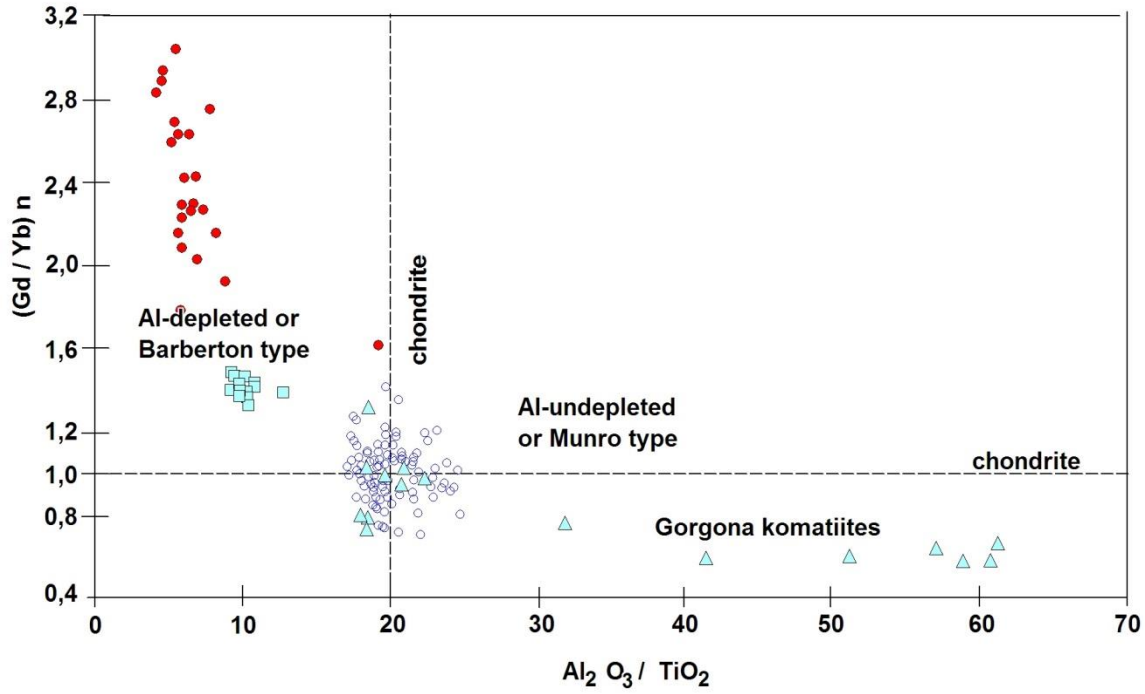


***Figure. 5.9.*** *Variation diagram $Al_2O_3/TiO_2$ vs. $(Gd/Yb)_n$, showing the compositions of the main types of komatiites. Symbols are the same as in Fig. 5.7.*

Arndt and Lesher (2004) distinguish an additional type of komatiites called Ti-enriched komatiites. This type is not indicated in fig. 5.8 and fig. 5.9, but from the $TiO_2$ vs MgO plot (Fig. 5.8), a relative enrichment in Ti of the studied rock can be observed relative to other types of komatiites. According to Arndt and Lesher (2004) these Ti-enriched komatiites occure in the Fennoscandian Shield and in Ontario.

The diagram $TiO_2$ and $SiO_2$ versus MgO including different types of komatiites and also fields of komatiitic basalts and modern mafic magmas after (Parman, 2004) is given in Fig. 5.10. The diagram shows komatiites from Barberton (South Africa, 3.5 Ga), Commondale (South Africa, 3.3 Ga), Tisdale (Canada, 2.7 Ga), Ball (Canada, 2.9 Ga), Munro (Canada, 2.7 Ga) and Gorgona (South America, 88 Ma), together with modern magmas represented by ocean island basalts and boninites. From the $TiO_2$ versus MgO plot it can be observed that the rock studied here with its high $TiO_2$ and MgO does not fit any field of komatiites; its composition is far from modern magmas as well. From the $SiO_2$ versus MgO plot in Fig. 5.10 it is obvious that studied rock is

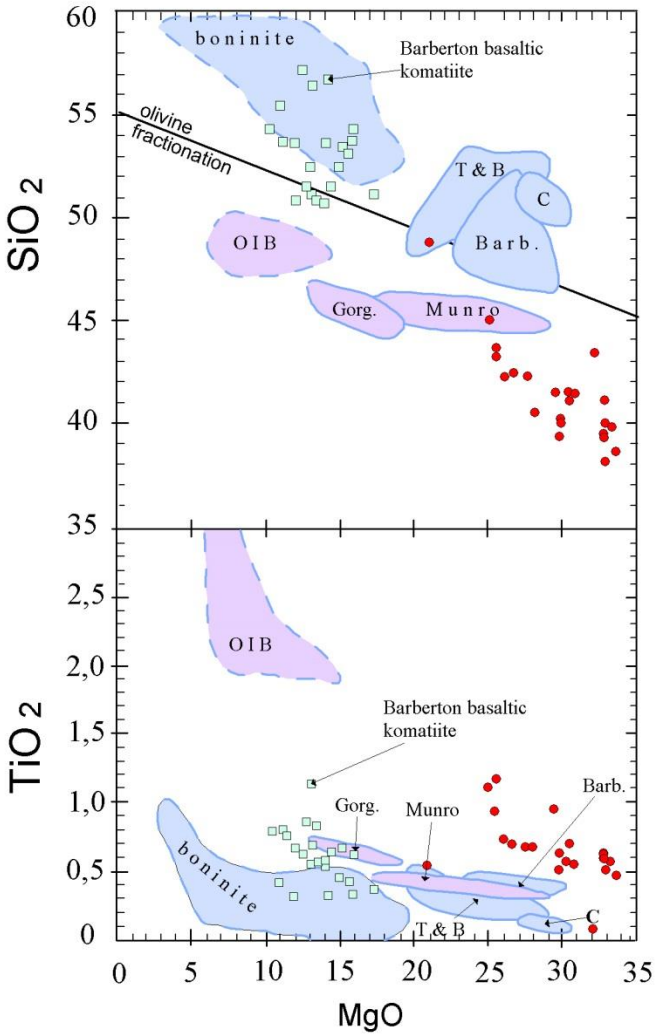


***Figure 5.10.*** *$SiO_2$ and $TiO_2$ versus MgO in komatiites (fields with solid boundaries), basaltic komatiites (green filled squares) and modern mafic magmas (ocean islands basalts and boninites). The solid line in the $SiO_2$ vs. MgO diagram (olivine fractionation) shows the compositional effect that olivine fractionation would have on the most MgO-rich Barberton komatiite. Komatiites: Barb. (Barberton, South Africa, 3.5 Ga,), C (Commondale, South Africa, 3.3 Ga), T (Tisdale, Canada, 2.7 Ga), B (Ball, Canada, 2.9 Ga), Munro (Munro, Canada, 2.7 Ga) and Gorg. (Gorgona, South America, 88 Ma). Modern magmas: OIB (ocean island basalt, GeoRoc online database http://georoc.mpch-mainz.gwdg.de/georoc/), boninites (GeoRoc online database).*

undersaturated in silica compared to the different komatiites that are shown. The compositional data of the studied rock form a trend in the diagram that suggests that the rock underwent differentiation. Only one sample of the studied rock plot in the field of Tisdale and Ball komatiites (shown in the same field). For most of the samples of the studied rock, the MgO content is higher than that for komatiites.

The diagrams after Coleman (1977) (Figs. 5.11 and 5.12) differentiate between mafic and ultramafic cumulates. Indeed, in the Al2O3–CaO–MgO diagram (Fig. 5.11), the compositional data for most of the samples of Kvaløya ultramafic rock plot in the field of ultramafic cumulates, quite far from the field of komatiites. Some samples plot outside the field of ultramafic cumulates toward the field of metamorphic peridotite.

In contrast, the diagram SiO2 vs. Fe2O3total/( Fe2O3total+MgO) (Fig. 5.12) shows that SiO2 content is not constant and exceeds that for ultramafic cumulates. As a result, the compositional data of the samples is distributed both in the field of ultramafic and mafic cumulates and in the transition zone between these fields.

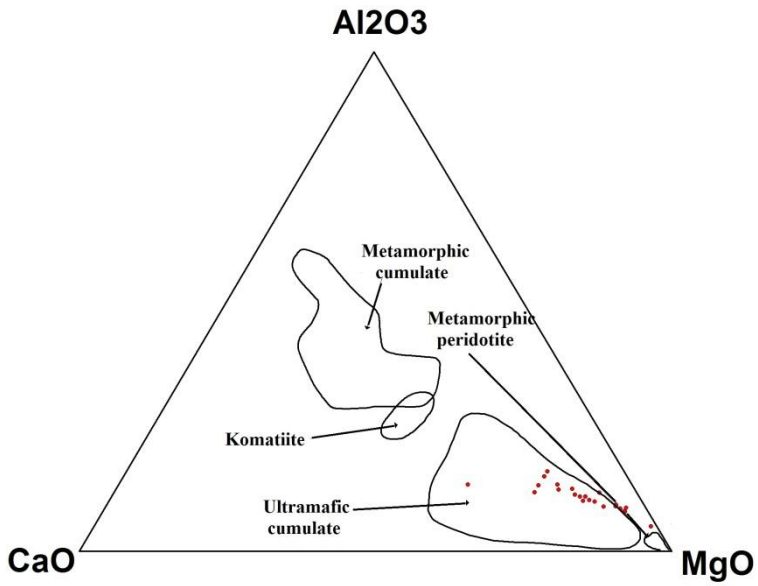


***Figure 5.11.*** *Compositional data of the samples of the ultramafic rock from the Kvaløya Island in the discrimination diagram CaO-$Al_2O_3$-MgO after Coleman (1977).*

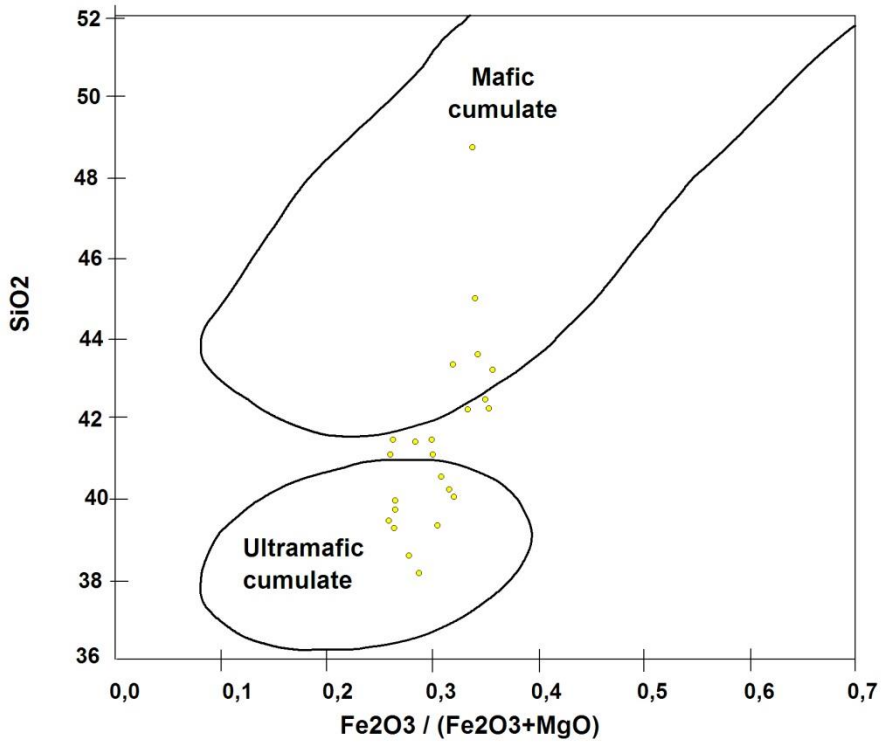


***Figure 5.12*** *Compositional data of samples of the ultramafic rock from the Kvaløya Island in the discrimination diagram* $SiO_2$ *vs.*$Fe_2O_3^{total}/(Fe_2O_3^{total} + MgO)$ *after Coleman (1977).*

## CIPW norm calculations

Since there has not been observed any primary magmatic minerals for the studied rock, CIPW normative mineralogy calculations have been carried out, in order to approach the primary mineralogy of the rock. The program used, which can be downloaded from: www.minerva.union.edu/hollochk/c_petrology/norms.htm, was written by Kurt Hollocher, Geology Department, Union College, Schenectady, NY.

A CIPW norm is a set of idealized minerals that are calculated from a bulk chemical analysis of a rock. The normative minerals are calculated to represent, in many ways, the minerals that might crystallize if the rock were cooled under perfect equilibrium and dry conditions at low pressure. (see link above). Norms may be used for volcanic rocks, which have glass and/or so small crystals that make determination of a

mineral mode impossible, and, as in the case of this study, for metamorphosed igneous rocks that no longer have the original igneous mineralogy and any textures preserved. Due to the length of the norm calculation procedure it is not presented here, but can be viewed on the web page at http://minerva.union.edu. The procedure is similar to the standard done for common rocks, but procedures to calculate normative leucite in strongly silica-undersaturated rocks, aegirine in alumina-undersaturated alkalic rocks, or hematite in oxidized rocks have been omitted.

The results obtained from the CIPW norm calculation are given in Appendix II.

The compositional data is graphically presented in the Ol-Cpx(+Opx)-Pl ternary diagram (Fig. 5.13). The majority of the samples of the studied ultramafic rock plot in the field of Feldspatitic Peridotite. One sample represents the composition of peridotite and three samples fit the field of Feldspatitic Clinopyroxenite. All samples plot within the field of ultramafic rocks.

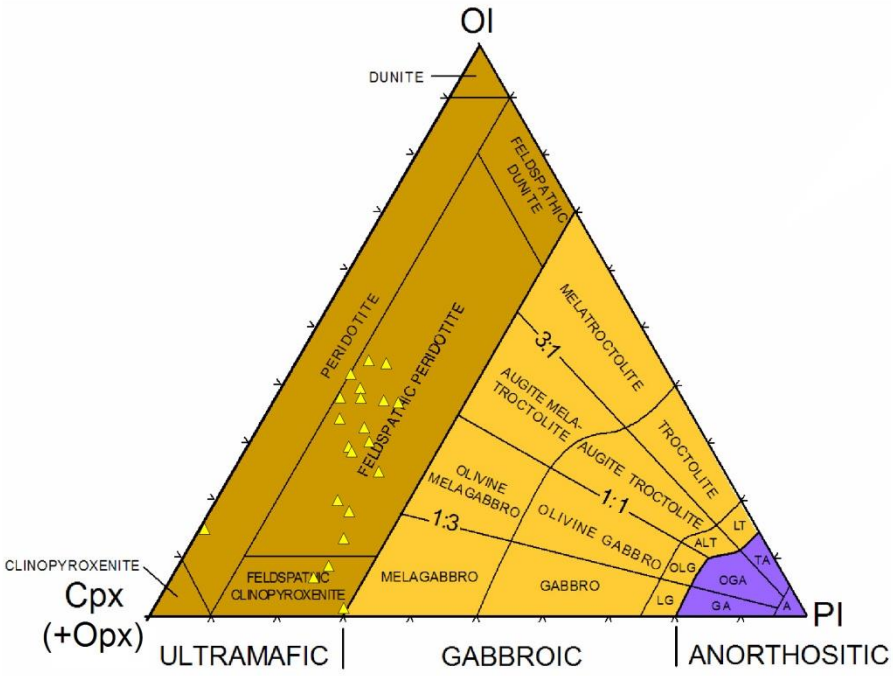


***Figure 5.13.*** *Ol - Cpx(+Opx) - Pl classification diagram for the ultramafic rock from the Kvaløya Island.*

The Ol - Cpx(+Opx) - Pl classification ternary diagram is used to distinguish between different types of ultramafic-mafic plutonic rocks based on the mineral contents of the intrusive rocks. As seen from Fig. 5.13, the majority of the analysed samples are peridotitic in composition. However, since the field relationships between the studied rock and the hosting gneisses are not clear due to tectonic reworking of the contacts, it should not be excluded that the rock might have a volcanic origin. Melting of garnet peridotite under different conditions is recognized as a major process responsible for the origin of different magma types that produce rocks as picrites and basalts, komatiites and komatiitic basalts, and alkaline rocks as kimberlites and carbonatites (Walter, 1998; Wilson, 1989).

## Chapter 6. Mineral chemistry

*Analytical procedure*

Mineral analyses have been performed at the Department of Geosciences at the University of Oslo, Norway with a Cameca SX100 electron microprobe. The analyses were carried out at 15 kV accelerating voltage, 15 nA beam current, focused beam and 10s counting time on peak for major and 20s or 30 s for minor elements. Standardisation was made on synthetic oxides, metal and on natural minerals. PAP matrix corrections were applied.

*Results*

For this work microprobe analyses were carried out only for sulfides and oxides. No silicates have been analysed. In total, 23 analyses of sulfides were carried out. Sulfide analyses are given in Tab. 6.1.

All sulfides show some amounts of Ni present in their mineral composition. Pyrite contains from 0.03up to 0.05 Ni p.f.u. (per formula unit). Co is absent in the lattice of some analysed pyrite grains while other grains contain up to 0.045 Co p.f.u. The copper content of pyrite is low (0.33 Cu p.f.u. is the highest concentration that was analysed). The one pyrrhotite analysis that was performed shows Ni content of 0.002 p.f.u., while chalcopyrite contains from 0.001 to 0.008 Ni p.f.u.

Nickel sulfides mostly show close to stoichiometric compositions. Pentlandite contains from 4.2 to 5.5 Ni p.f.u., from 3.5 to 4.4 Fe p.f.u. and up to 0.3 Co p.f.u. The most Ni enriched samples show (Fe + Co) / Ni ratios of about 1/1.4. The nickel content of millerite varies insignificantly from 0.96 to 0.97 p.f.u., which is close to its stoichiometric formula. Millerite contains up to 0.026 Fe p.f.u. The composition of violarite varies significantly. It contains high amounts of cobalt from 0.28 to 1.12 a.p.f.u,

from 2.9 to 3.7 Ni p.f.u. and from 1.27 to 2.16 Fe p.f.u. Violarite shows compositional variations towards siegenite along the violarite - siegenite solid solution series (Fig 6.1).

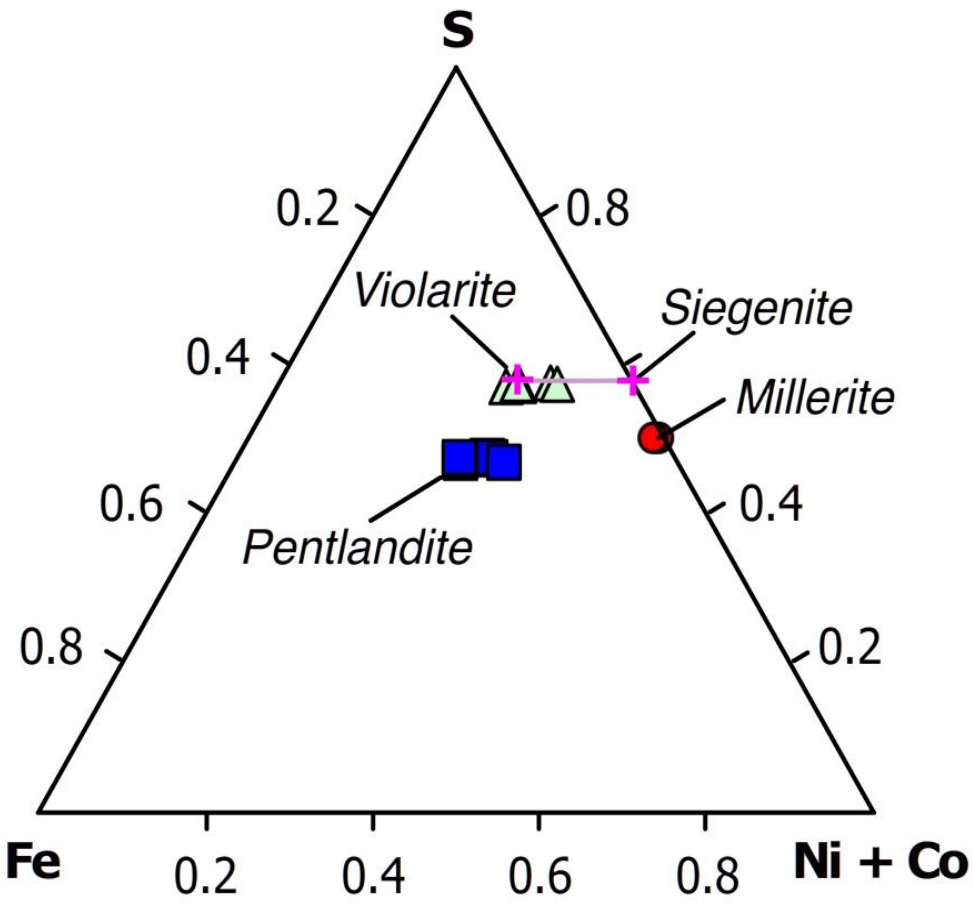


***Figure 6.1.*** *S – Fe–Ni+Co ternary plot for Ni-sulfides analysed from the studied ultramafic rock form the Kvaløya Island. Millerite shows very close to stoichiometric compositions. Pentlandite shows minor variations in composition due to different Co content of different grains, causing variations in the Fe/Ni+Co ratios. Violarite shows compositional variations towards siegenite. The pink line indicates the violarite – siegenite solid solution series.*

## *Table 6.1. Microprobe analyses of sulfides of the studied ultramafic rock from the Kvaløya Island*

Mineral analyses (elements in wt%)

| | Pn | Pn | Pn | Pn | Pn | Pn | Pn | Pn | Vl | Vl | Vl |
|---|---|---|---|---|---|---|---|---|---|---|---|
| S | 33.50 | 32.29 | 33.87 | 33.43 | 33.55 | 33.69 | 33.83 | 33.39 | 42.93 | 42.63 | 43.06 |
| Fe | 28.29 | 26.33 | 27.24 | 32.13 | 32.30 | 32.08 | 31.89 | 25.60 | 20.19 | 17.72 | 18.07 |
| Ni | 38.10 | 36.69 | 38.73 | 32.75 | 32.61 | 32.74 | 32.32 | 41.76 | 34.82 | 28.35 | 29.23 |
| Co | <d.l. | 0.19 | 0.54 | 2.31 | 2.20 | 2.24 | 2.14 | 0.01 | 2.78 | 11.00 | 9.91 |
| Cu | <d.l. | <d.l. | <d.l. | <d.l. | <d.l. | <d.l. | <d.l. | <d.l. | <d.l. | <d.l. | 0.06 |
| Total | 99.89 | 95.49 | 100.38 | 100.61 | 100.66 | 100.75 | 100.18 | 100.77 | 100.72 | 99.71 | 100.32 |
| Structural formulae: | | | | | | | | | | | |
| S | 8.000 | 8.000 | 8.000 | 8.000 | 8.000 | 8.000 | 8.000 | 8.000 | 8.000 | 8.000 | 8.000 |
| Fe | 3.877 | 3.744 | 3.693 | 4.414 | 4.422 | 4.374 | 4.330 | 3.521 | 2.160 | 1.909 | 1.928 |
| Ni | 4.970 | 4.964 | 4.996 | 4.281 | 4.248 | 4.247 | 4.174 | 5.465 | 3.545 | 2.906 | 2.967 |
| Co | <d.l. | 0.025 | 0.069 | 0.301 | 0.285 | 0.289 | 0.275 | 0.001 | 0.282 | 1.123 | 1.001 |
| Cu | <d.l. | <d.l. | <d.l. | <d.l. | <d.l. | <d.l. | <d.l. | <d.l. | <d.l. | <d.l. | 0.005 |
| Total - S | 8.847 | 8.734 | 8.758 | 8.996 | 8.954 | 8.910 | 8.779 | 8.987 | 5.986 | 5.938 | 5.901 |

Mineral analyses (elements in wt%)

| | Vl | Vl | Po | Ccp | Ccp | Mlr | Mlr | Py | Py | Py | Py |
|---|---|---|---|---|---|---|---|---|---|---|---|
| S | 42.72 | 43.61 | 39.21 | 35.16 | 35.43 | 36.26 | 36.42 | 54.31 | 54.26 | 54.77 | 54.62 |
| Fe | 12.78 | 12.06 | 60.87 | 30.78 | 30.61 | 0.87 | 1.63 | 44.02 | 44.70 | 45.92 | 44.72 |
| Ni | 31.91 | 36.70 | 0.12 | 0.27 | 0.02 | 64.67 | 64.08 | 1.49 | 2.41 | 0.02 | 0.01 |
| Co | 12.12 | 9.63 | <d.l. | <d.l. | <d.l. | 0.12 | 0.14 | <d.l. | <d.l. | 1.48 | 2.28 |
| Cu | <d.l. | <d.l. | <d.l. | 32.49 | 33.34 | <d.l. | <d.l. | <d.l. | 0.33 | 0.03 | <d.l. |
| Total | 99.53 | 102.00 | 100.21 | 98.69 | 99.40 | 101.92 | 102.28 | 99.82 | 101.69 | 102.21 | 101.63 |
| Structural formulae: | | | | | | | | | | | |
| S | 8.000 | 8.000 | 1.000 | 2.000 | 2.000 | 1.000 | 1.000 | 2.000 | 2.000 | 2.000 | 2.000 |
| Fe | 1.374 | 1.270 | 0.891 | 1.005 | 0.992 | 0.014 | 0.026 | 0.930 | 0.946 | 0.963 | 0.940 |
| Ni | 3.265 | 3.677 | 0.002 | 0.008 | 0.001 | 0.974 | 0.961 | 0.030 | 0.048 | <d.l. | <d.l. |
| Co | 1.235 | 0.960 | <d.l. | <d.l. | <d.l. | 0.002 | 0.002 | <d.l. | <d.l. | 0.029 | 0.045 |
| Cu | <d.l. | <d.l. | <d.l. | 0.932 | 0.950 | <d.l. | <d.l. | <d.l. | 0.006 | 0.001 | <d.l. |
| Total - S | 5.873 | 5.908 | 0.893 | 1.946 | 1.942 | 0.990 | 0.989 | 0.960 | 1.001 | 0.993 | 0.986 |

Note: <d.l. – below detection limit

# Chapter 7. Discussion

## 7.1. Tectonic settings

In order to place the studied ultramafic rock from the Kvaløya Island in the tectonic framework of the region some constrains were made by comparing geochemical data from the studied rock with geochemical data from other mafic-ultramafic rocks known in the region. Intermediate and felsic rocks were also included when there were strong evidences of their affinity to the same rock suite.

Rocks suites and localities from which the analyses were taken are described in Section 1.2.

Due to the fact that rocks of the whole region have a complex metamorphic history, mainly immobile elements were used. To sum up the previous description, the oldest mafic metavolcanics occurring in the Sjangeli area in the Rombak Tectonic Window has an age of 2.3 Ga (Romer 1989). These rocks are suggested to have formed in an intra-oceanic volcanic arc environment. Arc-related volcanites with compositions varying from basalts to rhyolites and an age of 1.9 Ga are also found in the Rombak Tectonic Window. Similar rocks are found in the Lofoten-Vesterålen area. These rocks have not been dated, but the age is assumed to be Paleoproterozoic (Griffin et al., 1978). The origin of the supracrustal rocks from the Lofoten-Vesterålen area is interpreted to be arc-related. Further north, data provided from the Torsnes supracrustal sequence suggest a maximum deposition age of metapsammites from this supracrustal unit to be 1970±14 Ma (Myhre et al. 2011), which place the formation of Torsnes to be earlier than the Svecofennian tectonothermal event. The Mjelde-Skorelvvatn Belt, which has been dated to 1992±2 Ma (zircon data from metagabbro, coeval with the hosting metabasaltic supracrustal sequence) is proposed to have an allochthonous origin with its later

transportation during the Svecofennian Orogeny to the present-day position. The Ringvassøya Greenstone Belt formed as a pre-orogenic basin, with the age 2.85 – 2.83 Ga (Motuza et. al., 2001). The age of the Vanna group sediments is constrained to the interval 2.40–2.20 Ga (Bergh et. al., 2007). For the last three culminations of basement provinces in Western Finnmark dating has not been performed, but the age of the metamorphic event for amphibolite from the Holmvann group of the Reppafjord Window was obtained at 1840 Ma (Jensen 1996). Bergh and Torske (1988) suggest 2.0 – 1.8 Ga age for the Kvenvik Greenstone Formation. The origin of the mafic rocks from that area interpreted to be arc-related.

In contrast, a layered mafic-ultramafic rock association from the Senja Island is interpreted as olivine-amphibole cumulates formed in a MORB-like environment.

By comparing major and trace element geochemistry of ultramafic-mafic to intermediate rocks from all known basement provinces in North Norway (sometimes felsic rocks from same suites are also included) with of the rock studied here, we make an attempt to place the ultramafic rock from Kvaløya into the tectonic framework of the region.

First of all, geochemical data of the studied rock has been plotted on Harker binary diagrams along with the data from other localities. It is visible from Fig. 8.1 that the compositional data from all localities except for Senja and Kvaløya are similar and often show same trends. In contrast to this, compositional data of samples from the mafic-ultramafic rock association from Senja and from the Kvaløya ultramafic rock plot apart from the rest of the data and sometimes show different trends, e.g. CaO vs. $SiO_2$ plot in Fig. 8.1. A similar situation can be observed on the trace element vs. $SiO_2$ plots in Fig. 8.2.

On the V vs. Ti diagram, selected data of all mafic-ultramafic suites from the supracrustal units of basement provinces in North Norway have been plotted (Fig. 8.3). The data are mostly concentrated in the fields of MORB and IAT,

while the data representing the mafic-ultramafic association from Senja tend to plot in the field of low-Ti bonninites and IAT with only 2 samples plotting in the field of MORB. This suggests that these rocks are different from the majority of mafic-ultramafic rocks in North Norway. Analyses of the rocks from Aisaroaivi formation of the Reppafjord Window plot along the boundary between the MORB and IAT fields. Data from Ringvassøya GB scatter within the fields of

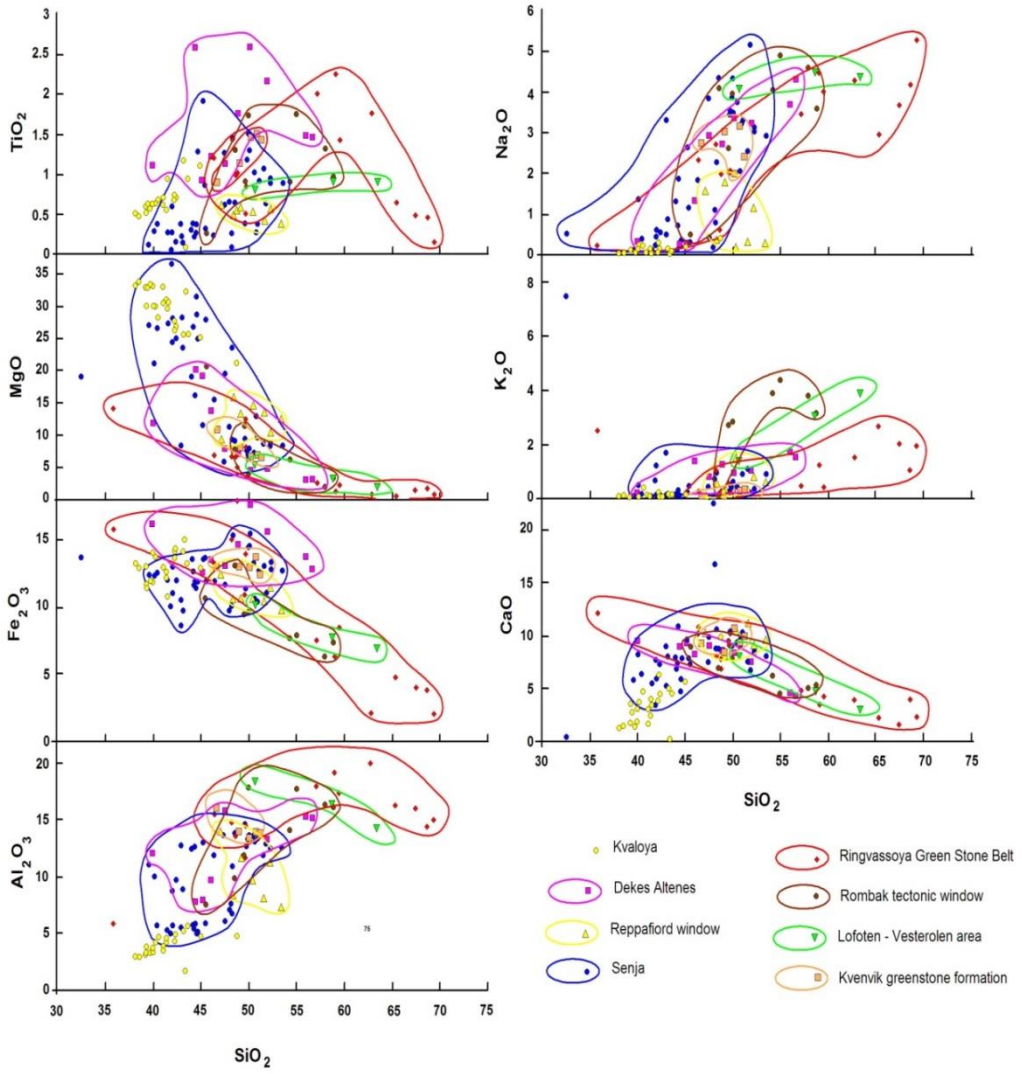


***Figure 8.1.*** *Binary Harker diagrams showing major oxides vs $SiO_2$. Symbols are given in the legend. Note that the compositional data from the Kvaløya ultramafic rock plot within or close to the field of the compositional data from samples from the layered mafic-ultramafic rock association from the Senja Island.*

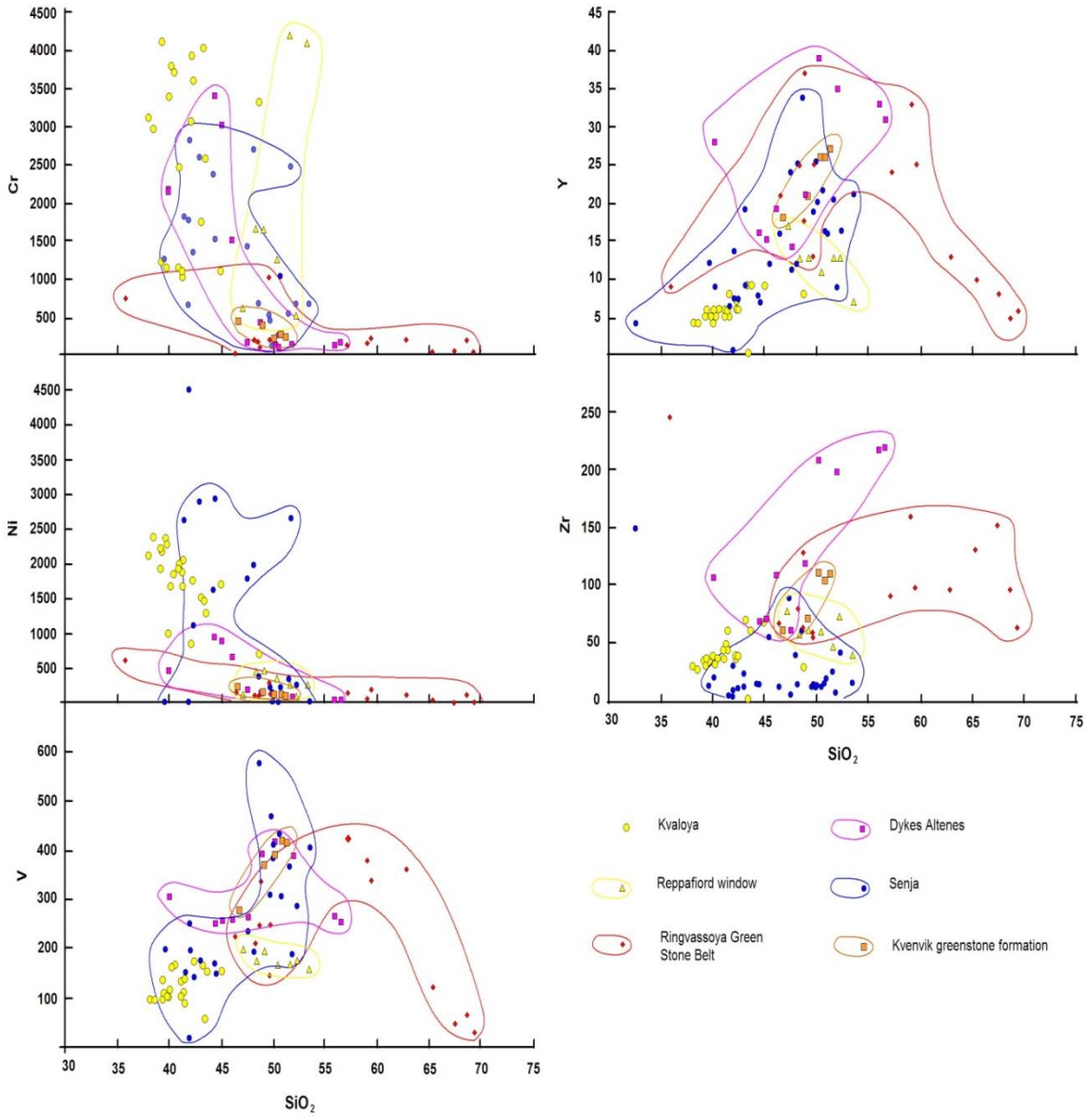


***Figure 8.2.*** *Binary Harker diagrams showing trace elements vs. $SiO_2$. Symbols are given in the legend.*

MORB and IAT. From the diagram it is obvious that the analyses of the studied rock from Kvaløya have Ti/V ratio higher than 20, which characterize MORB (Goodenough et al., 2010), but some of them plot in the field of IAT, showing lower Ti/V ratios, similar to the majority of the data from the other North Norwegian mafic-ultramafic suites. Anyhow, on this diagram the compositional data from the Kvaløya ultamafic rock and the majority of the data from Senja are plotted spatially close to each other.

To compare rock samples analyses from Senja and Kvaløya, the ternary Nb*2 – Zr/4 – Y diagram has been used (Fig. 8.4). However, here we can see that compositional data for the Senja rocks is scattered with just some samples plotting within MORB fields, while the compositional data from the Kvaløya ultramafic rock plot within the fields of within plate tholeiites.

In the Th/Yb versus Ta/Yb diagram (Fig.8.5), the compositional data of the ultramafic rock from the Kvaløya island plots within the field MORB+WPB. Within plate basalts usually have Ta/Yb ratio from slightly less than 0.1 up to 0.2 (Pearce 1983), while the studied rock has slightly higher values.

In the ternary diagram Hf/3 – Th - Ta (Fig. 8.6a), the compositional data of the Kvaløya ultramafics plot in the field of E-type MORB+Tholeitic WPB and differentiates. According to Workman et al. (2004), E-type MORB should have more than 0.2% $K_2O$ and more than 1.0% $TiO_2$. Following this differentiation between E-type and N-type MORB, the studied rock does not represent E-type MORB. The $K_2O$ content of the rock varies from < 0.01 wt % to 0.07 wt %, slightly exceeding 0.1 wt % in two samples. The $TiO_2$ content is always less than 1.0 wt % with the exception of one sample. This suggests that the rock represents within plate tholeiite and differentiates. However, the compositional data for some samples plot in the field of island arc tholeiites.

Furthermore, in the discrimination triangular plot Ti/100 – Zr – Y*3 (Fig. 8.6b) all compositional data of studied rock plot within the field of within plate basalts, except from one sample, which plot in the field of MORB+IAT+CAB.

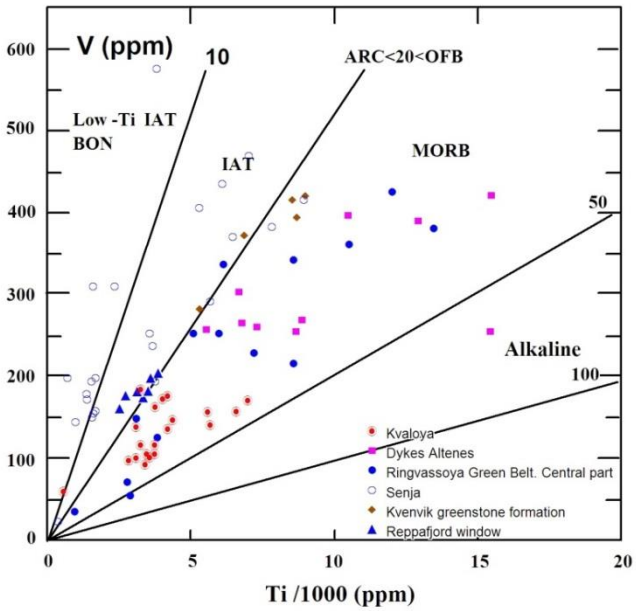


***Figure 8.3.*** *Ti/1000 vs. V discriminant plot for mafic-ultramafic rocks from supracrustal units of North Norway. Lines indicate constant Ti/V ratio. IAT: Island arc tholeiite; BON: boninite; MORB: mid-ocean ridge basalt; OFB: ocean floor basalts. After Goodenough (2010).*

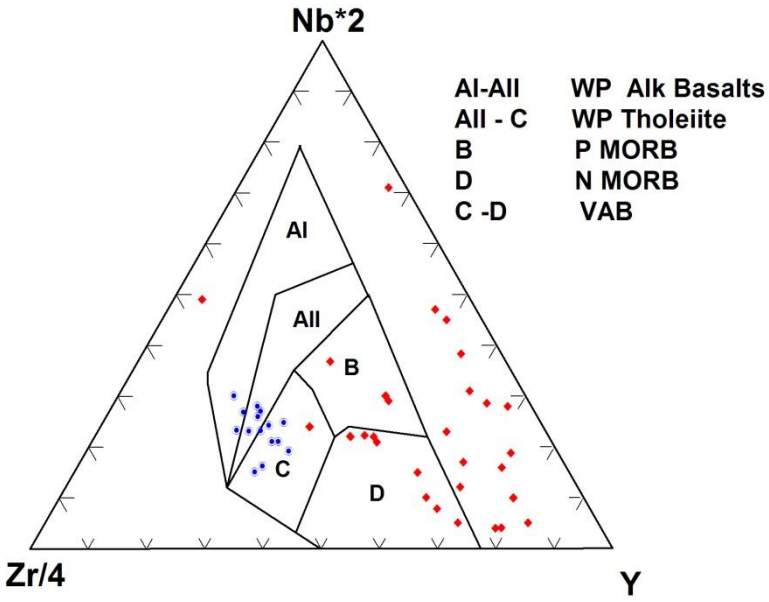


***Figure 8.4.*** *Nb*2 – Zr/4 – Y ternary plot for the compositional data of samples from the mafic-ultramafic rock association at NW Senja and from the ultramafic rock from the Kvaløya Island. Red rhombs – Senja; blue circles – Kvaløya.*

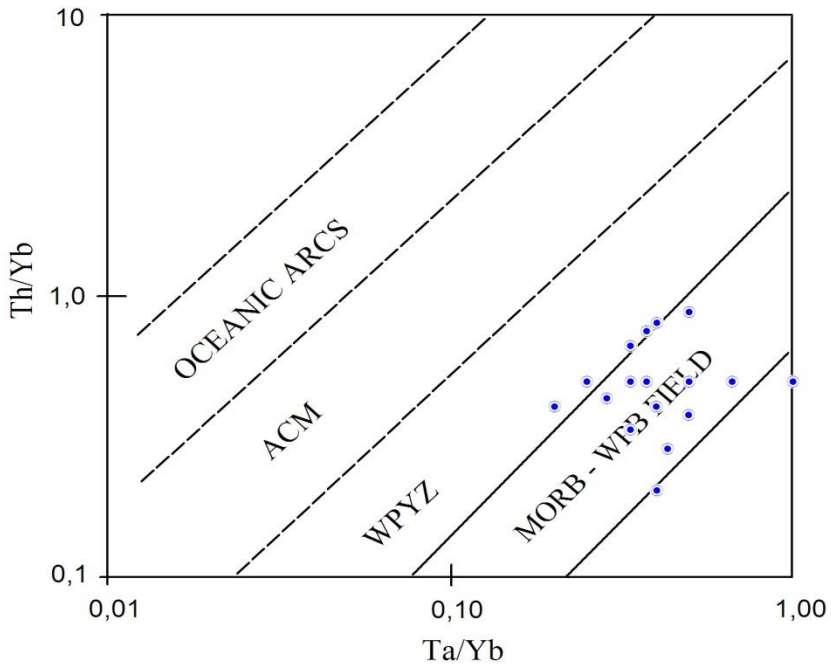


***Figure 8.5.*** *Th/Yb versus Ta/Yb diagram. ACM - active continental margin; WPYZ - within plate volcanic zone; WPB-within plate basalts. After Muñoz et al., (2006).*

In the ternary Y – La - Nd tectonic setting discrimination diagram in Fig. 8.7, the compositional data for the Kvaløya ultramafic rock is scattered. Most of the data plot in the fields of continental tholeiites and calc-alkaline basalts. The latter rock type can be excluded due to geochemical features of the rock and can be explained by slight variations of Y, La and Nd (compositional data plotted in the field of calc-alkaline basalts tend to plot close to the boundary of continental tholeiites field). Some samples lying in the field of Tholeites+Calc-alkaline rocks most likely resemble tholeiites.

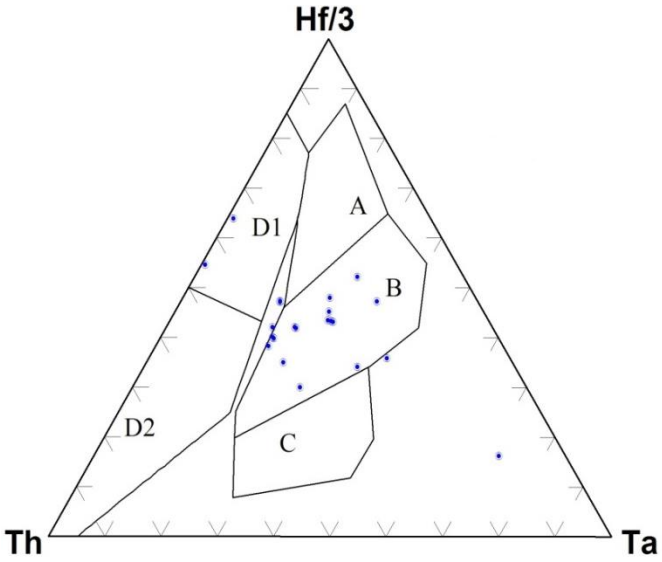


(a)

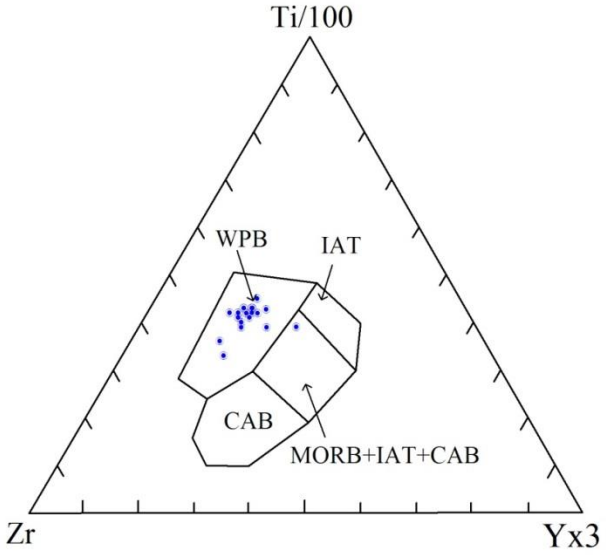


(b)

***Figure 8.6.*** *(a) in Data from the ultramafic rock from the Kvaløya island shown in the Hf-Th-Ta tectonic setting discrimination diagram. A: N-MORB; B: E-MORB+Within plate tholeiites and differentiates; C: Alkaline within plate basalts and differentiates (Rift); D1: Island arc tholeiites; D2: Destructive plate-margin basalts. After Ortega-Obregón et al., (2010). (b) Data from the ultramafic rock from the Kvaløya Island in the Zr-Ti-Y tectonic setting discrimination diagram. WPB: Within plate basalts; IAT: Island arc tholeiites; CAB: Calc-alkaline basalts; MORB: Mid ocean ridge basalts. After Pearce & Cann (1973).*

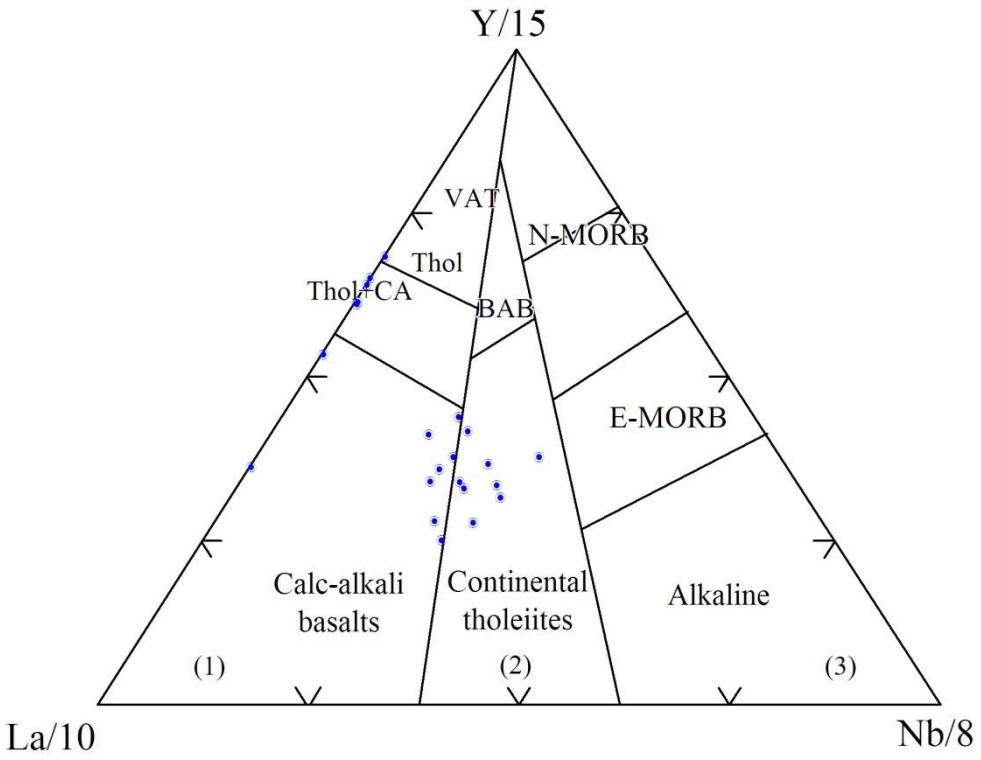


***Figure 8.7.*** *Data from the ultramafic rock from Kvaløya in the ternary Y – La - Nb tectonic setting discrimination diagram. 1 - Orogenic domains; 2 – Intracontinental and postorogenic domains; 3 – Anorogenic domains. VAT: Volcanic arc tholeiites; BAB: Basalts generated in fore- and back-arc basins; CA: Calc-alkaline basalts. After Oliveros et al. (2007).*

One explanation for the scattering of the compositional data from the Kvaløya ultramafic rock are scattered in some diagrams, e.g. Fig 8.6a and Fig. 8.7 can be that the studied rock represents cumulates. However, the majority of the results obtained suggests that the studied rock is a product of intraplate magmatism. According to the geochemical data, the studied ultramafic rock most likely is different from the majority of the mafic to felsic magmatic suites known in the region and interpreted to have formed in a volcanic arc environment. Some similarities exist between the studied rock and rocks of the layered mafic-ultramafic rock association from NW Senja (Figures 8.1 and 8.2). However, it seems form Fig. 8.4 and number of other diagrams (not shown) that

the rocks from these two localities were formed in different tectonic settings. However, differentiation between tectonic settings is obstructed by the possibility that the rocks from Kvaløya and from NW Senja are cumulative rocks.

## 7.2. The protolith of the investigated rock

Whole rock chemical analyses suggest that the studied rock belongs to the ultramafic rock class. Most of the discrimination diagrams that have been used in this thesis show that the rock can be considered to be a komatiite. According to Dostal (2008), komatiites are ultramafic volcanic rocks with low $SiO_2$ content, low $TiO_2$ content (< 1 wt %) and low $K_2O$ (< 0.5wt %). The MgO content of komatiites exceeds 18 wt % (Arndt &Lesher 2004). A lot of authors insist on the necessity of adding spinifex texture in the definition of komatiites (Arndt &Lesher 2004; Dostal 2008; Nesbit 1979).

For the ultramafic rock studied here, the MgO content is > 20 wt % for all samples, with average content of 29.5 wt % MgO, the $TiO_2$ content is usually < 1 wt % with an average content of 0.65 wt %, the $K_2O$ content rarely exceed 0.1 wt % and the sum of alkalis ($K_2O+Na_2O$) is lower than 0.5 wt % for all samples. The $SiO_2$ content of the rock is as typical for ultramafic rocks. REE pattern interpretation combined with Harker diagrams suggests that the analysed samples represent a co-magmatic series, and belong to the same magmatic suite. Moderate depletion in HREE relative to LREE, suggest some small degree of crustal contamination (Hanski et. al., 2001). This is in agreement with the conventional idea that komatiites are often susceptible to contamination due to the high temperatures of their parental magmas (Dostal 2008; Jochum et al. 1991). The Th/Ce ratio of the rock varies from 0.01 to 0.05, which is similar to the Th/Ce ratio of mantle derived magmas (Sun and McDonough, 1989).This is much lower than 0.15, which corresponds to the Th/Ce ratio of continental crust

(Taylor & McLennan, 1995). The Th/Yb ratio of the ultramafic rock from the Kvaløya Island is about 4 in average, which is much lower than that for the continental crust (28.2, Wang et. al., 2013). The rock shows Zr/Sm ratios in the range 20.5-30, and Hf/Sm ratios in the range 0.5 - 0.84, which is similar to the primitive mantle ratios of Zr/Sm = 25 and Hf/Sm = 0.69 ( Xie et al., 1995). The Ce/Yb ratio varies from 1 to 1.5, which is higher than that for primitive mantle and chondrite (= 0.39, Sun & McDonough, 1989).

Other possibilities for the origin of the studied ultramafic rock, which did not inherit any original textures and have complicated relationships with the host rock should not be excluded. However, the low $TiO_2$ content and the low concentration of REE do not allow classifying the studied rock as a meimechite (Le Bas, 2000). Essexite should contain elevated amounts of such elements as K, Ba, Rb, Cs, and Sr. Due to the mobility of these elements and the fact that the studied rock underwent metamorphism it is difficult to argue about the initial concentrations of these elements. However, there are not enough alkalis in the studied rock to be classified as essexite, since the normal content of alkalis in essexite exceeds 3 wt %. Picrite is another type of high-Mg rock of volcanic origin having similar features as the rock from Kvaløya. The IUGS classification scheme for high-Mg and picritic volcanic rocks (Le Bas, 2000) has an overlap in contents of major oxides that allow differentiating between komatiites, meimechites and picrites. CIPW calculations show that the theoretical mineral composition of the ultramafic rock from the Kvaløya Island resembles that for peridotite and feldspaitic peridotite. In the Kluane mafic-ultramafic belt (Yukon, Canada), feldspatic peridotite occurs near the basal contact of the intrusion and there is a gradual transition upwards into non-feldspatic peridotite and dunite (Hulbert, 1995). For the Eagle intrusion feldspathic peridotite (Michigan, USA), the most olivine-rich unit of the intrusion containing 30 to 60 % olivine, 5 to 15 % clinopyroxene, 15 to 40% orthopyroxene and 15 to 25 % plagioclase occurs as a sheet at the top of the sequence (http://www.portgeo.com.au).Thus, this

rock-type occurs as a part of a layered intrusion and represents a unit crystallized at moderate depths.

When discussing the whole rock composition of the Kvaløya ultramafic rock, it should not be excluded that element mobility might result in addition of some and removal of other element during metamorphism. This could have affected the primary chemical composition of the studied rock, for example under the influence of fluids associated with the intrusion of the Ersfjord Granite. Modification of the primary chemical composition of an igneous rock will affect the precision of CIPW calculations. For example, mobilization of CaO will affect the amount of plagioclase from the CIPW calculations. This might explain why the studied ultramafic rock, which is very similar in composition to komatiites and picrites, with REE ratios close to that of mantle rocks, plot in the field of feldspatic peridotite in the Ol – Cpx(+Opx) – Pl diagram in Fig. 5.13.

There are several possible interpretations of what type of magmatic body that the studied rock could represent. Due to its high MgO content and its position on differentiation diagrams for mafic- ultramafic cumulates (see Chapter 5, Fig. 5.11 and 5.12), it might be referred as a cumulate layer. Thus, the rock might represent the lower part of a layered intrusive body, or it could represent the stratigrafically lower part of a high-Mg lava flow (e.g. komatiite). Another possibility is that the studied ultramafic rock represents a boudinaged supracrustal unit. The evidence for this can be that the strike of the lenses is subparallel to parallel with the main foliation in the gneiss. However, Arndt and Lesher (2004) suggest that 28wt % MgO is the maximum possible MgO content of magma. Thus, a cumulate origin of the studied ultramafic rock is probably the most plausible model.

## 7.3. Origin of the sulfides

The opaque mineral content is dominated by ilmenite, magnetite as well as pyrrhotite, pentlandite, millerite and violarite, with minor amount of other sulfides such as pyrite, chalcopyrite, sphalerite and galena. In general, the opaque mineral content of the studied rock is similar to mineral assemblages reported from Ni-Cu-PGE deposits hosted in mafic-ultramafic rocks (Voisey's Bay, Kambalda) (Cowden & Woolrich, 1987; Naldrett et al., 2000). With reference to unpublished data of Gedeminas Motuza (personal communication to Kåre Kullerud 2011), reporting up to 10 ppb Pt and 300 ppb Pd from the studied rock, more investigations on the PGE content of the ultramafic rock at Kvaløya could be of interest.

The sulfides occurring in the ultramafic rock from Kvaløya are disseminated and quite small in size. It is clear that they do not represent a primary magmatic phase, but rather were formed during low-grade metamorphic processes. Olivine can contain up to 5 000 ppm of Ni in mafic-ultramafic rocks and even more for olivine from Ni-PGE ore (up to 14 000 ppm, Yang et. al., 2013). Most likely, all Ni that initially was contained in olivine was incorporated in the crystalline lattice of sulfides during metamorphism and olivine break-down.

The presence of violarite and millerite, that are quite abundant relative to other sulfides indicate that the rocks underwent secondary alteration within the supergene zone. From the S – Fe – Ni+Co ternary diagram (see Chapter 6 and Fig. 6.1), the Ni-sulfides from the studied ultramafic rock does not show any transitional compositions between pyrrhotite and violarite. This attests that the violarite present in the rock formed at the expense of pentlandite, most likely by dissolution-precipitation rather than by progressive conversion of pentlandite.

Variations in pyrite chemistry, e.g. the presence of Ni for some analysed grains and the absence in others can be explained by 2 generations of pyrite. The

earliest generation of pyrite contains small amounts of Co and Ni, while the second generation of pyrite, which probably occurs as pseudomorphs from pentlandite is Ni-rich. This feature is quite common in pyrite from base metal sulfide deposits (Nkoumbou et al. 2009). A similar process with Ni enrichment of secondary pyrite was noted in sulfides from the Mamb pyroxenite intrusion in Cameron (Nkoumbou et. al., 2009).

The temperature during the formation of the sulfides in the rock corresponds to the temperature range of upper greenschist – lower amphibolite metamorphic facies conditions. Nkoumbou et al. (2009) propose the formation of pyrrhotite + pentlandite+ violarite + chalcopyrite assemblage at temperatures below 400 °C. Ramdor (1962) suggests that millerite forms at temperatures below 395 °C, arguing that at higher temperatures it is almost always enough iron to form pentlandite. If this is the case, we are dealing with the low-temperature variety β-millerite, which is a product of decomposition of Ni-bearing sulfides. The Cu-free nature of pyrrhotite is indicative of re-equilibration around 200 °C (Lorand et al., 2006; Vaughan & Craig, 1978). Ilmenite, which is a wide-spread mineral in the rock is considered to be a "thermometer" because of its formation at exclusively high temperatures exceeding 500 °C according to Ramdor (1962) or > 650° according to Voitkevich (1979).

Chalcopyrite that occurs as small inclusions in sphalerite is probably not a result of chalcopyrite – sphalerite solid solution decay, but rather a result of substitution. Evidence for such kind of chalcopyrite inclusions in sphalerite includes random orientation of chalcopyrite "droplets" in sphalerite grains along with limited dissolution of Cu in the Cu – Fe – Zn - S system at temperatures below 700°.

## 7.4. Sulfur source

Another question concerns the source of sulfur. For many Archean komatiite hosted Ni deposits, the presence of an adequate sulfur source plays an important role. For instance, rocks from the Australian Agnew-Wiluna and Alexo deposits reached sulfur saturation by contamination from underlying volcanogenic massive sulfide deposits. For the Dundonald and Kambalda deposits in Australia, sulfur was probably derived from the wallrock sediments (Bekker et al., 2009; Florentini et al., 2006).

The host rock of the ultramafic rock at Kvaløya is referred to as a TTG-gneiss, implying a primary magmatic origin for the protolith of the gneiss. However, no particular research has been done on the country rock. Isotope studies of both the ultramafic rock and the hosting gneiss can be of importance for identifying the source of sulfur. In case a major sulfur source were available during metamorphism of the studied ultramafic rock it is possible that not only the supergene zone have high Ni concentrations, but the whole volume of the ultramafic rock could have enhanced Ni concentrations. However, due to the unclear field relationships between the studied ultramafic rock and the host rock, there are no plausible interpretations or even suggestions of the real size of the bodies of ultramafic rock.

In summary, lenses of the studied ultramafic rock probably represent ultramafic cumulates with up to 2500 ppm of Ni. Ni was incorporated in sulfides that formed due to low-grade metamorphism during breakdown of olivine and possibly pyroxene. The sulfides were subsequently subjected to supergene alteration that increased the Ni grade. At present, Ni ores with 0.2-0.5 wt % of Ni is considered to be low-grade. Determination of sulfur isotopes from the ultramafic rock and the host rock can shed light on the sulfur source during

metamorphism and sulfide formation. In case of the existence of a major sulfur source, not only the supergene zone, but also the hypogene zone might have high Ni concentrations.

### 7.5. Economical evaluation of the rock

Traditional mining of a low-grade ore deposit represent a serious environmental problem, because of the large amounts of waste rock that is produced. One of the most important challenges for modern mining industry is to find new solutions concerning making the production waste-free and find out possible alternatives to use the materials that traditionally have been deposited in tailings. The excess material after extracting Ni (and, possibly, Co, Cr, and Fe) from the ultramafic rock would be dominated by serpentine. The possible use of waste serpentine that might be of economic and ecological interest, and might decrease mining expenses is $CO_2$-sequestration. The reaction between serpentine and $CO_2$ can be formulated accordingly:

$$Mg_3Si_2O_5(OH)_4+3CO_2=3MgCO_3+2SiO_2+2H_2O$$

which shows that $CO_2$ through reaction with serpentine can be permanently sequestrated in magnesite. Carbonation of large volumes of serpentine in excess from mining may in this way be used for permanent storage of large quantities of $CO_2$. These carbonates are thermodynamically stable, and the storage of $CO_2$ is therefore a safe and long-term solution. Also avoided is the risk of any accidental release of stored $CO_2$ leaking from underground (Li et al., 2013). Furthermore, magnesite being produced during this process might also be of economic interest. Through comprehensive Aspen modelling, Brent et al. (2011) proposed that co-location of mineral carbonation plants and $CO_2$ producing industries could lead to synergies and added value for both parts. Captured $CO_2$

will help to reduce the atmospheric level of greenhouse gas as part of the climate change mitigation strategy, where most of it would remain isolated from the atmosphere (Li et al., 2013) Therefore, for a complete evaluation of the economic potential of the ultramafic rock studied here, the economic benefits of carbon sequestration using the materials in excess from metal extraction should be evaluated in a larger context, in order to decide whether the rock is of economic interest or not.

¶

## Conclusions

- Determination of the tectonic setting of the studied rock is difficult because of metamorphic alteration and the possibility of compositional modification of the rock caused by element migration. Geochemical investigations suggest that the studied rock was formed in an intracontinental environment. The rock has some similarities in chemical composition with the layered mafic-ultramafic rock association from NW Senja, rather than with any other mafic to intermediate rock sequence from the region.

- The studied rock represents an ultramafic rock metamorphosed under greenschist to lower amphibolite facies metamorphic conditions. The mineral content of the rock is dominated by serpentine, amphibole, chlorite and talk. Primary minerals or relics of them along with primary magmatic textures have not been observed in the rock.

- CIPW calculations suggest that the protolith of the rock was a felspatic peridotite.

- Due to the relatively high MgO content of the rock, it is inferred that the studied rock represent a cumulative layer formed either at the lower part of a komatiitic (or picritic) lava flow or as a basal part of a layered intrusion.

- The rock contains a number of Ni-sulfides that formed due to low-grade metamorphism and break down of primary olivine and possibly pyroxene that contained significant amount of Ni in their crystalline lattice.

- The temperature of sulfide formation did not exceed 400 - 450° C. The presence of violarite and millerite indicate alteration in the supergene zone, where pentlandite was replaced by these two minerals due to secondary alteration.

- The Ni content of the rock is up to 2 500 ppm, which presently is considered to be a low-grade Ni ore*. The results of PGE analyses show only very low concentrations of Pt, Pd and Au, but it is important to mention, that

only 5 samples were analysed for this work, while according to unpublished data of Motuza concentrations of Pd up to 300 ppb and Pt up to 10 ppb were identified in this rock.

- Sulfur isotope investigations are required to determine the source of S in the rock.

- The possibility of using the studied serpentinized ultramafic for $CO_2$ sequestration in carbonates allows to increase the economic potential of the rock.

- *If the tonnage is appropriate .

## References


33 IGC excursion guide. Metallogeny and tectonic evolution of the Northern Fennoscandian Shield. Edited by V. Juhani Ojala and Markku Iljina

Aitken B.G., Echeverria L.M., 1984. Petrology and geochemistry of komatiites and tholeiites from Gorgona Island, Colombia. Contribution to Mineralogy and Petrology 86, pp. 394-405.

Arndt N.T., Lesher C.M., 2004. Komatiite. http://hal.archives-ouvertes.fr/docs.

Barnes S., Osborne G, Cook D., Barnes L.,4 Maier D.W., Godel B., 2011. The Santa Rita nickel sulfide deposit in the Fazenda Mirabela intrusion, Bahia, Brazil: geology, sulfide geochemistry, and genesis. Economic Geology 106, pp. 1083–1110.

Barton P., Bethke Ph., 1987. Chalcopyrite disease in sphalerite: pathology and epidemiology. American mineralogist 72, 451-467.

Bergh G.F., Corfu F., Myhre P.I., Kullerud K., Armitage P.E.B., Zwaan K.B., Ravna E.K., Holdsworth R.E., Chattopadhya A., 2012. Was the Precambrian basement of Western Troms and Lofoten-Vesterålen in Northern Norway linked to the Lewisian of Scotland?A comparison of crustal components, tectonic evolution and amalgamation history. INTECH 2012 ISBN 978-953-51-0675-3.s 283 - 330.

Bergh S.G., 1986. The Kvenvik greenstone formation in Alta, Northern Norway: geotectonic setting and geochemical alterationof a Proterozoic metabasaltic sequence. UiT. PhD thesis.

Bergh S.G., Kullerud K., Armitage P., Zwaan K.B., Corfu F., Ravna E.K., Myhre P., 2010. Neoarchaean to Svecofennian tectono-magmatic evolution of the West Troms Basement Complex, North Norway. Norwegian Journal of Geology 90, pp 21-48. Trondheim.

Bergh S.G., Torske T., 1988. Palaeovolcanology and tectonic setting of a proterozoic metatholeiitic sequence near the baltic shield margin, Northern Norway. Precambrian Research 39, pp. 227–246.

Block of the Bird River Sill, Manitoba; in Report of Activities. Manitoba Industry, Trade and Mines, Manitoba Geological Survey, p. 250–254.

Bortnikov N. S., Genkin A.D., Dobrovol'skaya M. G., Muravitskaya N., Filimonova A.A., 1991. The nature of chalcopyrite inclusions in sphalerite:

Brent G.F., Allen J.D., Eichler R.B., Petrie J.G., Mann J.P., Haynes B.S., 2011. Mineral carbonation as the core of an industrial symbiosis for energy-intensive minerals conversion. Journal of Industrial Ecology 16, pp.94-104.

Corfu F., 2004. U–Pb Age, Setting and Tectonic Significance of the Anorthosite–Mangerite–Charnockite–Granite Suite, Lofoten–Vesterålen, Norway. Journal of Petrology 45, pp. 1799–1819 DOI

Corfu F., 2007. Multistage metamorphic evolution and nature of the amphibolite–granulite facies transition in Lofoten–Vesterålen, Norway, revealed by U–Pb in accessory minerals. Chemical Geology 241, pp.108–128.

Corfu F., Armitage P., Kullerud K., Bergh S.G., 2003. Preliminary U-Pb geochronology in the West Troms Basement Complex, North Norway: Archaean and Palaeoproterozoic events and younger overprints NGU-BULL 441, p. 61.

Dostal J., 2008. Komatiites. Journal of the Geological Association of Canada 35, pp. 21-31.

Exsolution, Coprecipitation, or "Disease"? Economic Geology 86, pp. 1070-1082.

Goodenough K.M., Styles M.T., Schofield D., Thomas R. J., Crowley Q. C., Lilly R.M., McKervey J., Stephenson D., Carney J. N., 2010. Architecture of the Oman–UAE ophiolite: evidence for a multi-phase magmatic history. British Geological Survey ©.

Griffin, W.L., Taylor, P.N., Hakkinen, J.W., Heier, K.S., Iden, I.K., Krogh, E.J., Malm, O., Olsen, K.I., Ormaasen, D.E. & Tveten, E. 1978: Archean and Proterozoic crustal evolution in Lofoten-Vesterålen, N Norway. Journal of the Geological Society, London 135, 629-647.

Grove T.L., Parmam S.W., 2004. Thermal evolution of the earth as recorded by komatiites. Earth and Planetary Science Letters 219, 173-187.

Ha-Duong M., Keith D.W., 2003. Carbon storage: the economic efficiency of storing CO2 in leaky reservoirs. Clean Techn Environ Policy 5, pp. 181–189.

Hanski E., Huhma H., Pastas P., Kamenetsky V.S., 2001. The Paleoproterozoic komatiite-picrite association of Finnish Lapland. Joutnal of Petrology 42, pp. 855-876.

Heier K.S., Thoresen K., 1971. Geochemistry of high grade metamorphic rocks, Lofoten-Vesterålen North Norway. Geochimica et Cosmochimica Acta 35, pp. 89-99.

Hui1 W.Y., Tenailleau1 Ch., Pring A., Brugger J., 2004. Experimental study of the transformation of pentlandite/pyrrhotite to violarite. Regolith pp. 146-150.

Interpretation of Geochemical data. Intermet Engineering, Moscow 2001. pp. 146-148. Domorackiy. (In Russian).

Jensen L.S., 1976. A new cation plot for classifying subalkalic volcanic rocks. Ontario Division of Mines, Miscallaneous Paper 66, 27p.

Jensen P.A., 1996. The Altenes and Repparfjord tectonic windows, Finnmark, Northern Norway: Remains of Paleoproterozoic Andean type plate margine at the rim of the Baltic Shield. UiT, PhD thesis.

Jochum K.P., Hafmann A.W., Pfander J., 1998. Constraints on the abundances and abundance ratios of Nb, Ta, Th and U in the Earth's Mantle and crust using high precision MIC-SSMS data. GERM workshop. La Jolla, p. 45-47.

Kullerud G., 1962. Thermal stabitity of pentlandite. Canadian Mineralogist 7, pp. 353-366.

Kullerud, K., Corfu, F., Bergh, S.G., Davidsen, B. & Ravna, E. K. 2006a: U-Pb constraints on the Archaean and Early Proterozoic evolutionof the West Troms Basement Complex, North Norway (Abstract). Bulletin of the Geological Society of Finland Special Issue I, p. 79.

Kullerud K., Skjerlie K.P., Corfu F., Rosa J.D., 2006b. The 2.40 Ga Ringvassøya mafic dykes, West Troms Basement Complex, Norway: The concluding act of early Palaeoproterozoic continental breakup. Precambrian Research 150, pp. 183–200.

Le Bas M.J., 2000. IUGS Reclassification of the high-Mg and picritic volcanic rocks. Journal of petrology 41, 1467-1470.

Le Bas M.J., Streckeisen A.L., 1991. The IUGS systematic of igneous rocks. Journal of Geological Society, London 148, pp. 825-833.

Le Maitre R. W., 2005. Igneous Rocks: A Classification and Glossary of Terms. Cambridge University Press, p. 256.

Li C., Naldrett A.J., 1999. Geology and petrology of the Voisey's Bay intrusion: reaction of olivine with sulfide and silicate liquids. Lithos 47, 1–31.

Li L., Zhao N., Wei W., Sun Yu., 2013. A review of research progress on CO2 capture, storage, and utilization. Fuel 108, pp.112–130.

Lorand J.P., Grégoire M., 2006. Petrogenesis of base metal sulphide assemblages of some peridotites from the Kaapvaal craton (South Africa). Contribution to Mineralogy and Petrology 151, pp. 521–538.

Markl G., Bucher K., 1988. Proterozoic eclogites from the Lofoten islands, Northern Norway. Precambrian Research, 39, pp. 227-246.

Motuza G., Motuza V., Beliatsky B., Savva E., 2010. Igneous and Metamorphic GeologyVolcanic Rocks of the Ringvassøya Green Stone Belt (North Norway): Implication for the Stratigraphy and Tectonic Setting. Abst. EUG XI Symposium OS07.

Motuza G., 2000. Description to the geological map of the central part of the Ringvassøya greenstone belt, Troms country, Northern Norway. NGU, Vilnius University.

Muñoz M., Fuentes F., Vergara M., Aguirre L., Nyström J.O., Féraud G., Demant A., 2006.Abanico East Formation: petrology and geochemistry of volcanic rocks behind the Cenozoic arc front in the Andean Cordillera, central Chile (33°50'S). Revista geológica de Chile 33, pp. 109-140.

Myhre P., Corfu F., Bergh S.G., 1997. Palaeoproterozoic (2.0–1.95 Ga) pre-orogenic supracrustal sequences in the West Troms Basement Complex, North Norway. Lithos 42, pp. 15-35.

Naldrett A. J., Singh J., Krstic S., and Li Ch., 2000. The mineralogy of the Voisey's Bay Ni-Cu-Co deposit, Northern Labrador, Canada: Influence of oxidation state on textures and mineral compositions. Economic Geology 95, pp. 889–900.

Nesbitt R.W., Sun Sh., Purvis A.C., 1979. Komatiites: geochemistry and genesis. Canadian Mineralogist 17, pp. 165-186.

Ni–Cu–PGE-mineralized intrusion, Northern Finland. Contribution to Mineralogy and Petrology 166, 81–95.

Nisbet E.G., 1982. Komatiites. The tectonic setting and petrogenesis of komatiites. (Eds.), London, George Allen and Unwin, p. 501-520.

Nisbet E.G., Cheadle M.J., Arndt N.T., Bickle M.J., 1993. Constraining the potential temperature of the Archaean mantle: a review of the evidence from komatiites. Lithos, 291Elsevier Science Publishers 30, 291-307.

Nkoumbou Ch., Villiéras F., Barbey P., Ngoune C.Y., Joussemet R., Diot F., Njopwouo D., Yvon J., Rendus C., 2009. Ni-Co sulphide segregation in the Mamb pyroxenite intrusion, Cameroon. Geoscience 341, pp. 517–525.

Obregón C.O., Keppie1J.D., Murphy B.J., 2010. Geochemistry of Carboniferous low metamorphic grade sedimentary and tholeiitic igneous rocks in the western Acatlán Complex, Southern Mexico: deposition along the active western margin of Pangea. Revista Mexicana de Ciencias Geológicas, 27, pp. 238-253.

Parman S., 2004. Komatiites and Plume Debate. http://www.mantleplumes.org/Komatiites.html

Pearce J. and Norry M., 1979. Petrogenetic implications of Ti, Zr, Y, and Nb variations in volcanic rocks. Contribution to Mineralogy and Petrology 69, 33-47.

Pichler H., Schmitt-Riegraf C., 1997. Rock-forming Minerals in Thin Section. 220 p.

Theyer P., 2002. Platinum group element investigations in the Peterson

Vaughan D.J., Craig J.R., 1978. Mineral chemistry of metal sulfides. Cambridge University Press, Cambridge, 493 p.

Voytkevich G.V., Miroshnikov A.E., Povarennih A.S., Prokhorov V.G., 1979. Short manual in Geochemistry. Moscow. Nedra. 444p. (in Russian).

Walter M.J., 1998. Melting of garnet peridotite and the origin of komatiite and depleted lithosphere. Journal of Petrology 39, pp. 29–60.

Wanga M., Wanga C. Ya., Sund ya., 2013. Mantle source, magma differentiation and sulfide saturation of the ~637 ma Zhouan mafic–ultramafic intrusion in the northern margin of the Yangtze block, Central China. Precambrian research 228, 206– 222.

Whitney **D.L.,** Evans **B.W.,** 2010. Abbreviations for names of rock-forming minerals. American Mineralogist, 95, pp. 185–187.

Woolrich P., Cowden A., 1987. Geochemistry of the Kambalda iron-nickel sulfides: implications for models of sulfide-silicate partitioning. Canadian Mineralogist 25, pp. 2l-36.

Workman R.K., Hart S.R., 2004. Major and Trace Element Composition of the Depleted MORB Mantle (DMM). Earth and Planetary Science Letters. Abst.

Xia F., Brugger J., Chen G., Ngothai Yu., O'neill B., Putnis A, Pring A., 2009. Mechanism and kinetics of pseudomorphic mineral replacement reactions: a case study of the replacement of pentlandite by violarite. Geochimica et Cosmochimica Acta 73, 1945–1969.

Xie Q., Kerrich R., Fan J., 1993. HFSE/REE fractionations recorded in three komatiite-basalt sequences, Archean Abitibi Greenstone Belt: implications for multiple plume sources and depths. Geochimica et Cosmochimica Acta 57, pp. 4111-4118.

Xie Q., McCuaig T.C., Kerrich R., 1995. Secular trends in the melting depths of mantle plumes: Evidence from HFSE/REE systematics of Archean high-Mg lavas and modern oceanic basalts. Chemical Geology 126, pp. 29-42.

Yang Sh., Maier D.W., Hanski J.E., Lappalainen M., Santaguida F., Maatta S., 2013. Origin of ultra-nickeliferous olivine in the Kevitsa

Zhang V., Mao J., Cai J., Kusky T., Zhou G., Yan Sh., Zhao L., 2008. Geochemistry of picrites and associated lavas of a Devonian island arc in the northern Junggar Terrane, Xinjiang (NW China): Implications for petrogenesis, arc mantle sources and tectonic settings . Lithos 105, 379–395.

Zhang Z., Mao J., Saunders A., Ai Yu, Li Y., Zhao L., 2009. Petrogenetic modeling of three mafic–ultramafic layered intrusions in the Emeishan large igneous province, SW China, based on isotopic and bulk chemical constraints Lithos 113, 369–392.

# **Appendix I.** Whole rock chemical analysis

| Sample | SiO2 (%) | TiO2 (%) | Al2O3 (%) | Cr2O3 (%) | Fe2O3 (%) | MnO (%) | MgO (%) | NiO (%) | CaO (%) | Na2O (%) | K2O (%) | P2O5 (%) | total | H2O (%) |
|---|---|---|---|---|---|---|---|---|---|---|---|---|---|---|
| **AP-33_A** | 37,87 | 0,10 | 3,52 | 0,87 | 10,00 | 0,17 | 34,40 | 0,26 | 0,36 | 0,10 | 0,01 | 0,03 | 87,68 | 12,34 |
| **AP-34_A** | 42,73 | 0,56 | 4,46 | 0,17 | 10,58 | 0,16 | 29,96 | 0,27 | 3,32 | 0,08 | 0,02 | 0,09 | 92,39 | 7,61 |
| **AP-035_A** | 36,16 | 0,50 | 2,92 | 0,09 | 9,86 | 0,16 | 30,40 | 0,26 | 1,55 | 0,01 | 0,03 | 0,07 | 82,00 | 17,99 |
| **AP-036_A** | 40,29 | 0,61 | 3,52 | 0,11 | 11,09 | 0,17 | 32,05 | 0,31 | 2,70 | 0,04 | 0,02 | 0,08 | 90,99 | 9,00 |
| **AP-37_A** | 41,15 | 0,68 | 3,86 | 0,35 | 12,84 | 0,17 | 29,64 | 0,28 | 2,99 | 0,03 | 0,01 | 0,08 | 92,08 | 7,94 |
| **AP-38_A** | 42,42 | 0,59 | 4,48 | 0,49 | 13,08 | 0,18 | 26,05 | 0,22 | 5,66 | 0,06 | 0,02 | 0,06 | 93,31 | 6,69 |
| **AP-46_A** | 42,97 | 0,65 | 4,51 | 0,49 | 13,41 | 0,17 | 27,12 | 0,22 | 3,85 | 0,06 | 0,16 | 0,07 | 93,67 | 6,33 |
| **AP-47_A** | 41,44 | 0,66 | 4,64 | 0,43 | 12,62 | 0,19 | 27,60 | 0,23 | 4,72 | 0,26 | 0,36 | 0,06 | 93,20 | 6,81 |
| **AP-49_A** | 32,79 | 0,37 | 2,61 | 0,32 | 10,05 | 0,15 | 29,08 | 0,26 | 1,25 | 0,04 | 0,01 | 0,05 | 76,98 | 23,01 |
| **AP-50_A** | 42,81 | 0,70 | 4,31 | 0,37 | 13,97 | 0,19 | 25,43 | 0,13 | 6,07 | 0,29 | 0,03 | 0,07 | 94,38 | 5,62 |
| **AP-51_A** | 40,69 | 0,59 | 4,22 | 0,55 | 13,29 | 0,18 | 28,75 | 0,24 | 3,56 | 0,34 | 0,04 | 0,05 | 92,51 | 7,49 |
| **AP-54_A1** | 48,14 | 0,53 | 4,86 | 0,37 | 10,87 | 0,20 | 20,54 | 0,11 | 9,43 | 0,37 | 0,04 | 0,04 | 95,50 | 4,50 |
| **AP-52_A** | 41,66 | 0,92 | 4,32 | 0,19 | 12,02 | 0,19 | 28,40 | 0,21 | 3,90 | 0,09 | 0,02 | 0,11 | 92,02 | 7,98 |
| **AP-53_A** | 43,82 | 1,04 | 4,57 | 0,19 | 12,18 | 0,16 | 23,27 | 0,23 | 5,40 | 0,20 | 0,06 | 0,12 | 91,24 | 8,76 |
| **AP-54_A** | 42,66 | 0,67 | 4,84 | 0,55 | 14,05 | 0,18 | 25,68 | 0,27 | 4,39 | 0,13 | 0,02 | 0,07 | 93,51 | 6,49 |
| **AP-55_A** | 43,05 | 1,12 | 5,29 | 0,28 | 14,22 | 0,18 | 24,37 | 0,23 | 4,87 | 0,12 | 0,11 | 0,13 | 93,96 | 6,04 |
| **AP-56_A** | 39,52 | 0,58 | 3,46 | 0,20 | 11,79 | 0,17 | 32,00 | 0,32 | 1,79 | 0,04 | 0,02 | 0,08 | 89,97 | 10,03 |
| **AP_57_A** | 39,79 | 0,55 | 3,27 | 0,21 | 11,52 | 0,17 | 32,17 | 0,33 | 1,39 | 0,05 | 0,02 | 0,08 | 89,55 | 10,45 |
| **AP-58_A** | 41,41 | 0,59 | 3,62 | 0,12 | 11,12 | 0,18 | 31,57 | 0,28 | 1,65 | 0,04 | 0,08 | 0,08 | 90,73 | 9,27 |
| **AP-59_A** | 40,52 | 0,62 | 3,68 | 0,50 | 13,73 | 0,17 | 29,35 | 0,15 | 3,21 | 0,15 | 0,03 | 0,09 | 92,20 | 7,80 |
| **AP-60_A** | 43,98 | 0,09 | 1,75 | 0,61 | 14,39 | 0,16 | 31,17 | 0,20 | 0,19 | 0,02 | 0,01 | 0,03 | 92,60 | 7,41 |
| **AP-61_A** | 42,49 | 0,10 | 4,27 | 0,81 | 11,26 | 0,17 | 30,17 | 0,29 | 1,87 | 0,09 | 0,02 | 0,02 | 91,56 | 8,44 |
| **AP-63_A** | 41,81 | 0,54 | 4,43 | 0,11 | 12,15 | 0,19 | 29,77 | 0,28 | 2,48 | 0,05 | 0,04 | 0,07 | 91,92 | 8,07 |
| **AP_63_A** | 39,66 | 0,14 | 4,82 | 0,66 | 11,66 | 0,16 | 30,45 | 0,19 | 2,18 | 0,05 | 0,01 | 0,03 | 90,01 | 10,00 |
| **AP-64_A** | 43,58 | 0,90 | 5,52 | 0,39 | 13,24 | 0,17 | 24,87 | 0,18 | 4,61 | 0,03 | 0,01 | 0,12 | 93,63 | 6,39 |
| **659** | 39,29 | 0,44 | 3,04 | n.a. | 11,23 | 0,16 | 33,90 | n.a. | 1,64 | 0,00 | 0,01 | 0,06 | 89,77 | 9,68 |
| **660** | 38,47 | 0,39 | 2,83 | n.a. | 12,89 | 0,17 | 33,53 | n.a. | 1,31 | 0,00 | 0,00 | 0,04 | 89,65 | 9,71 |
| **662** | 39,69 | 0,37 | 3,54 | n.a. | 12,81 | 0,18 | 30,77 | n.a. | 3,59 | 0,00 | 0,01 | 0,04 | 91,01 | 8,26 |
| **664** | 40,66 | 0,46 | 3,95 | n.a. | 12,32 | 0,15 | 30,48 | n.a. | 3,74 | 0,08 | 0,01 | 0,05 | 91,91 | 7,58 |

**n.a. – not analyzed**

| Sample | Sc (PPM) | V (PPM) | Cr (PPM) | Co (PPM) | Ni (PPM) | Cu (PPM) | Zn (PPM) | Ga (PPM) | Rb (PPM) | Sr (PPM) | Y (PPM) | Zr (PPM) | Nb (PPM) |
|---|---|---|---|---|---|---|---|---|---|---|---|---|---|
| **AP-33** | 13,70 | 48,40 | 5087,20 | 92,70 | 2032,00 | 17,60 | 80,00 | 2,90 | 1,40 | 2,80 | 5,70 | 4,20 | 1,40 |
| **AP-34** | 12,40 | 86,20 | 948,00 | 82,70 | 2019,40 | 89,70 | 84,90 | 6,10 | 2,00 | 35,80 | 9,90 | 43,10 | 4,30 |
| **AP-35** | 13,20 | 102,90 | 1082,50 | 102,20 | 2230,90 | 42,60 | 90,10 | 3,80 | 1,00 | 15,20 | 8,30 | 29,10 | 3,40 |
| **AP-36** | 12,00 | 121,30 | 966,60 | 95,90 | 2265,20 | 43,20 | 94,30 | 4,60 | 1,80 | 14,80 | 8,00 | 30,80 | 3,20 |
| **AP-37** | 18,00 | 161,30 | 2466,80 | 113,40 | 2139,60 | 62,40 | 88,30 | 6,70 | 1,10 | 19,60 | 9,70 | 39,00 | 3,80 |
| **AP-38** | 22,90 | 180,70 | 4083,40 | 86,00 | 1574,20 | 57,80 | 70,00 | 10,70 | 1,30 | 26,90 | 10,00 | 33,60 | 2,10 |
| **AP-46** | 21,10 | 188,80 | 3425,80 | 96,00 | 2042,40 | 165,10 | 78,90 | 6,20 | 14,30 | 35,50 | 8,70 | 33,20 | 2,00 |
| **AP-47** | 23,10 | 196,80 | 3238,90 | 107,10 | 1842,50 | 57,10 | 88,20 | 9,20 | 18,80 | 20,10 | 8,90 | 32,50 | 2,60 |
| **AP-49** | 13,50 | 105,90 | 2790,20 | 111,10 | 2450,80 | 7,40 | 94,90 | 5,70 | 0,80 | 7,80 | 7,80 | 21,60 | 2,60 |
| **AP-50** | 27,20 | 166,90 | 3007,70 | 78,50 | 943,80 | 48,50 | 58,20 | 6,10 | 2,70 | 20,20 | 9,20 | 34,50 | 3,30 |
| **AP-51** | 21,50 | 200,50 | 3839,60 | 94,30 | 1659,40 | 9,30 | 89,60 | 7,30 | 2,70 | 21,10 | 8,20 | 27,70 | 2,20 |
| **AP-52** | 19,10 | 154,90 | 1073,80 | 79,30 | 1709,20 | 60,30 | 112,20 | 6,70 | 2,10 | 12,40 | 12,00 | 51,60 | 5,00 |
| **AP-53** | 18,20 | 161,00 | 1040,70 | 86,30 | 1965,60 | 79,80 | 91,00 | 9,20 | 4,10 | 26,20 | 11,80 | 63,40 | 5,60 |
| **AP-54** | 25,30 | 211,50 | 3902,30 | 137,50 | 2114,80 | 85,70 | 96,20 | 7,70 | 0,40 | 18,90 | 8,50 | 34,10 | 2,50 |
| **AP-54A** | 20,40 | 217,10 | 3181,20 | 88,00 | 756,70 | 22,20 | 92,50 | 9,40 | 0,40 | 24,60 | 11,00 | 24,30 | 2,30 |
| **AP-55** | 22,60 | 165,90 | 1737,20 | 76,60 | 1649,40 | 90,00 | 90,40 | 10,30 | 8,00 | 18,40 | 12,80 | 68,20 | 5,60 |
| **AP-56** | 15,50 | 119,40 | 1109,70 | 98,90 | 2372,70 | 59,00 | 123,90 | 6,70 | 1,50 | 10,90 | 8,50 | 31,60 | 3,20 |
| **AP-57** | 13,70 | 115,40 | 1205,30 | 98,80 | 2507,80 | 25,80 | 111,00 | 4,50 | 2,00 | 6,90 | 8,50 | 29,50 | 3,20 |
| **AP-58** | 14,50 | 115,90 | 1018,80 | 79,40 | 2156,00 | 124,20 | 83,70 | 6,10 | 6,40 | 4,80 | 7,90 | 30,30 | 3,90 |
| **AP-59** | 17,50 | 143,00 | 3019,90 | 88,40 | 1067,40 | 14,00 | 77,40 | 6,40 | 2,60 | 13,00 | 8,10 | 34,00 | 3,30 |
| **AP-60** | 7,60 | 47,70 | 3648,20 | 104,40 | 1457,20 | 5,10 | 84,90 | 3,10 | 1,60 | 3,80 | 4,10 | 0,40 | 1,40 |
| **AP-61** | 15,40 | 43,50 | 5355,50 | 92,60 | 2045,30 | 22,30 | 73,70 | 2,80 | 2,40 | 7,20 | 8,10 | 5,60 | 1,80 |
| **AP-62** | 19,00 | 83,20 | 3997,10 | 89,90 | 1445,40 | 5,10 | 74,20 | 3,00 | 1,40 | 7,80 | 6,00 | 5,00 | 1,40 |
| **AP-63** | 10,50 | 120,20 | 1039,40 | 87,40 | 2103,40 | 69,70 | 94,10 | 6,30 | 9,90 | 19,90 | 9,20 | 42,30 | 3,70 |
| **AP-64** | 22,10 | 173,70 | 2615,70 | 101,80 | 1331,00 | 56,50 | 90,10 | 8,40 | 0,80 | 24,40 | 11,20 | 54,50 | 4,80 |
| **659** | 9,61 | 108,46 | 1222,47 | 119,87 | 2364,85 | 36,37 | 64,34 | 4,19 | 0,28 | 4,39 | 5,10 | 1,63 | 3,12 |
| **660** | 16,58 | 133,10 | 4045,99 | 174,38 | 5640,62 | 5,69 | 150,64 | 5,01 | 0,33 | 6,38 | 6,67 | 2,68 | 3,84 |
| **662** | 12,42 | 127,25 | 3422,46 | 119,08 | 5632,74 | 21,92 | 64,91 | 4,06 | 0,61 | 13,44 | 5,45 | 2,15 | 1,28 |
| **664** | 18,30 | 164,19 | 3669,39 | 60,35 | 1508,42 | 25,92 | 62,64 | 5,80 | 0,27 | 11,66 | 6,60 | 3,94 | 1,74 |

| Sample | Ag (PPM) | Cu (%) | As (PPM) | Bi (PPM) | Sb (PPM) | Se (PPM) | S (%) | Zn (%) | Pb (%) | Sn (PPM) |
|---|---|---|---|---|---|---|---|---|---|---|
| **AP-33_ore** | 1,80 | 0,00 | 14,00 | 0,00 | 4,30 | 0,00 | 0,13 | 0,01 | 0,00 | 1,30 |
| **AP-34_ore** | 6,60 | 0,01 | 17,00 | 2,00 | 4,10 | 0,00 | 0,27 | 0,01 | 0,00 | 1,40 |
| **AP-35_ore** | 3,30 | 0,00 | 19,00 | 0,00 | 3,90 | 0,00 | 0,08 | 0,01 | 0,00 | 0,00 |
| **AP-36** | 1,50 | 0,00 | 10,00 | 0,00 | 5,40 | 0,00 | 0,20 | 0,01 | 0,00 | 0,00 |
| **AP-37** | 0,30 | 0,00 | 15,00 | 0,00 | 1,30 | 0,00 | 0,33 | 0,01 | 0,00 | 2,80 |
| **AP-38_ore** | 4,70 | 0,01 | 15,00 | 0,00 | 3,10 | 0,00 | 0,17 | 0,01 | 0,00 | 5,70 |
| **AP-46** | 1,20 | 0,02 | 13,00 | 0,00 | 1,30 | 0,00 | 0,29 | 0,01 | 0,00 | 3,60 |
| **AP-47** | 5,60 | 0,01 | 15,00 | 1,00 | 6,10 | 0,00 | 0,11 | 0,01 | 0,00 | 0,00 |
| **AP-49_ore** | 3,50 | 0,00 | 18,00 | 2,00 | 6,00 | 0,00 | 0,06 | 0,01 | 0,00 | 5,40 |
| **AP-50** | 8,40 | 0,00 | 18,00 | 0,00 | 8,80 | 0,00 | 0,02 | 0,01 | 0,00 | 2,70 |
| **AP-51** | 2,90 | 0,00 | 17,00 | 0,00 | 2,80 | 0,00 | 0,06 | 0,01 | 0,00 | 5,70 |
| **AP-52_ore** | 7,50 | 0,01 | 21,00 | 0,00 | 3,10 | 0,00 | 0,12 | 0,01 | 0,00 | 0,00 |
| **AP-53** | 2,10 | 0,01 | 14,00 | 1,00 | 6,80 | 0,00 | 0,05 | 0,01 | 0,00 | 0,00 |
| **AP-54** | 9,40 | 0,01 | 19,00 | 0,00 | 1,30 | 0,00 | 0,17 | 0,01 | 0,00 | 0,00 |
| **AP-54a** | 2,40 | 0,00 | 14,00 | 0,00 | 3,10 | 0,00 | 0,22 | 0,01 | 0,00 | 0,00 |
| **AP-55_ore** | 5,90 | 0,00 | 16,00 | 1,00 | 6,70 | 0,00 | 0,10 | 0,01 | 0,00 | 0,00 |
| **AP-56_ore** | 3,80 | 0,01 | 15,00 | 0,00 | 5,90 | 0,00 | 0,06 | 0,02 | 0,00 | 0,80 |
| **AP-57_ore** | 5,40 | 0,00 | 13,00 | 0,00 | 8,60 | 0,00 | 0,12 | 0,01 | 0,00 | 0,00 |
| **AP-58** | 2,60 | 0,01 | 15,00 | 0,00 | 3,10 | 0,00 | 0,04 | 0,01 | 0,00 | 0,00 |
| **AP-59** | 1,10 | 0,00 | 19,00 | 0,00 | 3,50 | 0,00 | 0,01 | 0,01 | 0,00 | 0,00 |
| **AP-60_ore** | 4,90 | 0,00 | 12,00 | 0,00 | 6,80 | 0,00 | 0,02 | 0,01 | 0,00 | 2,80 |
| **AP-61_ore** | 1,80 | 0,00 | 12,00 | 1,00 | 1,30 | 0,00 | 0,09 | 0,01 | 0,00 | 0,00 |
| **AP-62_ore** | 3,10 | 0,00 | 21,00 | 0,00 | 7,00 | 0,00 | 0,01 | 0,01 | 0,00 | 0,00 |
| **AP-63_ore** | 1,90 | 0,00 | 10,00 | 1,00 | 3,20 | 0,00 | 0,41 | 0,01 | 0,00 | 6,00 |
| **AP-64** | 6,10 | 0,01 | 15,00 | 2,00 | 5,70 | 0,00 | 0,20 | 0,01 | 0,00 | 0,00 |

| Analyte Symbol | SiO2 | Al2O3 | Fe2O3(T) | MnO | MgO | CaO | Na2O | K2O | TiO2 | P2O5 | LOI | Total |
|---|---|---|---|---|---|---|---|---|---|---|---|---|
| Unit Symbol | % | % | % | % | % | % | % | % | % | % | % | % |
| **AP-34** | 41,46 | 4,42 | 10,77 | 0,14 | 30,37 | 3,34 | 0,08 | < 0.01 | 0,56 | 0,08 | 7,89 | 99,11 |
| **AP-35** | 39,29 | 3,20 | 11,66 | 0,15 | 32,75 | 1,75 | 0,03 | 0,02 | 0,59 | 0,08 | 9,65 | 99,16 |
| **AP-36** | 39,42 | 3,39 | 11,39 | 0,16 | 32,79 | 2,75 | 0,04 | < 0.01 | 0,63 | 0,07 | 9,30 | 99,94 |
| **AP-37** | 41,06 | 3,80 | 12,99 | 0,16 | 30,46 | 3,01 | 0,03 | < 0.01 | 0,70 | 0,07 | 8,30 | 100,60 |
| **AP-46** | 42,24 | 4,47 | 13,65 | 0,15 | 27,60 | 3,86 | 0,07 | 0,15 | 0,67 | 0,05 | 6,95 | 99,86 |
| **AP-47** | 40,53 | 4,61 | 12,44 | 0,18 | 28,07 | 4,77 | 0,25 | 0,34 | 0,67 | 0,05 | 7,63 | 99,53 |
| **AP-49** | 38,57 | 3,01 | 12,88 | 0,15 | 33,63 | 1,49 | 0,04 | < 0.01 | 0,47 | 0,04 | 9,92 | 100,20 |
| **AP-50** | 42,26 | 4,30 | 14,13 | 0,18 | 26,07 | 6,16 | 0,30 | 0,02 | 0,73 | 0,06 | 5,90 | 100,10 |
| **AP-51** | 40,23 | 4,15 | 13,66 | 0,18 | 29,83 | 3,63 | 0,26 | 0,03 | 0,62 | 0,03 | 8,05 | 100,70 |
| **AP-52** | 41,43 | 4,29 | 12,53 | 0,19 | 29,49 | 4,01 | 0,13 | < 0.01 | 0,94 | 0,09 | 7,76 | 100,90 |
| **AP-53** | 44,99 | 4,71 | 12,90 | 0,15 | 25,09 | 5,60 | 0,19 | 0,05 | 1,10 | 0,12 | 5,98 | 100,90 |
| **AP-54** | 42,41 | 4,85 | 14,25 | 0,17 | 26,69 | 4,49 | 0,15 | 0,02 | 0,70 | 0,06 | 6,20 | 99,97 |
| **AP-54a** | 48,73 | 4,79 | 10,65 | 0,20 | 20,98 | 9,89 | 0,39 | 0,03 | 0,54 | 0,02 | 3,83 | 100,10 |
| **AP-56** | 39,96 | 3,37 | 11,86 | 0,17 | 32,86 | 1,84 | 0,03 | 0,02 | 0,59 | 0,08 | 9,88 | 100,70 |
| **AP-57** | 39,76 | 3,31 | 11,94 | 0,16 | 33,28 | 1,39 | 0,03 | < 0.01 | 0,57 | 0,06 | 9,92 | 100,40 |
| **AP-58** | 41,07 | 3,54 | 11,47 | 0,17 | 32,81 | 1,68 | 0,03 | 0,07 | 0,62 | 0,06 | 9,36 | 100,90 |
| **AP-59** | 40,02 | 3,72 | 13,96 | 0,16 | 29,83 | 3,09 | 0,13 | 0,02 | 0,63 | 0,07 | 8,22 | 99,84 |
| **AP-60** | 43,36 | 1,72 | 14,94 | 0,16 | 32,10 | 0,20 | 0,01 | < 0.01 | 0,09 | 0,01 | 7,82 | 100,40 |
| **AP-63** | 41,36 | 4,49 | 12,13 | 0,18 | 30,80 | 2,38 | 0,04 | 0,04 | 0,54 | 0,07 | 8,07 | 100,10 |
| **AP-64** | 43,62 | 5,68 | 13,30 | 0,15 | 25,53 | 4,51 | 0,07 | 0,01 | 0,93 | 0,11 | 5,68 | 99,61 |
| **KV-660** | 38,12 | 3,01 | 13,25 | 0,17 | 32,93 | 1,30 | 0,03 | < 0.01 | 0,51 | 0,06 | 9,62 | 99,00 |
| **KV-662** | 39,31 | 3,76 | 13,02 | 0,18 | 29,77 | 3,60 | 0,11 | 0,02 | 0,51 | 0,05 | 8,42 | 98,75 |
| **AP-55** | 43,19 | 5,27 | 14,15 | 0,16 | 25,57 | 4,98 | 0,14 | 0,11 | 1,17 | 0,12 | 5,74 | 100,60 |

| Analyte Symbol | Sc | Be | V | Ba | Sr | Y | Zr | Cr | Co | Ni | Cu | Zn | Ga | Ge |
|---|---|---|---|---|---|---|---|---|---|---|---|---|---|---|
| Unit | ppm | ppm | ppm | ppm | ppm | ppm | ppm | ppm | ppm | ppm | ppm | ppm | ppm | ppm |
| Detection Limit | 1 | 1 | 5 | 3 | 2 | 2 | 4 | 20 | 1 | 20 | 10 | 30 | 1 | 1 |
| **AP-34** | 10 | < 1 | 87 | 4 | 38 | 5 | 44 | 1030 | 103 | 2040 | 100 | 80 | 8 | 1 |
| **AP-35** | 12 | < 1 | 94 | 9 | 16 | 5 | 34 | 1200 | 118 | 2210 | 50 | 90 | 6 | 2 |
| **AP-36** | 12 | < 1 | 110 | 5 | 15 | 6 | 35 | 1050 | 98 | 2160 | 50 | 90 | 6 | 1 |
| **AP-37** | 14 | < 1 | 132 | < 3 | 20 | 6 | 43 | 2450 | 112 | 1920 | 60 | 80 | 8 | 3 |
| **AP-46** | 17 | < 1 | 169 | 12 | 35 | 6 | 35 | 3920 | 119 | 1750 | 180 | 80 | 9 | 2 |
| **AP-47** | 17 | < 1 | 168 | 20 | 20 | 6 | 35 | 3680 | 112 | 1840 | 60 | 90 | 9 | 2 |
| **AP-49** | 11 | < 1 | 93 | < 3 | 8 | 4 | 26 | 2960 | 131 | 2380 | < 10 | 110 | 6 | 2 |
| **AP-50** | 21 | < 1 | 142 | 4 | 20 | 7 | 37 | 3070 | 74 | 840 | 50 | 50 | 8 | 2 |
| **AP-51** | 17 | < 1 | 160 | 6 | 22 | 5 | 30 | 3780 | 92 | 1660 | < 10 | 100 | 8 | 2 |
| **AP-52** | 15 | < 1 | 136 | < 3 | 13 | 8 | 60 | 1100 | 91 | 1680 | 70 | 110 | 8 | 2 |
| **AP-53** | 17 | < 1 | 153 | 5 | 27 | 9 | 67 | 1100 | 90 | 1680 | 90 | 80 | 9 | 2 |
| **AP-54** | 19 | < 1 | 171 | < 3 | 18 | 6 | 37 | 3580 | 128 | 1750 | 90 | 80 | 8 | 2 |
| **AP-54a** | 17 | < 1 | 179 | < 3 | 25 | 8 | 27 | 3290 | 101 | 710 | 20 | 100 | 11 | 2 |
| **AP-56** | 12 | < 1 | 99 | < 3 | 11 | 4 | 36 | 1130 | 109 | 2260 | 100 | 130 | 6 | 1 |
| **AP-57** | 11 | < 1 | 101 | < 3 | 7 | 5 | 32 | 1150 | 107 | 2380 | 30 | 110 | 6 | 1 |
| **AP-58** | 12 | < 1 | 101 | 4 | 5 | 5 | 35 | 1140 | 82 | 1990 | 140 | 80 | 7 | 2 |
| **AP-59** | 13 | < 1 | 114 | 4 | 13 | 6 | 37 | 3380 | 81 | 980 | < 10 | 90 | 7 | 2 |
| **AP-60** | 7 | < 1 | 56 | < 3 | 4 | < 2 | < 4 | 4010 | 111 | 1460 | < 10 | 120 | 4 | 2 |
| **AP-63** | 9 | 4 | 111 | 4 | 21 | 6 | 48 | 1090 | 101 | 1860 | 80 | 90 | 8 | 3 |
| **AP-64** | 17 | < 1 | 151 | 4 | 26 | 9 | 59 | 2560 | 100 | 1290 | 60 | 80 | 9 | 1 |
| **KV-660** | 11 | < 1 | 94 | < 3 | 4 | 4 | 28 | 3100 | 117 | 2110 | 10 | 120 | 6 | 2 |
| **KV-662** | 14 | < 1 | 134 | 3 | 16 | 6 | 29 | 4090 | 122 | 1920 | 30 | 90 | 7 | 2 |
| **AP-55** | 18 | < 1 | 165 | 7 | 19 | 9 | 70 | 1730 | 83 | 1500 | 100 | 80 | 10 | 2 |

| Analyte Symbol | As | Rb | Nb | Mo | Ag | In | Sn | Sb | Cs | La | Ce | Pr | Nd | Sm |
|---|---|---|---|---|---|---|---|---|---|---|---|---|---|---|
| Unit | ppm | ppm | ppm | ppm | ppm | ppm | ppm | ppm | ppm | ppm | ppm | ppm | ppm | ppm |
| Detection Limit | 5 | 2 | 1 | 2 | 0.5 | 0.2 | 1 | 0.5 | 0.5 | 0.1 | 0.1 | 0.05 | 0.1 | 0.1 |
| **AP-34** | < 5 | < 2 | 3 | < 2 | < 0.5 | < 0.2 | < 1 | < 0.5 | < 0.5 | 6,3 | 13,9 | 1,73 | 7,8 | 1,8 |
| **AP-35** | < 5 | < 2 | 3 | < 2 | < 0.5 | < 0.2 | < 1 | 0,8 | < 0.5 | 5,2 | 11,1 | 1,41 | 6,5 | 1,5 |
| **AP-36** | < 5 | < 2 | 2 | < 2 | < 0.5 | < 0.2 | < 1 | < 0.5 | < 0.5 | 4,2 | 11 | 1,51 | 7 | 1,7 |
| **AP-37** | < 5 | < 2 | 3 | < 2 | < 0.5 | < 0.2 | < 1 | < 0.5 | < 0.5 | 6,5 | 15,1 | 1,88 | 8,3 | 1,9 |
| **AP-46** | < 5 | 11 | < 1 | < 2 | < 0.5 | < 0.2 | < 1 | < 0.5 | 0,8 | 2,5 | 6,8 | 1,02 | 5,4 | 1,6 |
| **AP-47** | < 5 | 18 | < 1 | < 2 | < 0.5 | < 0.2 | < 1 | < 0.5 | 1,9 | 3,5 | 8,6 | 1,18 | 5,8 | 1,7 |
| **AP-49** | < 5 | < 2 | 1 | < 2 | < 0.5 | < 0.2 | < 1 | < 0.5 | < 0.5 | 2,6 | 7,4 | 1,05 | 4,8 | 1,2 |
| **AP-50** | < 5 | < 2 | 2 | < 2 | < 0.5 | < 0.2 | < 1 | < 0.5 | < 0.5 | 3,8 | 10,7 | 1,44 | 6,9 | 1,7 |
| **AP-51** | < 5 | < 2 | < 1 | < 2 | < 0.5 | < 0.2 | < 1 | < 0.5 | < 0.5 | 1,9 | 4,8 | 0,71 | 3,6 | 1,3 |
| **AP-52** | < 5 | < 2 | 4 | < 2 | < 0.5 | < 0.2 | < 1 | < 0.5 | < 0.5 | 5,8 | 15 | 1,95 | 9,3 | 2,4 |
| **AP-53** | < 5 | < 2 | 5 | < 2 | < 0.5 | < 0.2 | < 1 | < 0.5 | < 0.5 | 7,1 | 18,6 | 2,56 | 12,1 | 2,9 |
| **AP-54** | < 5 | < 2 | < 1 | < 2 | < 0.5 | < 0.2 | < 1 | < 0.5 | < 0.5 | 1,9 | 5,4 | 0,79 | 4,1 | 1,3 |
| **AP-54a** | < 5 | < 2 | < 1 | < 2 | < 0.5 | < 0.2 | < 1 | < 0.5 | < 0.5 | 2,9 | 8,3 | 1,19 | 6,1 | 1,8 |
| **AP-56** | < 5 | < 2 | 2 | < 2 | < 0.5 | < 0.2 | 4 | < 0.5 | < 0.5 | 2,1 | 5,7 | 0,81 | 4,1 | 1,2 |
| **AP-57** | < 5 | < 2 | 2 | < 2 | < 0.5 | < 0.2 | < 1 | < 0.5 | < 0.5 | 3,2 | 8,3 | 1,07 | 5,3 | 1,3 |
| **AP-58** | < 5 | 5 | 2 | < 2 | < 0.5 | < 0.2 | < 1 | < 0.5 | 0,6 | 3,9 | 10,6 | 1,48 | 7 | 1,7 |
| **AP-59** | < 5 | < 2 | 2 | < 2 | < 0.5 | < 0.2 | < 1 | < 0.5 | < 0.5 | 4,5 | 11,1 | 1,46 | 6,8 | 1,8 |
| **AP-60** | < 5 | < 2 | < 1 | < 2 | < 0.5 | < 0.2 | < 1 | < 0.5 | < 0.5 | 0,8 | 1,6 | 0,2 | 0,7 | 0,2 |
| **AP-63** | < 5 | 7 | < 1 | < 2 | < 0.5 | < 0.2 | 3 | < 0.5 | 1,2 | 6,7 | 15 | 1,85 | 7,9 | 1,7 |
| **AP-64** | < 5 | < 2 | 3 | < 2 | < 0.5 | < 0.2 | < 1 | < 0.5 | < 0.5 | 7,7 | 18,8 | 2,38 | 10,7 | 2,5 |
| **KV-660** | < 5 | < 2 | 1 | < 2 | < 0.5 | < 0.2 | < 1 | < 0.5 | < 0.5 | 2,1 | 5,7 | 0,81 | 4,1 | 1,1 |
| **KV-662** | < 5 | < 2 | < 1 | < 2 | < 0.5 | < 0.2 | < 1 | < 0.5 | < 0.5 | 2,6 | 7 | 0,97 | 4,8 | 1,3 |
| **AP-55** | < 5 | 7 | 4 | < 2 | < 0.5 | < 0.2 | < 1 | < 0.5 | 0,8 | 7,2 | 18,7 | 2,57 | 11,6 | 3 |

| Analyte Symbol | Eu | Gd | Tb | Dy | Ho | Er | Tm | Yb | Lu | Hf | Ta | W | Tl | Pb |
|---|---|---|---|---|---|---|---|---|---|---|---|---|---|---|
| Unit | ppm | ppm | ppm | ppm | ppm | ppm | ppm | ppm | ppm | ppm | ppm | ppm | ppm | ppm |
| Detection Limit | 0.05 | 0.1 | 0.1 | 0.1 | 0.1 | 0.1 | 0.05 | 0.1 | 0.04 | 0.2 | 0.1 | 1 | 0.1 | 5 |
| **AP-34** | 0,5 | 1,7 | 0,2 | 1,3 | 0,2 | 0,6 | 0,08 | 0,5 | 0,08 | 1,2 | 0,2 | 3 | 0,1 | < 5 |
| **AP-35** | 0,37 | 1,5 | 0,2 | 1,2 | 0,2 | 0,6 | 0,07 | 0,4 | 0,07 | 1 | 0,4 | 2 | < 0.1 | < 5 |
| **AP-36** | 0,51 | 1,6 | 0,2 | 1,3 | 0,2 | 0,6 | 0,09 | 0,5 | 0,08 | 1,1 | 0,2 | 2 | 0,3 | < 5 |
| **AP-37** | 0,42 | 2 | 0,3 | 1,6 | 0,3 | 0,7 | 0,1 | 0,6 | 0,09 | 1,3 | 0,2 | 2 | 0,5 | 9 |
| **AP-46** | 0,25 | 1,7 | 0,3 | 1,5 | 0,3 | 0,7 | 0,1 | 0,6 | 0,1 | 1,1 | < 0.1 | 2 | 0,1 | 13 |
| **AP-47** | 0,47 | 1,8 | 0,3 | 1,6 | 0,3 | 0,8 | 0,1 | 0,6 | 0,1 | 1,1 | 0,4 | 2 | 0,2 | < 5 |
| **AP-49** | 0,34 | 1,3 | 0,2 | 1,1 | 0,2 | 0,5 | 0,07 | 0,4 | 0,07 | 0,8 | 0,1 | 2 | < 0.1 | < 5 |
| **AP-50** | 0,53 | 1,8 | 0,3 | 1,5 | 0,3 | 0,7 | 0,1 | 0,7 | 0,1 | 1,1 | 0,2 | 2 | < 0.1 | < 5 |
| **AP-51** | 0,3 | 1,4 | 0,2 | 1,2 | 0,2 | 0,6 | 0,08 | 0,5 | 0,08 | 0,8 | 0,1 | 2 | < 0.1 | < 5 |
| **AP-52** | 0,51 | 2,5 | 0,4 | 1,9 | 0,3 | 0,9 | 0,12 | 0,7 | 0,11 | 1,6 | 0,3 | 2 | < 0.1 | < 5 |
| **AP-53** | 0,44 | 2,8 | 0,4 | 2,2 | 0,4 | 1 | 0,14 | 0,8 | 0,13 | 1,8 | 0,4 | 2 | < 0.1 | < 5 |
| **AP-54** | 0,29 | 1,5 | 0,2 | 1,3 | 0,3 | 0,7 | 0,09 | 0,6 | 0,11 | 1,1 | < 0.1 | 2 | < 0.1 | < 5 |
| **AP-54a** | 0,55 | 1,9 | 0,3 | 1,9 | 0,3 | 0,9 | 0,13 | 0,8 | 0,12 | 0,9 | 0,3 | 4 | < 0.1 | < 5 |
| **AP-56** | 0,36 | 1,3 | 0,2 | 1,1 | 0,2 | 0,5 | 0,07 | 0,4 | 0,07 | 1 | 0,2 | 2 | < 0.1 | 27 |
| **AP-57** | 0,23 | 1,1 | 0,2 | 1 | 0,2 | 0,5 | 0,08 | 0,5 | 0,08 | 0,8 | 0,2 | 1 | < 0.1 | < 5 |
| **AP-58** | 0,31 | 1,6 | 0,2 | 1,4 | 0,3 | 0,7 | 0,09 | 0,6 | 0,09 | 0,9 | 0,2 | 1 | < 0.1 | 21 |
| **AP-59** | 0,52 | 1,7 | 0,3 | 1,5 | 0,3 | 0,7 | 0,1 | 0,6 | 0,09 | 1,1 | 0,2 | 1 | < 0.1 | < 5 |
| **AP-60** | < 0.05 | 0,2 | < 0.1 | 0,2 | < 0.1 | 0,1 | < 0.05 | 0,1 | < 0.04 | < 0.2 | < 0.1 | 2 | < 0.1 | < 5 |
| **AP-63** | 0,52 | 1,6 | 0,2 | 1,3 | 0,2 | 0,7 | 0,09 | 0,6 | 0,09 | 1,2 | 0,2 | 1 | < 0.1 | 8 |
| **AP-64** | 0,76 | 2,4 | 0,4 | 2 | 0,4 | 0,9 | 0,13 | 0,8 | 0,12 | 1,7 | 0,3 | 2 | < 0.1 | < 5 |
| **KV-660** | 0,21 | 1,1 | 0,2 | 1 | 0,2 | 0,5 | 0,06 | 0,4 | 0,07 | 0,8 | 1,2 | 1 | < 0.1 | < 5 |
| **KV-662** | 0,3 | 1,4 | 0,2 | 1,2 | 0,2 | 0,6 | 0,08 | 0,5 | 0,07 | 0,9 | 0,2 | 1 | < 0.1 | < 5 |
| **AP-55** | 0,66 | 2,9 | 0,4 | 2,2 | 0,4 | 1 | 0,13 | 0,8 | 0,12 | 2 | 0,4 | 2 | < 0.1 | < 5 |

| Analyte Symbol | Bi | Th | U |
|---|---|---|---|
| Unit | ppm | ppm | ppm |
| Detection Limit | 0.4 | 0.1 | 0.1 |
| **AP-34** | < 0.4 | 0,4 | 0,2 |
| **AP-35** | < 0.4 | 0,2 | 0,2 |
| **AP-36** | 0,4 | 0,2 | < 0.1 |
| **AP-37** | 0,6 | 0,4 | 0,2 |
| **AP-46** | < 0.4 | 0,3 | 0,3 |
| **AP-47** | < 0.4 | 0,3 | 0,6 |
| **AP-49** | < 0.4 | 0,2 | 0,6 |
| **AP-50** | < 0.4 | 0,3 | 3,1 |
| **AP-51** | < 0.4 | 0,2 | 1,7 |
| **AP-52** | < 0.4 | 0,2 | 0,2 |
| **AP-53** | < 0.4 | 0,7 | 0,5 |
| **AP-54** | < 0.4 | 0,2 | 0,7 |
| **AP-54a** | < 0.4 | 0,4 | 0,7 |
| **AP-56** | < 0.4 | 0,2 | 0,1 |
| **AP-57** | < 0.4 | 0,1 | 0,4 |
| **AP-58** | < 0.4 | 0,2 | 0,5 |
| **AP-59** | < 0.4 | 0,3 | 0,2 |
| **AP-60** | < 0.4 | 0,9 | 0,3 |
| **AP-63** | 0,6 | 0,4 | 0,2 |
| **AP-64** | < 0.4 | 0,6 | 0,3 |
| **KV-660** | < 0.4 | 0,2 | 0,1 |
| **KV-662** | < 0.4 | 0,2 | 1,6 |
| **AP-55** | < 0.4 | 0,3 | 0,3 |

| Analyte Symbol | Y | La | Ce | Pr | Nd | Sm | Eu | Gd | Tb | Dy | Ho | Er | Tm | Yb | Lu |
|---|---|---|---|---|---|---|---|---|---|---|---|---|---|---|---|
| Unit | ppm | ppm | ppm | ppm | ppm | ppm | ppm | ppm | ppm | ppm | ppm | ppm | ppm | ppm | ppm |
| Detection Limit | 2 | 0.1 | 0.1 | 0.05 | 0.1 | 0.1 | 0.05 | 0.1 | 0.1 | 0.1 | 0.1 | 0.1 | 0.05 | 0.1 | 0.04 |
| AP-34 | 5 | 6,3 | 13,9 | 1,73 | 7,8 | 1,8 | 0,5 | 1,7 | 0,2 | 1,3 | 0,2 | 0,6 | 0,08 | 0,5 | 0,08 |
| AP-35 | 5 | 5,2 | 11,1 | 1,41 | 6,5 | 1,5 | 0,37 | 1,5 | 0,2 | 1,2 | 0,2 | 0,6 | 0,07 | 0,4 | 0,07 |
| AP-36 | 6 | 4,2 | 11 | 1,51 | 7 | 1,7 | 0,51 | 1,6 | 0,2 | 1,3 | 0,2 | 0,6 | 0,09 | 0,5 | 0,08 |
| AP-37 | 6 | 6,5 | 15,1 | 1,88 | 8,3 | 1,9 | 0,42 | 2 | 0,3 | 1,6 | 0,3 | 0,7 | 0,1 | 0,6 | 0,09 |
| AP-46 | 6 | 2,5 | 6,8 | 1,02 | 5,4 | 1,6 | 0,25 | 1,7 | 0,3 | 1,5 | 0,3 | 0,7 | 0,1 | 0,6 | 0,1 |
| AP-47 | 6 | 3,5 | 8,6 | 1,18 | 5,8 | 1,7 | 0,47 | 1,8 | 0,3 | 1,6 | 0,3 | 0,8 | 0,1 | 0,6 | 0,1 |
| AP-49 | 4 | 2,6 | 7,4 | 1,05 | 4,8 | 1,2 | 0,34 | 1,3 | 0,2 | 1,1 | 0,2 | 0,5 | 0,07 | 0,4 | 0,07 |
| AP-50 | 7 | 3,8 | 10,7 | 1,44 | 6,9 | 1,7 | 0,53 | 1,8 | 0,3 | 1,5 | 0,3 | 0,7 | 0,1 | 0,7 | 0,1 |
| AP-51 | 5 | 1,9 | 4,8 | 0,71 | 3,6 | 1,3 | 0,3 | 1,4 | 0,2 | 1,2 | 0,2 | 0,6 | 0,08 | 0,5 | 0,08 |
| AP-52 | 8 | 5,8 | 15 | 1,95 | 9,3 | 2,4 | 0,51 | 2,5 | 0,4 | 1,9 | 0,3 | 0,9 | 0,12 | 0,7 | 0,11 |
| AP-53 | 9 | 7,1 | 18,6 | 2,56 | 12,1 | 2,9 | 0,44 | 2,8 | 0,4 | 2,2 | 0,4 | 1 | 0,14 | 0,8 | 0,13 |
| AP-54 | 6 | 1,9 | 5,4 | 0,79 | 4,1 | 1,3 | 0,29 | 1,5 | 0,2 | 1,3 | 0,3 | 0,7 | 0,09 | 0,6 | 0,11 |
| AP-54a | 8 | 2,9 | 8,3 | 1,19 | 6,1 | 1,8 | 0,55 | 1,9 | 0,3 | 1,9 | 0,3 | 0,9 | 0,13 | 0,8 | 0,12 |
| AP-56 | 4 | 2,1 | 5,7 | 0,81 | 4,1 | 1,2 | 0,36 | 1,3 | 0,2 | 1,1 | 0,2 | 0,5 | 0,07 | 0,4 | 0,07 |
| AP-57 | 5 | 3,2 | 8,3 | 1,07 | 5,3 | 1,3 | 0,23 | 1,1 | 0,2 | 1 | 0,2 | 0,5 | 0,08 | 0,5 | 0,08 |
| AP-58 | 5 | 3,9 | 10,6 | 1,48 | 7 | 1,7 | 0,31 | 1,6 | 0,2 | 1,4 | 0,3 | 0,7 | 0,09 | 0,6 | 0,09 |
| AP-59 | 6 | 4,5 | 11,1 | 1,46 | 6,8 | 1,8 | 0,52 | 1,7 | 0,3 | 1,5 | 0,3 | 0,7 | 0,1 | 0,6 | 0,09 |
| AP-60 | < 2 | 0,8 | 1,6 | 0,2 | 0,7 | 0,2 | < 0.05 | 0,2 | < 0.1 | 0,2 | < 0.1 | 0,1 | < 0.05 | 0,1 | < 0.04 |
| AP-63 | 6 | 6,7 | 15 | 1,85 | 7,9 | 1,7 | 0,52 | 1,6 | 0,2 | 1,3 | 0,2 | 0,7 | 0,09 | 0,6 | 0,09 |
| AP-64 | 9 | 7,7 | 18,8 | 2,38 | 10,7 | 2,5 | 0,76 | 2,4 | 0,4 | 2 | 0,4 | 0,9 | 0,13 | 0,8 | 0,12 |
| KV-660 | 4 | 2,1 | 5,7 | 0,81 | 4,1 | 1,1 | 0,21 | 1,1 | 0,2 | 1 | 0,2 | 0,5 | 0,06 | 0,4 | 0,07 |
| KV-662 | 6 | 2,6 | 7 | 0,97 | 4,8 | 1,3 | 0,3 | 1,4 | 0,2 | 1,2 | 0,2 | 0,6 | 0,08 | 0,5 | 0,07 |
| AP-55 | 9 | 7,2 | 18,7 | 2,57 | 11,6 | 3 | 0,66 | 2,9 | 0,4 | 2,2 | 0,4 | 1 | 0,13 | 0,8 | 0,12 |

| Analyte Symbol | Au | Pt | Pd |
|---|---|---|---|
| Unit | ppb | ppb | ppb |
| Detection Limit | **1** | **0.5** | **0.5** |
| **662 KV** | 1 | 4,1 | 3,9 |
| **660KV** | 3 | 1,5 | 1,4 |
| **AP-038** | < 1 | 11 | 11,3 |
| **AP-62** | < 1 | 1,4 | 2,4 |
| **AP-61** | 5 | 1 | 0,7 |
| **AP-33** | < 1 | 1,6 | 1,3 |

# **Appendix II.** Whole rock chemical analysis for mafic-ultramafic associations from basement provinces in Northern Norway

**Alta-Kvænangen tectonic window**
**Kvenvik greenstone formation**
**Least altered lavas**

| Sample | SiO2 % | Al2O3 % | Fe2O3(T) % | MnO % | MgO % | CaO % | Na2O % | K2O % | TiO2 % | P2O5 % |
|---|---|---|---|---|---|---|---|---|---|---|
| **2-1** | 46,70 | 16,08 | 13,00 | 0,38 | 10,75 | 9,29 | 2,75 | 0,10 | 0,89 | 0,07 |
| **203E/H** | 49,07 | 14,03 | 12,97 | 0,24 | 7,97 | 8,38 | 3,02 | 0,12 | 1,14 | 0,07 |
| **195** | 50,13 | 13,45 | 12,95 | 0,19 | 6,64 | 10,69 | 2,01 | 0,35 | 1,45 | 0,12 |
| **146** | 50,82 | 14,02 | 13,76 | 0,20 | 6,74 | 9,36 | 3,17 | 0,32 | 1,50 | 0,12 |
| **5-D** | 51,25 | 13,83 | 12,38 | 0,19 | 6,49 | 9,98 | 2,41 | 0,35 | 1,42 | 0,12 |

| Sample | Cr ppm | Ni ppm | V ppm | Zr ppm | Y ppm |
|---|---|---|---|---|---|
| **2-1** | 425,00 | 222,00 | 279,00 | 59,00 | 18,00 |
| **203E/H** | 382,00 | 130,00 | 369,00 | 70,00 | 21,00 |
| **195** | 216,00 | 87,00 | 391,00 | 110,00 | 26,00 |
| **146** | 259,00 | 101,00 | 419,00 | 103,00 | 26,00 |
| **5-D** | 234,00 | 90,00 | 413,00 | 109,00 | 27,00 |

**Aisaroavi formation of Holmvann Group Reppafjord window**

| Sample | SiO2 % | Al2O3 % | Fe2O3(T) % | MnO % | MgO % | CaO % | Na2O % | K2O % | TiO2 % | P2O5 % |
|---|---|---|---|---|---|---|---|---|---|---|
| **12B** | 47,14 | 14,24 | 12,43 | 0,19 | 9,48 | 10,48 | 1,64 | 0,10 | 0,64 | 0,09 |
| **83B** | 48,35 | 8,56 | 10,65 | 0,18 | 16,22 | 10,72 | 0,43 | 0,59 | 0,51 | 0,08 |
| **50A** | 49,19 | 11,80 | 10,74 | 0,17 | 13,57 | 8,33 | 1,83 | 0,36 | 0,60 | 0,12 |
| **61** | 50,36 | 9,84 | 10,66 | 0,20 | 14,92 | 10,63 | 0,26 | 1,54 | 0,55 | 0,14 |
| **11A** | 51,59 | 8,25 | 10,50 | 0,20 | 13,70 | 11,29 | 0,37 | 0,34 | 0,45 | 0,08 |
| **53C** | 52,22 | 11,38 | 11,57 | 0,18 | 10,65 | 9,31 | 1,21 | 0,82 | 0,58 | 0,08 |
| **11D** | 53,41 | 7,55 | 9,86 | 0,19 | 12,78 | 9,76 | 0,35 | 0,63 | 0,41 | 0,05 |

| Sample | Cr ppm | Ni ppm | V ppm | Zr ppm | Y ppm |
|---|---|---|---|---|---|
| **12B** | 626,00 | 137,00 | 201,00 | 78,00 | 17,00 |
| **83B** | 1681,00 | 467,80 | 178,80 | 57,50 | 13,00 |
| **50A** | 1673,00 | 485,00 | 196,00 | 62,00 | 13,00 |
| **61** | 1281,00 | 373,00 | 170,00 | 60,00 | 11,00 |
| **11A** | 4217,00 | 279,00 | 173,00 | 48,00 | 13,00 |
| **53C** | 544,50 | 112,00 | 178,70 | 74,00 | 13,00 |
| **11D** | 4128,00 | 276,00 | 161,00 | 40,00 | 7,00 |

**Altenes Tectonic Window**
**Dykes**

| Sample | SiO2 % | Al2O3 % | Fe2O3(T) % | MnO % | MgO % | CaO % | Na2O % | K2O % | TiO2 % | P2O5 % |
|---|---|---|---|---|---|---|---|---|---|---|
| **A332** | 40.0 | 12,13 | 16,20 | 0,23 | 11,75 | 9,46 | 0,34 | 0,20 | 1,11 | 0,15 |
| **A85** | 44,44 | 7,76 | 11,96 | 0,19 | 20,11 | 8,87 | 0,27 | 0,05 | 2,58 | 0,12 |
| **A86** | 45,14 | 7,99 | 12,53 | 0,21 | 19,05 | 9,30 | 0,30 | 0,13 | 0,92 | 0,1 |
| **A262** | 46,06 | 9,81 | 13,54 | 0,23 | 13,68 | 8,22 | 1,34 | 1,37 | 1,22 | 0,16 |
| **A481** | 47,54 | 15,83 | 13,08 | 0,20 | 7,79 | 9,03 | 2,92 | 0,77 | 1,13 | 0,13 |
| **A483** | 48,92 | 13,02 | 14,64 | 0,22 | 7,06 | 8,61 | 2,71 | 1,23 | 1,75 | 0,17 |
| **A44** | 50,16 | 12,95 | 17,60 | 0,26 | 4,41 | 8,27 | 3,36 | 0,89 | 2,58 | 0,28 |
| **A42** | 51,92 | 13,28 | 15,65 | 0,21 | 4,81 | 7,50 | 3,23 | 1,02 | 2,16 | 0,25 |
| **A273** | 55,95 | 15,29 | 13,71 | 0,07 | 3,06 | 4,50 | 3,69 | 1,69 | 1,48 | 0,23 |
| **A274** | 56,58 | 15,19 | 12,81 | 0,07 | 3,18 | 4,29 | 4,33 | 1,50 | 1,45 | 0,22 |

| Sample | Cr ppm | Ni ppm | V ppm | Zr ppm | Y ppm |
|---|---|---|---|---|---|
| **A332** | 2154,00 | 439,00 | 300,00 | 105,00 | 28,00 |
| **A85** | 3384,00 | 950,00 | 250,00 | 67,00 | 16,00 |
| **A86** | 3030,00 | 874,00 | 254,00 | 70,00 | 15,00 |
| **A262** | 1515,00 | 655,00 | 257,00 | 107,00 | 19,00 |
| **A481** | 166,00 | 166,00 | 261,00 | 60,00 | 14,00 |
| **A483** | 436,00 | 124,00 | 392,00 | 118,00 | 21,00 |
| **A44** | 127,00 | 53,00 | 420,00 | 208,00 | 39,00 |
| **A42** | 134,00 | 60,10 | 387,00 | 197,00 | 35,00 |
| **A273** | 131,00 | 27,00 | 266,00 | 217,00 | 33,00 |
| **A274** | 174,00 | 41,00 | 251,00 | 219,00 | 31,00 |

**Mafic-ultramafic layered association**

**The Senja Island**

| Sample | SiO2 | TiO2 | Al2O3 | Fe2O3 | MnO | MgO | CaO | Na2O | K2O | P2O5 | H2O | Total |
|---|---|---|---|---|---|---|---|---|---|---|---|---|
| **514** | 49,75 | 1,17 | 12,66 | 13,94 | 0,22 | 7,46 | 10,39 | 3,53 | 0,39 | 0,14 | 0,60 | 100,24 |
| **515** | 49,97 | 1,31 | 13,28 | 14,55 | 0,22 | 6,36 | 8,89 | 4,32 | 0,50 | 0,15 | 0,27 | 99,83 |
| **521/1** | 52,27 | 0,88 | 12,55 | 13,34 | 0,17 | 8,26 | 8,53 | 3,04 | 0,33 | 0,06 | 0,39 | 99,81 |
| **521/2** | 52,28 | 0,95 | 12,47 | 12,87 | 0,17 | 8,75 | 8,33 | 3,15 | 0,33 | 0,10 | 0,38 | 99,78 |
| **523** | 53,53 | 0,89 | 12,62 | 12,70 | 0,18 | 8,21 | 8,05 | 2,91 | 0,86 | 0,08 | 0,50 | 100,52 |
| **526** | 44,52 | 0,25 | 5,87 | 11,50 | 0,18 | 31,36 | 4,73 | 0,23 | 0,09 | 0,02 | 0,79 | 99,52 |
| **527/2** | 43,01 | 0,22 | 5,53 | 10,50 | 0,16 | 28,20 | 5,27 | 0,51 | 1,68 | 0,02 | 4,43 | 99,51 |
| **527/1** | 42,00 | 0,27 | 5,75 | 11,00 | 0,17 | 28,03 | 5,90 | 0,45 | 1,20 | 0,02 | 4,69 | 99,46 |
| **528** | 42,43 | 0,16 | 9,79 | 12,02 | 0,20 | 24,79 | 7,22 | 0,56 | 0,12 | 0,02 | 2,21 | 99,52 |
| **529** | 39,58 | 0,11 | 11,01 | 12,35 | 0,16 | 26,89 | 5,82 | 0,13 | 0,08 | 0,02 | 3,41 | 99,56 |
| **530/2** | 44,63 | 0,37 | 5,02 | 11,96 | 0,18 | 28,72 | 5,93 | 0,37 | 0,09 | 0,03 | 2,18 | 99,48 |
| **533** | 51,06 | 0,92 | 13,38 | 12,67 | 0,25 | 6,73 | 10,20 | 3,32 | 0,87 | 0,14 | 0,30 | 99,84 |
| **534** | 44,29 | 0,22 | 5,40 | 11,65 | 0,22 | 26,55 | 7,30 | 0,74 | 0,11 | 0,02 | 3,06 | 99,56 |
| **535/2** | 40,47 | 0,38 | 5,70 | 12,51 | 0,30 | 26,46 | 6,30 | 0,41 | 0,15 | 0,04 | 6,74 | 99,45 |
| **536** | 50,06 | 1,30 | 13,69 | 15,40 | 0,23 | 7,69 | 7,76 | 3,49 | 0,61 | 0,10 | 0,20 | 100,52 |
| **537** | 48,25 | 0,08 | 6,71 | 10,03 | 0,19 | 23,39 | 8,69 | 0,81 | 0,04 | 0,02 | 1,28 | 99,49 |
| **539** | 50,74 | 0,26 | 13,17 | 10,54 | 0,20 | 12,84 | 8,90 | 2,06 | 0,06 | 0,02 | 1,03 | 99,81 |
| **540** | 41,89 | 0,05 | 4,95 | 10,02 | 0,17 | 36,48 | 3,49 | 0,26 | 0,65 | 0,01 | 1,36 | 99,32 |
| **564/1** | 42,00 | 0,59 | 8,65 | 12,97 | 0,27 | 24,31 | 7,73 | 0,60 | 0,13 | 0,06 | 2,29 | 99,61 |
| **567** | 48,31 | 1,44 | 10,93 | 15,23 | 0,32 | 9,30 | 10,50 | 2,25 | 0,89 | 0,13 | 0,50 | 99,80 |

**Mafic-ultramafic layered association**
**The Senja Island**

| Sample | SiO2 | TiO2 | Al2O3 | Fe2O3 | MnO | MgO | CaO | Na2O | K2O | P2O5 | H2O |
|---|---|---|---|---|---|---|---|---|---|---|---|
| **585** | 44,40 | 0,21 | 12,64 | 11,92 | 0,22 | 16,00 | 10,80 | 1,87 | 0,30 | 0,02 | 1,34 |
| **593** | 44,02 | 0,30 | 12,47 | 13,58 | 0,20 | 19,01 | 7,89 | 1,31 | 0,12 | 0,03 | 0,90 |
| **613** | 43,17 | 0,14 | 8,88 | 9,72 | 0,17 | 23,44 | 8,01 | 0,88 | 0,17 | 0,02 | 4,97 |
| **627** | 49,65 | 0,39 | 14,70 | 11,39 | 0,23 | 9,33 | 9,50 | 3,44 | 0,27 | 0,03 | 0,90 |
| **630** | 48,18 | 0,26 | 7,60 | 12,90 | 0,55 | 9,15 | 16,73 | 1,11 | 0,71 | 0,12 | 2,08 |
| **635** | 44,17 | 0,38 | 5,69 | 12,58 | 0,23 | 26,64 | 6,75 | 0,14 | 0,07 | 0,04 | 2,84 |
| **636** | 48,60 | 0,64 | 13,94 | 13,61 | 0,23 | 9,04 | 8,69 | 4,33 | 0,07 | 0,06 | 0,63 |
| **637** | 49,92 | 1,50 | 13,33 | 14,43 | 0,22 | 6,77 | 9,02 | 3,86 | 0,42 | 0,13 | 0,19 |
| **638** | 50,55 | 1,02 | 13,54 | 13,31 | 0,22 | 7,15 | 9,28 | 3,76 | 0,40 | 0,11 | 0,47 |
| **639** | 45,51 | 0,32 | 5,90 | 11,95 | 0,18 | 27,90 | 7,24 | 0,32 | 0,05 | 0,05 | 0,40 |
| **640** | 51,80 | 0,63 | 12,99 | 11,11 | 0,21 | 7,10 | 6,70 | 5,15 | 0,18 | 0,08 | 3,92 |
| **641** | 41,53 | 0,27 | 5,23 | 12,02 | 0,19 | 27,28 | 5,51 | 0,12 | 0,02 | 0,03 | 7,37 |
| **643** | 47,55 | 0,61 | 6,10 | 11,69 | 0,18 | 19,43 | 9,90 | 0,43 | 0,05 | 0,06 | 3,70 |
| **646** | 51,55 | 1,08 | 11,94 | 13,04 | 0,17 | 8,60 | 7,56 | 2,54 | 1,06 | 0,13 | 2,03 |
| **646 krok** | 44,74 | 1,28 | 5,04 | 11,96 | 0,17 | 24,80 | 7,85 | | 0,03 | 0,09 | 3,63 |
| **s12-2-1** | 40,17 | 0,28 | 10,02 | 12,30 | 0,22 | 21,01 | 8,20 | 1,37 | 0,51 | 0,04 | 5,53 |
| **s12-2-2** | 32,56 | 2,27 | 17,69 | 13,64 | 0,14 | 19,01 | 0,37 | 0,51 | 7,49 | 0,26 | 5,75 |
| **s12-2-3** | 45,26 | 1,91 | 13,04 | 13,57 | 0,25 | 11,46 | 9,57 | 2,67 | 0,22 | 0,18 | 1,82 |
| **2012-3** | 50,94 | 0,37 | 13,36 | 10,33 | 0,18 | 9,54 | 9,70 | 3,25 | 0,25 | 0,06 | 1,82 |
| **44-1** | 46,37 | 0,23 | 11,93 | 11,96 | 0,24 | 15,28 | 10,14 | 1,83 | 0,22 | 0,03 | 1,58 |
| **44-2** | 43,00 | 0,37 | 12,74 | 8,60 | 0,16 | 8,16 | 8,85 | 3,32 | 0,12 | 0,05 | 14,51 |
| **65-1** | 47,94 | 0,65 | 7,06 | 9,75 | 0,24 | 11,14 | 22,49 | 0,19 | 0,02 | 0,09 | 0,11 |
| **65-2** | 47,40 | 1,27 | 13,66 | 12,56 | 0,38 | 5,84 | 7,43 | 3,85 | 0,43 | 0,21 | 6,91 |
| **78-1** | 45,42 | 0,85 | 7,07 | 13,67 | 0,29 | 20,40 | 7,80 | 1,16 | 0,46 | 0,11 | 2,35 |

**Ringvassøya Green Stone Belt. Central part.**

| Sample | SiO2 % | Al2O3 % | Fe2O3(T) % | MnO % | MgO % | CaO % | Na2O % | K2O % | TiO2 % | P2O5 % |
|---|---|---|---|---|---|---|---|---|---|---|
| G11/1 | 35.78 | 5.88 | 15.81 | 0.33 | 14.15 | 12.14 | 0.26 | 2.49 | 2.84 | 0.2 |
| Gr23 | 49.58 | 11.8 | 10.91 | 0.18 | 12.49 | 9.1 | 2.04 | 0.54 | 0.51 | 0.15 |
| G3 | 49.67 | 14.62 | 13.97 | 0.2 | 8.02 | 10.29 | 2.09 | 0.19 | 0.85 | 0.13 |
| D47 | 48.63 | 13.67 | 13.02 | 0.23 | 6.62 | 7.78 | 0.63 | 0.04 | 1.00 | 0.09 |
| G111/4 | 48.8 | 13.06 | 17.85 | 0.16 | 5.14 | 6.84 | 2.00 | 0.27 | 1.02 | 0.24 |
| II/4 | 48.2 | 14.83 | 15.04 | 0.21 | 6.63 | 8.1 | 2.73 | 1.03 | 1.43 | 0.17 |
| II/6 | 46.37 | 15.52 | 13.28 | 0.2 | 6.86 | 10.87 | 2.33 | 0.27 | 1.20 | 0.19 |
| III/122 | 59.07 | 19.20 | 6.30 | 0.12 | 1.30 | 3.54 | 4.47 | 1.25 | 2.25 | 0.22 |
| E80/1 | 59.48 | 17.39 | 8.45 | 0.19 | 2.19 | 4.24 | 4.02 | 0.42 | 1.43 | 0.15 |
| G98/3 | 62.76 | 20.02 | 2.12 | 0.01 | 0.73 | 3.93 | 4.28 | 1.52 | 1.76 | 0.12 |
| G98/1 | 57.14 | 18.02 | 7.50 | 0.14 | 2.55 | 4.84 | 3.46 | 0.45 | 2.01 | 0.17 |
| III/95 | 67.42 | 16.07 | 3.99 | 0.08 | 1.5 | 1.68 | 3.7 | 2.03 | 0.48 | 0.12 |
| G 2/3 | 69.30 | 15.06 | 2.08 | 0.05 | 0.83 | 2.29 | 5.27 | 1.91 | 0.15 | 0.11 |
| G 54 | 65.34 | 16.41 | 4.79 | 0.04 | 0.45 | 2.2 | 2.97 | 2.64 | 0.64 | 0.15 |
| C69 | 68.58 | 14.50 | 3.81 | 0.01 | 1.81 | 3.95 | 4.16 | 1.01 | 0.46 | 0.15 |

| Sample | Cr ppm | Ni ppm | V ppm | Zr ppm | Y ppm |
|---|---|---|---|---|---|
| G11/1 | 757 | 612 | 2500 | 246 | 9 |
| Gr23 | 1026 | 299 | 146 | 57 | 13 |
| G3 | 220 | 115 | 250 | 54 | 25 |
| D47 | 184.5 | 87 | 248 | 63.5 | 17.6 |
| G111/4 | 88.88 | 121 | 334 | 128 | 37 |
| II/4 | 216 | 101 | 211 | 79 | 25 |
| II/6 | 10 | 140 | 226 | 66 | 21 |
| III/122 | 178 | 49 | 377 | 159 | 33 |
| E80/1 | 239 | 191 | 338 | 98 | 25 |
| G98/3 | 225 | 106 | 360 | 95 | 13 |
| G98/1 | 143.5 | 131 | 424 | 90 | 24 |
| III/95 | 68 | 7 | 48 | 152 | 8 |
| G 2/3 | 31 | 8 | 30 | 62 | 6 |
| G 54 | 50 | 26 | 120 | 131 | 10 |
| C69 | 198 | 111 | 66 | 95 | 5 |

**Rombak tectonic window**

**Ruvssot area**

| | SiO2 | TiO2 | Al2O3 | Fe2O3 | MnO | MgO | CaO | Na2O | K2O | P2O5 | LOI |
|---|---|---|---|---|---|---|---|---|---|---|---|
| **R22.3** | 45.55 | 0.25 | 7.49 | 10.63 | 0.16 | 20.56 | 8.85 | 0.50 | 0.03 | 0.02 | 4.28 |
| **R1.3** | 48.57 | 1.30 | 9.88 | 13.04 | 0.09 | 7.75 | 6.86 | 4.10 | 0.17 | 0.12 | 6.68 |

**Sørdalen area**

| | | | | | | | | | | | |
|---|---|---|---|---|---|---|---|---|---|---|---|
| **M1** | 49.57 | 0.90 | 11.92 | 9.39 | 0.18 | 11.19 | 9.47 | 2.63 | 2.69 | 0.42 | 1.41 |
| **M6** | 49.99 | 1.72 | 17.91 | 9.64 | 0.13 | 3.75 | 7.83 | 3.97 | 2.84 | 0.68 | 0.92 |
| **M2** | 54.26 | 0.89 | 14.10 | 7.65 | 0.15 | 6.19 | 6.18 | 4.05 | 3.91 | 0.38 | 0.89 |
| **M5** | 54.99 | 1.73 | 17.80 | 7.92 | 0.08 | 1.74 | 4.48 | 4.90 | 4.36 | 0.76 | 0.38 |
| **M4** | 57.94 | 1.31 | 16.38 | 6.30 | 0.11 | 1.94 | 5.06 | 4.60 | 3.78 | 0.40 | 0.58 |
| **M3** | 58.83 | 0.96 | 16.18 | 7.35 | 0.13 | 3.20 | 5.35 | 3.59 | 3.12 | 0.24 | 0.86 |

**Lofoten - Vesterålen area**
**Early Proterozoic supracrustal rocks**

| | | SiO2 | Al2O3 | Fe2O3(T) | MnO | MgO | CaO | Na2O | K2O | TiO2 | P2O5 |
|---|---|---|---|---|---|---|---|---|---|---|---|
| | | % | % | % | % | % | % | % | % | % | % |
| **Langøy** | LV1 | 58.7 | 16.3 | 7.8 | 0.10 | 3.2 | 4.6 | 4.5 | 3.1 | 0.9 | 0.4 |
| **Austvågøy** | LV2 | 63.4 | 14.2 | 6.9 | 0.09 | 1.9 | 3.0 | 4.4 | 3.9 | 0.9 | 0.3 |
| **Moskenesøy** | LV3 | 50.7 | 18.5 | 10.2 | 0.15 | 5.2 | 8.1 | 4.1 | 1.4 | 0.8 | 0.4 |

# **Appendix III.** CIPW norms

| Normative Minerals | Volume % Norm | Volume % Norm | Volume % Norm | Volume % Norm | Volume % Norm | Volume % Norm | Volume % Norm | Volume % Norm | Volume % Norm | Volume % Norm | Volume % Norm |
|---|---|---|---|---|---|---|---|---|---|---|---|
| | AP-34 | AP-35 | AP-36 | AP-37 | AP-46 | AP-47 | AP-49 | AP-50 | AP-51 | AP-52 | AP-55 |
| Quartz | | | | | | | | | | | |
| Plagioclase | 16,22 | 11,28 | 12,48 | 13,70 | 15,56 | 15,56 | 10,06 | 16,64 | 16,07 | 15,85 | 18,57 |
| Orthoclase | | 0,15 | | | 1,23 | 1,23 | | 0,15 | 0,23 | | 0,92 |
| Nepheline | | | | | | | | | | | |
| Leucite | | | | | | | | | | | |
| Kalsilite | | | | | | | | | | | |
| Corundum | | 0,15 | | | | | 0,30 | | | | |
| Diopside | 3,14 | | 2,87 | 2,30 | 4,67 | 4,67 | | 15,03 | 5,27 | 5,27 | 6,16 |
| Hypersthene | 44,88 | 43,07 | 36,59 | 47,20 | 50,35 | 50,35 | 39,34 | 37,90 | 36,10 | 42,44 | 50,93 |
| Wollastonite | | | | | | | | | | | |
| Olivine | 26,96 | 35,93 | 38,56 | 25,80 | 16,63 | 16,63 | 40,07 | 18,47 | 30,95 | 25,56 | 10,83 |
| Larnite | | | | | | | | | | | |
| Acmite | | | | | | | | | | | |
| K2SiO3 | | | | | | | | | | | |
| Na2SiO3 | | | | | | | | | | | |
| Rutile | | 0,18 | | | | | 0,17 | | | | |
| Ilmenite | 0,51 | 0,57 | 0,56 | 0,35 | 0,16 | 0,16 | 0,39 | 0,11 | 0,20 | 0,51 | 0,35 |
| Magnetite | | | | | | | | | | | |
| Hematite | 7,39 | 8,26 | 7,94 | 8,92 | 9,26 | 9,26 | 9,09 | 9,49 | 9,32 | 8,49 | 9,42 |
| Apatite | 0,22 | 0,22 | 0,19 | 0,19 | 0,12 | 0,12 | 0,10 | 0,15 | 0,07 | 0,24 | 0,31 |
| Zircon | 0,01 | 0,01 | 0,01 | 0,01 | 0,01 | 0,01 | | 0,01 | | 0,01 | 0,01 |
| Perovskite | | | | | | | | | | | |
| Chromite | 0,15 | 0,18 | 0,16 | 0,38 | 0,59 | 0,59 | 0,47 | 0,45 | 0,57 | 0,16 | 0,26 |
| Sphene | 0,52 | | 0,62 | 1,14 | 1,41 | 1,41 | | 1,58 | 1,22 | 1,47 | 2,23 |
| Pyrite | | | | | | | | | | | |
| Halite | | | | | | | | | | | |
| Fluorite | | | | | | | | | | | |
| Anhydrite | | | | | | | | | | | |
| Na2SO4 | | | | | | | | | | | |
| Calcite | | | | | | | | | | | |
| Na2CO3 | | | | | | | | | | | |
| Total | | 100,00 | 99,98 | 99,99 | 99,99 | 99,99 | 99,99 | 99,98 | 100,00 | 100,00 | 99,99 |

| Normative Minerals | Volume % Norm | Volume % Norm | Volume % Norm | Volume % Norm | Volume % Norm | Volume % Norm | Volume % Norm | Volume % Norm | Volume % Norm | Volume % Norm | Volume % Norm |
|---|---|---|---|---|---|---|---|---|---|---|---|
| | AP-54 | AP-54a | AP-56 | AP-57 | AP-58 | AP-59 | AP-60 | AP-63 | AP-64 | KV-660 | KV-662 |
| Quartz | | 2,66 | | | | | | | | | |
| Plagioclase | 17,74 | 17,96 | 11,75 | 9,02 | 10,76 | 14,07 | 1,33 | 15,17 | 20,05 | 8,55 | 14,22 |
| Orthoclase | 0,15 | 0,23 | 0,15 | | 0,62 | 0,16 | | 0,31 | 0,08 | | 0,15 |
| Nepheline | | | | | | | | | | | |
| Leucite | | | | | | | | | | | |
| Kalsilite | | | | | | | | | | | |
| Corundum | | | 0,14 | 0,83 | 0,47 | | 1,27 | 0,23 | | 0,72 | |
| Diopside | 6,44 | 29,38 | | | | 2,94 | | | 3,16 | | 5,88 |
| Hypersthene | 48,99 | 41,21 | 43,91 | 46,17 | 48,19 | 42,95 | 72,91 | 49,27 | 57,82 | 42,38 | 37,52 |
| Wollastonite | | | | | | | | | | | |
| Olivine | 14,83 | | 34,61 | 34,47 | 30,93 | 27,94 | 13,22 | 25,66 | 7,19 | 37,59 | 31,19 |
| Larnite | | | | | | | | | | | |
| Acmite | | | | | | | | | | | |
| K2SiO3 | | | | | | | | | | | |
| Na2SiO3 | | | | | | | | | | | |
| Rutile | | | 0,15 | 0,14 | 0,21 | | 0,02 | 0,14 | | 0,25 | |
| Ilmenite | 0,23 | 0,09 | 0,60 | 0,62 | 0,54 | 0,08 | 0,10 | 0,55 | 0,20 | 0,35 | 0,22 |
| Magnetite | | | | | | | | | | | |
| Hematite | 9,59 | 6,84 | 8,28 | 8,41 | 7,93 | 9,68 | 10,49 | 8,31 | 8,90 | 9,50 | 9,12 |
| Apatite | 0,15 | 0,05 | 0,22 | 0,17 | 0,17 | 0,19 | 0,02 | 0,19 | 0,29 | 0,17 | 0,12 |
| Zircon | 0,01 | | 0,01 | | 0,01 | 0,01 | | 0,01 | 0,01 | | |
| Perovskite | | | | | | | | | | | |
| Chromite | 0,53 | 0,47 | 0,17 | 0,18 | 0,17 | 0,52 | 0,63 | 0,16 | 0,38 | 0,49 | 0,64 |
| Sphene | 1,34 | 1,12 | | | | 1,47 | | | 1,93 | | 0,92 |
| Pyrite | | | | | | | | | | | |
| Halite | | | | | | | | | | | |
| Fluorite | | | | | | | | | | | |
| Anhydrite | | | | | | | | | | | |
| Na2SO4 | | | | | | | | | | | |
| Calcite | | | | | | | | | | | |
| Na2CO3 | | | | | | | | | | | |
| Total | 100,00 | 100,01 | 99,99 | 100,01 | 100,00 | 100,01 | 99,99 | 100,00 | 100,01 | 100,00 | 99,98 |


UNIVERSITY OF TROMSØ